



HAL
open science

Nanoscale structuration effects on phonon transport at low temperatures

Christophe Blanc

► **To cite this version:**

Christophe Blanc. Nanoscale structuration effects on phonon transport at low temperatures. Condensed Matter [cond-mat]. Université de Grenoble, 2013. English. NNT: 2013GRENY079. tel-01291220v2

HAL Id: tel-01291220

<https://hal.science/tel-01291220v2>

Submitted on 28 Sep 2016

HAL is a multi-disciplinary open access archive for the deposit and dissemination of scientific research documents, whether they are published or not. The documents may come from teaching and research institutions in France or abroad, or from public or private research centers.

L'archive ouverte pluridisciplinaire **HAL**, est destinée au dépôt et à la diffusion de documents scientifiques de niveau recherche, publiés ou non, émanant des établissements d'enseignement et de recherche français ou étrangers, des laboratoires publics ou privés.

THÈSE

Pour obtenir le grade de

DOCTEUR DE L'UNIVERSITÉ DE GRENOBLE

Spécialité : **Physique**

Arrêté ministériel :

Présentée par

Christophe Blanc

Thèse dirigée par **Olivier Bourgeois**

préparée au sein de l'**Institut Néel**
et de l'**Ecole doctorale de Physique de Grenoble**

Nanoscale structuration effects on phonon transport at low temperatures

Thèse soutenue publiquement le **5 Novembre 2013**,
devant le jury composé de :

Henri Godfrin

Directeur de recherche, Institut Néel, Président

Francesco Giazotto

Professeur, Laboratoire Nest, Rapporteur

Ilari Maasilta

Professeur, Université de Jyväskylä, Rapporteur

Sebastian Volz

Directeur de recherche, Laboratoire d'Energétique Moléculaire et Macroscopique,
Examineur

Olivier Bourgeois

Chargé de recherche, Institut Néel, Directeur de thèse



Acknowledgements

Tout d'abord un grand merci à Olivier Bourgeois. Pendant ces trois années (plus celles du stage), tu m'as bien aidé à comprendre la physique compliqué du transport de phonons. Tu as été toujours disponible pour m'indiquer de nouvelles pistes de réflexion. Même si je n'ai pas toujours profiter de ton expérience, ton ouverture et ta disponibilité ont énormément contribué à que cette thèse se déroule aussi bien. J'ai aussi bien aimé que tu ais envie de profiter du temps avec ta famille, et donc me faire confiance pour aller présenter nos résultats à de grandes conférences.

Ensuite Jean-Savin Héron m'a beaucoup appris sur la fabrication et sur la physique. C'est vraiment génial de commencer une thèse avec une expérience qui tourne bien, de la fabrication à la mesure. Et pour l'analyse, avoir déjà une bonne bibliographie (presque) toute bien rangée a été très utile. J'espère que tout se passe bien pour toi maintenant.

Concernant la fabrication, merci aussi à Thierry Crozes et Thierry Fournier. Thierry Crozes, pour sa disponibilité dès que je n'étais pas sur de moi sur le MEB, pour tes petits conseils avec elphy. Dieu sait que ce logiciel n'est pas intuitif, et tu me l'as rendu quand même assez simple. Thierry Fournier, pour toute ta database, qui m'ont permis de construire de si belle corrugation.

Et bien sûr, merci au reste de la Nanofab team ! Bruno, Gwenaëlle, Sébastien, et Jean-François, mes presque voisins de bureau. C'était cool d'avoir une ambiance aussi sympa. Dès que j'avais besoin d'aide sur une machine vous étiez là. Et dans une ambiance plus qu'amicale, ce qui m'a rendu ces longs moments d'attentes en salle blanche un peu moins pénibles... Désolé pour les bechers cassés, la vaisselle oublié (oui, je peux l'avouer, cela m'ait arrivé...), et les mauvais réglages sur certaines machines. J'ai essayé d'être le plus propre en salle blanche, mais des erreurs sont inévitables. Merci d'avoir tous été là pour réparer mes bêtises.

J'aurais arrêté les mesures en deuxième année si je n'avais pas eu la chance, l'honneur même, d'avoir reçu l'aide de l'immense Pierre Brosse. Il y a presque trente ans tu as fabriqué un frigo, et il fonctionne toujours, en grande partie grâce à toi. Ton impressionnante maîtrise de la cryogénie m'a bluffé. Ton pouvoir de trouver même les plus petites fuites manquera beaucoup au labo... Merci beaucoup Pierre, et profite bien de ta retraite. Merci aussi au reste du pôle Cryogénie. Vous m'avez toujours bien accueilli, toujours prêt à donner un coup de main, et toujours très gentiment. Merci à tous.

Le liquéfacteur fait aussi un énorme travail. On a de l'hélium 24h/24 grâce à vous. Et même si des fois je suis venu un peu tard, j'ai l'impression d'avoir toujours eu quelqu'un pour m'aider. Alors désolé pour les vases vides (2 en trois ans...), et pour à chaque fois vous demander

Acknowledgements

d'enlever et remettre la tête, et merci de l'avoir toujours fait sans râler.

Un bon merci à Jean-Seb Roch et Bernard Maire-Amiot. J'ai eu plusieurs problèmes et vous étiez là très rapidement pour m'aider à les réparer. Vu comme l'informatique est indispensable dans un travail de thèse, sans vous j'aurais été bien plus mal. C'est super d'avoir ainsi des ordinateurs sur qui ont peu faire ce qu'on veut (même y mettre des virus). Et j'ai pu faire ça grâce à vous qui étiez là pour m'aider en amont et en aval. Merci beaucoup.

Merci aussi au électroniciens. J'ai finalement pas trop eu besoin de vous. Ça veut dire que les machines que vous avez faites sont super ! Mais les rares fois où j'ai eu besoin d'un coup de main pour commander des fils, des résistances, ou une machine, il y a toujours eu quelqu'un pour m'aider. Merci donc à Olivier, Christophe, Jean-Luc et Maurice.

Du coup, comme j'en suis aux achats, merci beaucoup au magasin. Moi qui perd mes stylos, mes clefs USB, qui ne suit pas bien rangé, cela m'a été très utile d'avoir un tel service juste à côté. Merci donc bien d'avoir tout ce qu'il faut, et tout le temps.

Et à côté du magasin il y avait Carmeline qui en a bien bavé à 17h pour m'aider à faire venir tous mon jury, payer un peu de mon pot de thèse,... J'ai pu voir comme les logiciels de gestion du CNRS sont contre-intuitifs et souvent répétitif. Merci beaucoup d'avoir passé du temps pour que tout se passe bien. Un gros merci aussi à Christine pour les papiers. J'ai oublié deux fois mon contrat, et sans toi j'aurais du passer du temps à chercher. En un coup de fil, tu avais tout de suite les infos. Bravo ! Merci aussi à Patricia. Mes missions ont toujours été traités rapidement et avec le sourire. Bonne continuation à toi. Et merci aussi à Cécile, toujours présente pour donner un coup de main sur un poster mal présenté.

Pour la recherche, un bon merci à Eddy Collin qui m'a montré que les phonons ne servaient pas que à transporter la chaleur. J'ai bien aimé faire des nano cages de foot. J'aurais bien aimé prendre le temps de te demander plus exactement ce que tu faisais avec. Mais merci d'avoir mis mon nom sur vos papiers. Thanks also to Kunal. I really liked working with you. Even if it wasn't for long and I should have worked more with you, it was a pleasure to work with someone smart and with a good knowledge. Et pendant qu'on est chez les UBT, merci Henri pour toutes tes corrections de mon manuscrit. J'ai voulu le faire en anglais sans avoir vraiment le niveau. Même s'il reste sûrement des coquilles, sans toi il y en aurait tellement plus...

Voilà, pour finir sur les permanents du CNRS, j'ai gardé les meilleurs pour la fin : la fameuse équipe TPS et le pôle capteur ! Difficile au début de savoir qui est dans quoi, mais en tout cas je me suis tout de suite senti bien avec cette équipe au sens large. Donc je vous regroupe tous ensemble, comme ça pas de jaloux ! Les repas, les cafés, et les débats lorsque je venais voir Olivier m'ont toujours amusés et intéressés. On se sent un peu comme dans une famille (malgré l'absence de présence féminine...). Il y avait : mon papa qui est le plus fort parce que c'est le chef ; Le grand-père qui sait plein de trucs et que malheureusement on voit de moins en moins ; l'oncle qui est jamais d'accord et qui le fait savoir ; l'autre oncle adepte des nouvelles technologies ; et le dernier qui a préféré émigré au Japon plutôt que rester avec les autres ; En parlant de rester il y a les deux jeunes cousins (l'un qui vient d'être papa et l'autre qui attends qu'un brevet lui fasse gagner plein d'argent) qui aimeraient bien y rentrer. Ah si, il y a aussi les cousines éloignés qui comme elles aiment pas le rugby et la politique, on les voit pas trop... Il y a bien sûr les amis de la famille, qui viennent donner un coup de main au

petits jeunes quand vous êtes trop occupé à parier des bières. Notamment un qui a respiré des vapeurs de HF grâce à moi. Il y a eu aussi des amis étrangers de passage. Ça a été toujours un plaisir de partager avec eux. Comme les glaces à l'azote lorsque l'un de vous devait faire la garderie. Et puis il y avait les autres enfants comme moi. Ceux qui sont arrivés en même temps que moi. Ceux qui sont arrivés un peu après. Avec tous, ça c'est bien passé, tant pour moi, que pour eux j'ai eu l'impression. J'espère que vous continuerez à bien intégrer les jeunes, sans trop leur faire peur. Mais je me fais pas de soucis pour vous. Je vous souhaite donc à tous de continuer à bien bosser tout en continuant à déconner. Vive la thermo !

Et enfin merci aux autres thésards de Néel. A Vito et Hadès pour ce bon voyage en China. Aux responsables des séminaires thésards. A ceux qui sont venus plusieurs fois présenter leur résultats parce que personnes d'autres voulaient venir. Aux irréductibles de 12h15 devant le bâtiment M. Bref à tous ceux qui ont fait que je me suis senti bien dans ce labo pendant plus de 3 ans, juste parce que j'étais pas tout seul. Merci à tous.

Et ceux qui se rappellent m'avoir donné un coup de main, mais qui ne se sentent pas inclus dans ces remerciements, je suis vraiment désolé. Trois ans, c'est long, il se passe beaucoup de choses et ma mémoire n'est plus ce qu'elle était. Donc un grand merci à toi, personne dont j'ai oublié le nom et dont j'ai oublié ce que tu as fait pour moi. Cette thèse t'est aussi dédié.

Voilà pour le côté boulot. Mais ma thèse ne se serait pas aussi bien passé sans plein de gens autour de moi pour me supporter. Encore une fois, cela me sera difficile de ne pas en oublier, donc si tu te sens oublié dans ces remerciements, j'en suis désolé. Je te remercie quand même...

Un grand merci à ma famille. Mes parents, pour tous ces dimanche soir où j'ai pu manger un bon repas. Pour votre support, même si vous ne connaissiez rien sur mon sujet. Et votre présence stable, comme un bon point d'accroche dans ma vie. Merci à Etienne, pour m'avoir donné envie de ne pas faire comme toi, et Estelle, pour m'avoir montré qu'une thèse c'est possible. Merci aussi à Briséis et Apolline, pour les couches et les vomis et maintenant les chevaliers-pompiers. Merci à Camille, pour son engagement associatif. Ça me montre qu'il est possible de continuer de penser aux autres. Merci à Thomas, je me sens un peu comme un exemple pour toi, même si tu te persistes à faire de l'informatique. Merci à Violaine et Yannick, pour tous ces samedi soir à supporter le AC Seyssinet Handball, et maintenant le AL Voiron Handball. Et merci Barth, qui prends la suite à Nancy. Amuses toi bien là-bas. Merci à Papi et Mamie, d'être toujours là et de rester comme vous êtes et de me faire un peu sentir Stéphanois et d'aimer la Badoit. Merci à Papaul et Magnès, pour m'avoir dit un jour que tout est intéressant et pour Saint Aupre. Merci à tous mes oncles et tantes. Désolé de ne pas tous vous citer ici, vous savez que vous êtes nombreux. Mais sachez que j'ai un réel plaisir à chaque fois lorsque je discute avec chacun d'entre vous. Une pensée spéciale à Maïe, pour me rappeler qu'il y a peut-être quelque chose de plus important, et pour les tournois de Baby-foot. Et pour les cousines et cousins, un autre merci général. Durant ces trois ans, vous n'avez peut-être pas tout suivi, mais je sais qu'on reste proche même si on se voit tous un peu moins.

Merci aussi à mes colocs. Rami, pour les discussions, la Xbox et tes repas équilibrés qui m'ont fait me sentir plus sain. Doris, pour avoir mis un peu d'organisation, les gâteaux, le frigo que t'as fini de dégeler et tes amies en culotte dans le salon...

Et ma thèse se serait bien moins passé sans des potes qui ont soutenus avant moi pour me

Acknowledgements

montrer que si même eux l'ont fait alors pourquoi pas moi. Merci donc encore à Rami pour ça ! A Lolo, mister best student paper. Poil, qui est venu en matière condensée, et qui a réussi malgré Starcraft. Rem's, qui s'est envoyé en l'air, courage mec, tu trouveras un boulot. Grand, pour les tournois de coinchés. Zouave, pour ses intestins intempestifs. Chloé, même si j'ai pas fait tes expériences, dire là pour une lampe allumé ça avait l'air rigolo. Boom's, pour le meilleur fêtage de soutenance possible. Warz, pour critiquer les gens qu'on aime pas au labo et t'avoir mis une pils à Civilization. Petit Cerise je t'aime beaucoup, et pour dirty old town. Val pour la bio, comme quoi j'ai bien fait de pas en faire. Fred, le survivor, l'autre rescapé du WEI 4A. Et à Pierrot, pour tes étagères, et tout les plans qu'on a imaginés les matins ou t'étais sur Grenoble. A tout notre salaire, bien dépensé en bière, au Cal'z, au Subway, ou au Monoprix. Merci aux autres potes, qui ont préférés gagner direct leur vie. A Fab et Sophie, le couple le plus mature de notre groupe et à Gaby Wellness. A Ju, le nouvel américain. A Carole, pour ton appart à Lyon. A Bastieng, le rescapé de l'île de la tentation (pour les otariophile). Et tous les autres de PG.

Merci aussi au CPPiste nancéen. A chaque fois qu'on se revoit, c'est presque comme avant, ça fait plaisir.

Un autre merci aux potes plus anciens. Même si on se voit moins, c'est souvent bien cool de voir comment on change, mais comment l'amitié est toujours présente. Merci surtout à So, pour aller boire des cafés, m'inviter à manger, et courage avec la petite. Une bonne pensée aussi à Cloclo. Ca y est t'es mariée ! J'ai vraiment apprécié de te voir aussi radieuse. Bonne chance à tous les deux.

Un grand merci aussi à tout les Monkey. Vive l'ultimate frisbee ! J'espère que la montée en D1 se fera cette année, comme ça j'y aurais contribué. Et bravo pour BO, c'est toujours un succès. Et last but not least, une énorme pensée à Barbara. Ca a pas toujours été facile. Mais tu as bien voulu de moi, comme j'ai bien voulu de toi. Ensemble on a réussi à traverser la distance. J'espère qu'on aura plus à vivre cela, qu'on enchaîne Pise, Marseille, San Francisco et Bordeaux ou pas, j'espère que désormais on sera ensemble. Sans tes corrections aussi cette thèse n'aurait pas été aussi bien écrite. Donc thanks a lot. (bandit).

Il me semble avoir fait le tour de la question. Vous pouvez maintenant lire cette thèse, tout en sachant à qui je suis redevable pour l'avoir faite. J'espère donc pour moi, et pour toutes ces personnes, que vous apprécierez ce travail.

Abstract

This PhD entitled *Nanoscale structuration effects on phonon transport at low temperatures* take place for three years in the Thermodynamique et Biophysique des Petits Systèmes of the Institut Néel.

The context of this PhD is to understand and control the heat transport in samples with variations at the nanoscale. These samples were mostly suspended silicon nanowires. The production was performed in the Néel Institute. During these three years, three important results have been demonstrated.

First, we verify that heat transport is not dominated by an effect due to the contact between the suspended nanowire and the thermal bath. This has been demonstrated by the agreement between the measurements and the model called Casimir-Ziman. It was also mainly verified with wires whose junction to the thermal bath has been adapted to allow transmission close to unity. These profiles nanowires have the same thermal conductance as a nanowire with abrupt junction to the thermal bath. This proves that the transmission is always close to 1.

Then measurements on nanowires whose section is corrugated have shown a reduction in thermal conductance. This reduction is explained by the presence of backscatter phonons at the surface, resulting in a large reduction of their mean free path. Thus, the phonons in a smooth nanowire have a mean free path up to 9 times greater than in these corrugated nanowires. Simulations with the Monte-Carlo method also demonstrate this effect.

If these first results were achieved for monocrystalline silicon nanowires, my last work has focused on the study sample of silicon nitride. This material is an amorphous one. Physics of heat transport in amorphous materials is not yet fully understood. However, measurements on these materials show a similar behavior, both qualitatively and quantitatively, for almost all amorphous materials. We have measured samples of different kinds, to see if this behavior was still valid when the sample size is reduced. The result of our measurements is that the size plays a role in transport. As in crystalline materials, the small sample size will limit the heat transport. However transport in low-dimensional samples shows the same behavior qualitatively as in bulk amorphous materials. This can help provide clues for understanding the heat transport in amorphous materials.

In conclusion, this work has allowed me to make and measure the heat transport in different types of samples. The results allow a better knowledge of the phonon transport, thus helping to pave the way towards a better control of heat transport.

Résumé

Cette thèse, intitulé « Effet de structuration à l'échelle du nanomètre sur le transport de phonon à basse température » c'est déroulé pendant trois ans au sein du groupe Thermodynamique et Biophysique des Petits Systèmes de l'Institut Néel.

Il s'agit de comprendre et de contrôler le transport de chaleur au sein d'échantillons ayant des variations de l'ordre du nanomètre. Ces échantillons ont surtout été des nanofils suspendus en silicium. La fabrication a été réalisée au sein de l'Institut Néel. Lors de ces trois années, trois résultats importants ont été réalisés.

Tout d'abord, il a fallu vérifier que le transport de chaleur ne soit pas dominé par un effet dû aux contacts entre le nanofil suspendu et le bain thermique. Cela a pu être mis en évidence grâce à la concordance entre les mesures et le modèle appelé Casimir-Ziman. Mais cela a surtout été vérifié avec des fils dont la jonction au bain thermique a été adaptée afin de permettre une transmission proche de l'unité. Ces fils profilés ayant la même conductance thermique que les fils avec une jonction abrupte au bain thermique, cela prouve que la transmission est toujours proche de 1.

Ensuite des mesures sur des fils dont la section est ondulée ont permis de montrer une réduction de la conductance thermique. Cette réduction est expliquée par la présence de rétrodiffusion des phonons à la surface, ce qui entraîne une grande réduction de leur libre parcours moyen. Ainsi, les phonons dans un nanofil droit ont un libre parcours moyen jusqu'à 9 fois plus grand que dans ces nanofils à la section ondulée. Des simulations avec la méthode de Monte-Carlo ont permis de mettre en évidence cet effet.

Si ces premiers résultats ont été réalisés pour des fils de silicium monocristallin, le dernier travail a porté sur l'étude d'échantillon en nitrure de silicium. Ce matériau est un matériau amorphe. La physique du transport de chaleur au sein des matériaux amorphes n'est pas encore complètement comprise. Cependant les mesures faites sur ces matériaux montrent un comportement similaire, tant qualitatif que quantitatif, pour presque tous les matériaux amorphes. Nous avons donc mesurés des échantillons de différentes sortes, afin de vérifier si ce comportement était toujours valable, lorsque la dimension de l'échantillon est réduite. Le résultat de nos mesures est que la dimension joue un rôle sur le transport. Tout comme dans les matériaux cristallins, la basse dimension de l'échantillon va limiter le transport de chaleur. Cependant le transport dans les échantillons de basses dimensions montre le même comportement qualitatif que les matériaux amorphes massifs. Ce travail peut permettre de donner des pistes pour la compréhension du transport de chaleur au sein des matériaux amorphes.

En conclusion ce travail m'a permis de fabriquer puis de mesurer le transport de chaleur dans différents types d'échantillons. Les résultats obtenus permettent une meilleure connaissance du transport des phonons, et donc aident à ouvrir la voie vers un meilleur contrôle du transport de la chaleur.

Contents

Acknowledgements	iii
Abstract (English/Français)	vii
Introduction	1
1 Physics of phonons in nanostructures at low temperature	3
1.1 Introduction	3
1.2 The heat carriers	3
1.3 Phonons	5
1.3.1 Definition and dispersion relation	5
1.3.2 The two characteristic lengths for phonon transport	8
1.4 Phonon transport at low dimensions and low temperatures	10
1.4.1 Introduction	10
1.4.2 Heat Capacity, and thermal conductance	10
1.4.3 The Casimir model	13
1.4.4 The Ziman model	14
1.4.5 The universal quantum of thermal conductance	15
1.4.6 The junction with the thermal bath	18
1.5 Phonon inside amorphous materials	21
1.6 Thermal transport by electrons	24
1.7 Nanophononics	25
1.8 Conclusion	26
2 Experimental techniques for thermal transport in small systems and at low temperatures	27
2.1 Introduction	27
2.2 Measurement of thermal conductance	28
2.2.1 The 3ω method for nanowires	28
2.2.2 The 3ω method for membranes	34
2.2.3 The Helium 3 fridge	38
2.2.4 Other method of measurement	40
2.3 Fabrication	45
2.3.1 Silicon nanowires	45

Contents

2.3.2	Fabrication of Si_3N_4 nanowires and slabs	47
2.3.3	Fabrication of the SiN membranes	48
2.4	Previous measurements of silicon nanowires	49
2.4.1	Introduction	49
2.4.2	Comparison with the Casimir-Ziman model	49
2.4.3	Influence of the dimensions	52
2.4.4	Influence of the contact	53
2.4.5	The other parasitic thermal paths	54
2.5	Conclusion	56
3	Investigation of the thermal transport at the junction between a nanowire and a thermal bath	57
3.1	Introduction	57
3.2	Theoretical works	57
3.3	Measurements and normalization	60
3.4	Conclusion	63
4	Modification of phonon transport in corrugated nanowires	65
4.1	Introduction	65
4.2	Measurements	65
4.3	Impact on the mean free path	69
4.4	Impact of the corrugation on the dispersion relation	71
4.5	Conclusion	73
5	Measurements on SiN structures	75
5.1	Introduction	75
5.2	The phenomenological approach	75
5.3	Measurements on nanowires, membranes and slabs	78
5.4	Comparison with the Casimir-Ziman model and the quantum of thermal conductance	83
5.5	Conclusion	85
	Conclusion	87
	Bibliography	87

Introduction

For thirty years, mesoscopic physics has drawn a strong activity in the condensed matter community. This field is at the border between quantum and classical physics. But the transition between these two fields is not a continuous process. When a macroscopic object is miniaturized, before reaching a pure quantum behavior with just a few atoms, the physical properties begin to change.

If electronic properties of meso-systems are much studied, thermal properties are a little left out. Heat exchange in most cases is undesirable, and responsible for losses of information (decoherence for instance). Thus, it needs to be controlled. Generally, most studies in mesoscopic physics deal with electrons. However, intermediate sizes also influence the physics of phonons, especially in dielectrics. This phonon meso-physics is now called nanophononics. This emerging field of research is dedicated to the understanding of the physics of phonon transfer at the nanoscale. Finally, in the energy recovery field of research, heat becomes a dominant factor, where phonons plays a major role. Heat management at the nanoscale requires the development of more efficient thermoelectric devices for instance.

This thesis focuses on the vast field of thermal phonon manipulation. Two characteristic lengths are used to describe phonon transport : the mean free path and the wavelength. Intuitively, one can think that when the size of the sample studied is of the same order of magnitude as these characteristic lengths, the phonons transport will be affected. This is our motivation to undertake the investigation of the effect of nanostructuration on the phonon transport.

In this work, three typical cases were investigated :

The influence of the contact between a nanowire and a thermal reservoir;

The influence of corrugation at the surface of a nanowire;

The thermal transport in nanoscale systems of amorphous materials.

The environment to perform these experiments was favorable, as the Thermodynamique des Petits Systemes group of the Institut Néel developed several very sensitive sensors for measuring thermal properties. In the particular field of phonon transport previous measurements have already been made. The presence of both nanofabrication and cryogenic facilities in the laboratory was also an advantage.

Contents

The present manuscript reports the work I have done during the last three years.

In the first chapter, theoretical works of the thermal transport at low temperature are presented.

The second chapter introduces the methods used for the measurement of phonon transport, the fabrication of the sample, and previous measurements made in the group.

The influence of the contact conductance between the nanowire and the thermal bath is investigated in the third chapter.

Chapter four shows how the thermal conductance of a nanowire is affected by the presence of a corrugation.

Finally, the chapter five introduces thermal transport in an amorphous materials (SiN) in three different kinds of samples.

1 Physics of phonons in nanostructures at low temperature

1.1 Introduction

The thermodynamic variable "temperature" has been studied for more than one century. The question of what is hot or what is cold has always interested physicists. The temperature is the intensive thermodynamic variable conjugated to the entropy. It can be macroscopically defined by means of the mean square value of the velocities of the atoms in a body. However when the samples to be studied reach nanometric scales, the notion of temperature could even be not well-defined. Nowadays, with the development of nanofabrication technologies, it is possible to design and build such nanometric samples.

On a macroscopic scale, heat can propagate in a material or between bodies following three different ways: conduction, convection and radiation. These three ways are schematically represented with a cup of coffee in Fig. 1.1. These modes of heat propagation are useful to obtain phenomenologically the flow values between bodies at different temperatures. However, if we want to know at a microscopic scale what exactly happens when heat propagates, it is important to know what the heat carriers are, and how they interact with their surroundings. In this case, a microscopic description of the transfer processes is required.

In this chapter the mechanism of heat transport at low temperature inside nanowires will be presented. The concept of phonon will be introduced to study heat transport.

1.2 The heat carriers

In the case of radiation, the heat carriers are called photons. The sun for instance radiates heat through the emission of photons. In fact all bodies at a temperature higher than 0 K emit photons. An idealized case is when one only takes the temperature into account for the creation of photons for a body. It is called the black body approximation. This case permits to calculate the emission of photons of such a body. The black body radiates according to Planck's law and the total emissive power of a blackbody is given by the Stefan-Boltzmann



Figure 1.1: Three mechanisms of heat propagation. The conduction come from contact with a low gradient of temperature; the convection happens when the heat carriers are able to move freely, so in a disorganized way; the radiation come with the creation of the photons, it happens as soon as the temperature differ from 0 K, and it propagates in every directions.

law. The power radiated per surface unit is directly proportional to the fourth power of the black body temperature. It is also interesting to notice that this heat transfer does not require a medium and can propagate in vacuum.

Convection happens in fluids or gases, where atoms are free to move. A hot atom moves faster than the others and then gives its energy through collisions. This process, although simple, may become chaotic due to the high number of atoms. Environmental factors have a huge impact on this process. No general law exists to quantify convection. One needs to write the convection-diffusion equation (or drift-diffusion) and solve it in the studied case. As the heat carriers in convection are atoms, this mechanism is also responsible for mass transport.

In our case we are interested in heat transport in condensed matter. Even if a photon can travel within matter, it will be absorbed soon. Therefore radiation is not appropriate. Neither is convection, as atoms do not flow inside bulk materials. Conduction remains the only relevant mechanism. In this case, the only known moving particle is the electron. While carrying electricity, electrons also carry heat. In the case of dielectrics, electrons do not move. However, an atom with an internal energy, can slightly move around its equilibrium position. This displacement will be seen by its neighbors. As masses linked by strings, this variation will propagate along the sample (see figure 1.2) [1].

If this process seems quite simple, in the case of a three dimensional system constituting the lattice, it becomes very complex. A model was proposed by Einstein in 1907 and another by Debye in 1912. Both models consider the atoms to be quantum harmonic oscillators. If the Einstein model considers that every atom oscillates at the same frequency, the Debye model introduces a linear frequency dependence to the wave vector of the oscillation. In 1932,

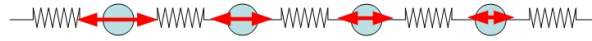


Figure 1.2: Schematic representation of a one dimensional atom chain.

Yakov Frenkel and Igor Tamm used the similarity between photons and these atomic quantum oscillators to introduce the concept of phonons.

As a final note one can argue that on the surface of a sample, radiation and convection mechanisms play a role in heat transfer. As it will be described later on, the samples are put under vacuum. No gas will permit thermal exchange and convection process cannot take place. As it has been said, the emitting power through radiation is proportional to the fourth power of the temperature. As in our studies, the temperature ranges from 0.27 K to 5 K, radiation processes can be neglected.

1.3 Phonons

1.3.1 Definition and dispersion relation

In a crystal, atoms are in an equilibrium position in a periodic structure, determined by the interactions. This position can be given by a Lennard-Jones potential for instance. However the atoms are not totally fixed at the equilibrium position. They vibrate around this position. Assuming that the vibrations are small, the position of an atom will be given by $r(R) = R + u(R)$; where R is the equilibrium position and $u(R)$ its deviation. Each atom pair adds a potential energy to the crystal, noted ϕ (with the assumption that just the first neighbor is taken into account). The total potential energy for a crystal is given by [1, 2, 3] :

$$U = \frac{1}{2} \sum_{R,R'} \phi(R - R' + u(R) - u(R')) \quad (1.1)$$

By using the Taylor theorem U may be approximated. It leads to : $U = U^{eq} + U^{harm}$. U^{eq} is the potential energy of equilibrium. It is a constant and determines the zero level of the internal energy of the crystal. U^{harm} on the other hand describes the energy stored by the atom vibrations. This term is the first order of the Taylor approximation. That is the reason why it is called the harmonic approximation.

$$U^{harm} = \frac{1}{2} \sum_{R,R'} \sum_{\mu,\nu} u_{\mu}(R) D_{\mu,\nu}(R - R') u_{\nu}(R') \quad (1.2)$$

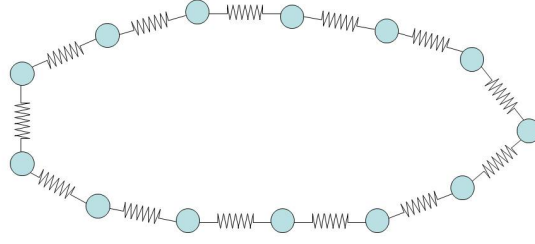


Figure 1.3: Schematic representation of an atom chain with Born-von Karman boundary conditions.

$D_{\mu,\nu}(R - R')$ is a matrix which characterises the system; μ and ν are the coordinates of the system.

Using the classical equation of motion, it leads to the displacement :

$$u(\mathbf{r}, t) = \sum e^{i(\mathbf{k}\cdot\mathbf{r} - \omega t)} \quad (1.3)$$

It is like a plane wave having a wave vector \mathbf{k} and a frequency ω . Furthermore, it reminds the wave function of a free particle in quantum physics. Landau in 1940, formally described this displacement as a quasiparticle with momentum $\mathbf{p} = \hbar\mathbf{k}$ and energy $E = \hbar\omega$. As the photon is the quantum of vibrations for the electromagnetic field, these new quasiparticles called phonons are the quanta of vibrations for a solid.

Another analogy for the atoms in a crystal can be done using an oscillator set. In this case, the energy allowed for an oscillator at the frequency ω is $(n + 1/2)\hbar\omega$, with $n = 0, 1, 2, \dots$. It is the same as the description used in the figure 1.2. The atoms have a mass m and are linked with strings of stiffness K . Equation 1.2 can be written as for a monoatomic one dimension chain of N atoms :

$$U^{harm} = \frac{1}{2}K \sum [u(na) - u((n+1)a)]^2 \quad (1.4)$$

Where a is the period of the lattice. With the assumption of Born-von Karman periodic boundary conditions (see figure 1.3), the displacement becomes $u(na, t) \propto \exp[ikna - i\omega t]$. One can notice when k changes of $2\pi/a$ the displacement remains unchanged (the range in phase space where $k < \pi/a$ is known as the first Brillouin zone). Furthermore the boundary condition requires $e^{ikNa} = 1$. This leads to :

$$k = \frac{2\pi n}{aN} \quad (1.5)$$

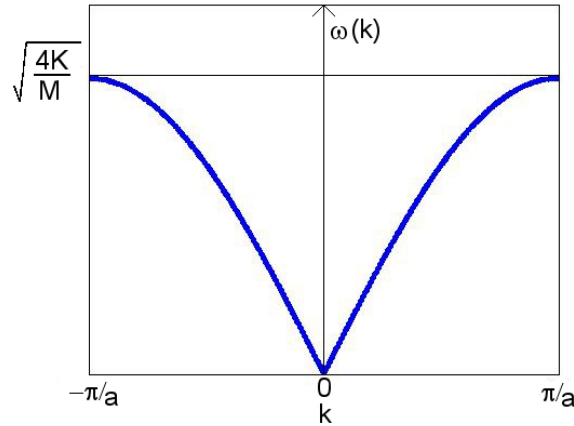


Figure 1.4: Dispersion curve for a one dimension monoatomic chain of atom with Born-von Karman periodic boundary conditions.

One can then write the equations of motion :

$$M\ddot{u}(na) = -\frac{dU^{harm}}{du(na)} - M\omega^2 e^{ii(kna-\omega t)} = -2K(1 - \cos(ka))e^{i(kna-\omega t)} \quad (1.6)$$

ω and k are thus linked by :

$$\omega(k) = \sqrt{\frac{2K(1 - \cos ka)}{M}} = 2\sqrt{\frac{K}{M}} \sin|ka/2| \quad (1.7)$$

This is the dispersion relation for a one dimension monoatomic chain of atoms with Born-von Karman periodic limit. It has been plotted on figure 1.3.1. It is interesting to notice that the group velocity is given by : $v_s = \partial\omega/\partial k$. For $k \rightarrow 0$ the dispersion relation becomes linear. And for $k = \pm\pi/a$ the speed of sound becomes zero.

In the case of a diatomic chain of atoms, with two different interaction energies, the dispersion relation has another branch. This branch has a peculiarity : $\omega(k=0) \neq 0$, and is almost flat (see figure 1.3.1). The phonons of this branch have a higher frequency, and interact mostly with photons. Therefore the higher branch is referred to as optical. The lower branch is called acoustic, because it is responsible of the transport of sound. As the speed of sound is equal to the derivative of ω , optical phonons will not contribute to heat transport. Also, at low temperature, the optical branches are not populated. Hence, in our case, only acoustic phonons will be investigated. These acoustic modes are also called propagative modes because they carry energy.

One can write the general case for a three dimensional monoatomic crystal. The typical sample in our study is a nanowire. Our nanowires are doubly clamped beams which cross section

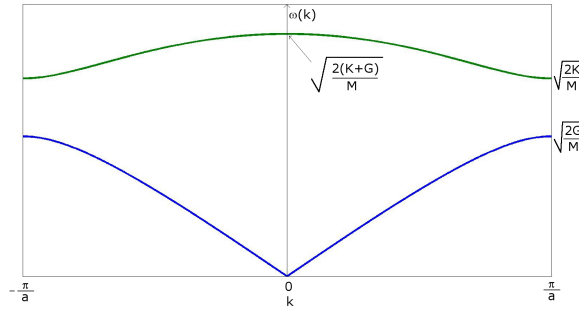


Figure 1.5: Dispersion curve for a one dimensional diatomic chain of atoms with Born-von Karman periodic boundary conditions.

is around $100 \text{ nm} \times 100 \text{ nm}$. Thus there is still about 200×200 atoms in one cross section. A nanowire cannot be considered as a one dimensional chain, but as a three dimensional medium with confinement, just like a classical beam (this dimension aspect will be discussed in the section 1.3.2). Then 3 different types of acoustic waves will propagate in a nanowire : one longitudinal and two transverses.

In a three-dimensional crystal, such as Si, the dispersion relation will depend on many factors, such as the propagative direction, the interaction with the neighbors, the lattice parameters,... However for all acoustic modes, the dispersion relation can always be considered as linear for small wave vectors. Thus the relation : $\omega_i = v_i \cdot k_i$, (where i stands for the mode, and v is the group velocity) will always be valid in our studies.

When the wire is small enough to be considered as one dimensional (this will be discussed in section 1.3.2), a flexural mode will appear. This mode is also an acoustic mode, and can be considered as linear at small wave vectors.

The wave vector $\mathbf{k} = 2\pi n/aN$ is quantized, so will be ω . The energy of the mode is $(n + 1/2)\hbar\omega$. The quantum number n is defined as the number of phonons of wave vector \mathbf{k} and at the frequency ω . The thermal energy is the sum of all these phonons (the s subscript is for the different modes):

$$E = \sum_{\mathbf{k},s} \left(n_{\mathbf{k},s} + \frac{1}{2} \right) \hbar\omega_s(\mathbf{k}) \quad (1.8)$$

1.3.2 The two characteristic lengths for phonon transport

As phonon transport is concerned, two lengths are important : the mean free path and the phonon wavelength.

Physically, the phonon mean free path is the distance a phonon will travel before being

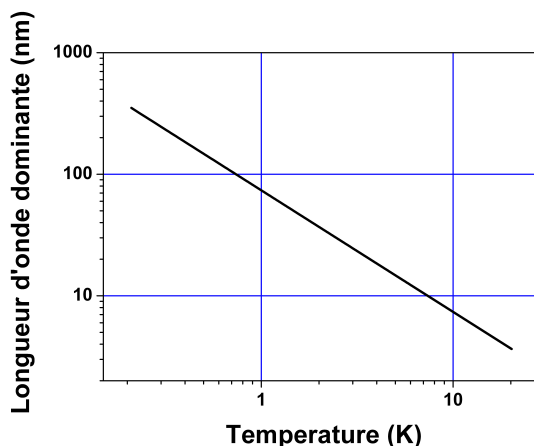


Figure 1.6: The dominant wavelength of phonons in Si against the temperature, in a log-log scale.

inelastically scattered. As a phonon is defined by its wavelength, a modification in its energy leads to a new definition for the phonon. Inelastic collisions may be of different types (phonon-phonon, phonon-electron, phonon-defect,...). At low temperature in dielectrics materials, only the crystalline defects will affect phonon transport, which means that phonon can travel centimeters into a single crystal. On the contrary, in a nanowire, the effect of surface becomes predominant. This has been studied especially by Casimir [4] and Ziman [5, 3], and will be presented in section 1.4.3 and 1.4.4.

The second significant length scale is the wavelength. To calculate it, the mostly used formalism is called the dominant wavelength approximation. The principle is similar to blackbody emission of photons, with an energy density following Planck's law. At the temperature T_0 , phonons will be emitted with frequencies determined by a Planck's law. Thus the majority of the phonons will have an energy approximatively equals to the maximum of the Planck's law : $h\nu_{max} = 2.82k_B T_0$; where h and k_B are the Planck and Boltzmann constant respectively. In the dominant wavelength approximation, it is assumed that the heat is carried predominantly by phonons of the same frequency. The model made by Debye considers a maximum frequency for the phonons. It changes the value of 2.82 by 3.83. Measurements of the phonons that contribute the most to heat storage was made by R. O. Pohl and T. Klistner [6]. These measurements show that $h\nu_{max} = 4.25k_B T_0$. The dominant wavelength ($\lambda = v_s$; v_s is the speed of sound) is then given by :

$$\lambda_{Dom} = \frac{h v_s}{4.25 k_B T_0} \quad (1.9)$$

To know if a wire can be considered as one dimensional or three dimensional, one must compare the cross section of the wire with the phonon dominant wavelength. If the cross

section is large as compared to the phonon wavelength, then the wire is three dimensional. On the contrary, if the cross section is small compared to the wavelength, the wire is considered as one dimensional. The samples studied in this thesis have a cross section around $100 \text{ nm} \times 100 \text{ nm}$. Thus it is the intermediate case where the cross section is of the same order of magnitude as the wavelength. The measurements of thermal properties will then depend on the dimension of the system. Therefore these measurements will also show if the wire can be considered as one or three dimensional.

1.4 Phonon transport at low dimensions and low temperatures

1.4.1 Introduction

A phonon, as defined in the first section, is a plane wave. The transport of such a wave has been understood for a long time. However, it can also be defined as a quasi-particle. The same rules as for electrons can thus be applied. Two differences are that phonons are bosons and electrically neutral. However the biggest difference between electronic transport and heat transport is within material properties. In terms of electronic transport, there exist almost perfect insulator materials, and on the contrary materials with almost no electrical resistance. This is not the case with phonons. Electronic transport can be measured with the electrical conductivity, whereas the heat transport is given by the thermal conductivity. For instance the electrical conductivity of silver is 6.10^5 S.m^{-1} , whereas it is around $10^{-17} \text{ S.m}^{-1}$ for glasses. Conversely, the thermal conductivity of silver (which is one of the best thermal conductors) is $4.10^2 \text{ W.m}^{-1}.\text{K}^{-1}$, and in glass wool (a material often used in thermal insulation), the thermal conductivity is $4.10^{-2} \text{ W.m}^{-1}.\text{K}^{-1}$. Because of this, phonons are quite difficult to guide. To improve phonon control, one can use nanofabrication. When the size of a nanosystem is on the same order of magnitude as the characteristic lengths of phonons, phonon transport will be modified. This is the new field of nanophononics.

In this section basic notions regarding thermal properties will be presented. Then the impact of nanostructuration will be investigated, with models taking into account both low dimensions and low temperatures. Finally, some special nanostructures which have effect on phonon transport will be discussed.

1.4.2 Heat Capacity, and thermal conductance

Four notions will be presented that are necessary to understand thermal properties in matter : heat capacity and specific heat, thermal conductance and thermal conductivity.

Heat capacity (C) represents the capacity of a body to change its temperature with a given amount of heat. It is defined by the ratio of heat energy (Q) transferred to a body to the resulting change of temperature : $C = \Delta Q / \Delta T$. It is an extensive property. When expressing the same phenomenon as an intensive property (depending just on bulk material), the heat

1.4. Phonon transport at low dimensions and low temperatures

capacity is divided by the amount of substance and is then called specific heat (c). As a general statement, one has to keep in mind that heat capacity is related to heat storage.

Thermal conductance (K) and thermal conductivity (κ) are characteristic of how a material conducts heat. If a body is heated at one side, temperature will tend to homogenize in all the body. Thermal conductance links the dissipated energy to the temperature gradient created, by $K = P/\Delta T$. Thermal conductivity is the related intensive property while conductance is its extensive version.

Heat capacity and specific heat

Heat capacity is defined by $C_v = \partial U/\partial T$, where U is the internal energy. As phonons are bosons, they follow Bose-Einstein statistics [1, 2] :

$$n_{\mathbf{k},s} = \frac{1}{\exp(\hbar\omega/k_B T) - 1} \quad (1.10)$$

Injecting equation 1.10 in equation 1.8 leads to :

$$U = \sum_{\mathbf{k},s} \frac{1}{2} \hbar\omega(\mathbf{k}) + \frac{\hbar\omega(\mathbf{k})}{\exp\left(\frac{\hbar\omega(\mathbf{k})}{k_B T}\right) - 1} \quad (1.11)$$

The first term corresponds to the zero level of the energy. It is a constant and can be neglected. Heat capacity is then :

$$C_v = \frac{1}{V} \sum_{\mathbf{k},s} \frac{\partial}{\partial T} \frac{\hbar\omega_s(\mathbf{k})}{e^{\hbar\omega_s(\mathbf{k})/k_B T} - 1} \quad (1.12)$$

To give an analytical expression of this equation, one can make some approximations. Two models are often used because of their accuracy with experimental data. The Einstein model, which considers that all phonons have the same frequency; and the Debye model, which considers that the dispersion relation is linear ($\omega = v_s k$) until a limit wave vector k_D . The Debye model usually provides a better accuracy of experimental results, especially at low temperature. k_D is defined by the density n , with $n = k_D^3/6\pi^2$. One can then define a Debye frequency : $\omega_D = k_D v_s$, and a Debye temperature : $\Theta_D = \hbar\omega_D/k_B$. In this model, heat capacity becomes :

$$C_v = 9nk_B \left(\frac{T}{\Theta_D}\right)^3 \int_0^{\Theta_D/T} \frac{x^4 e^x dx}{(e^x - 1)^2} \xrightarrow{\text{at low } T} 234nk_B \left(\frac{T}{\Theta_D}\right)^3 \quad (1.13)$$

The last term of this equation is for a three dimensional material. It is interesting to notice that C_v has a cubic dependence with the temperature. In this Debye model, heat capacity is actually proportional to T^d , where d is the dimension of the system studied.

Thermal conductance and thermal conductivity

Thermal energy can be stored by phonons in matter. Acoustic phonons have a non-zero group velocity. They are propagative and so, transport heat along a body. If there is a temperature gradient along the x axis, a thermal current $j(x)$ will be created. This thermal current can be written as :

$$j(x) = \frac{1}{V} \sum_k v_x E(k) f(\mathbf{k}, \mathbf{p}) \quad (1.14)$$

where V is the volume of the system, v_x the phonon velocity, E the energy of the phonons, and f the distribution function in the (\mathbf{r}, \mathbf{p}) space. Determining this distribution function is the main problem. To do so, one can use Boltzmann equation, which describes phonons as a classical particles gas :

$$\frac{\partial f}{\partial t} + \frac{d\mathbf{r}}{dt} \cdot \Delta f + \frac{d\mathbf{p}}{dt} \cdot \Delta f = \left(\frac{\partial f}{\partial t} \right)_{coll} \quad (1.15)$$

The term on the right of equation 1.15 is the collision term. Within the relaxation time approximation one can write :

$$\left(\frac{\partial f}{\partial t} \right)_{coll} = -\frac{f - f_0}{\tau} \quad (1.16)$$

where f_0 is the equilibrium distribution function (Bose-Einstein distribution for the phonons), and τ a characteristic diffusion time.

Using the hypothesis of stationarity ($\partial f / \partial t = 0$) and without external forces ($d\mathbf{p} / dt = 0$), one can use equation 1.16 to solve equation 1.15. The distribution function is then :

$$f(r, k) = f_0 - \tau \frac{df}{dT} \mathbf{v} \cdot \Delta T \quad (1.17)$$

This solution is quite interesting in itself, as a temperature gradient will create a deviation from the equilibrium function for the phonons, along a specific space direction. Heat transfer will thus be created. Using this solution with equation 1.14 leads to :

$$j = \sum_s \int_0^{\omega_{max}} d\omega \int_0^{2\pi} d\phi \int_0^\pi d\theta v_x \hbar \omega (f_0 - \tau \frac{df}{dT} \mathbf{v} \cdot \Delta T) \frac{D(\omega)}{4\pi} \quad (1.18)$$

This equation has been obtained by changing the sum over k in equation 1.14 by an integral over frequency. $D(\omega) = dk / d\omega$ is the phononic density of states. If the temperature gradient is

1.4. Phonon transport at low dimensions and low temperatures

just along one direction, then $\Delta T = dT/dx$, and one can make a comparison with Fourier's law :

$$j = \kappa \left(-\frac{\partial T}{\partial x} \right) \quad (1.19)$$

where the coefficient of proportionality κ is defined as the thermal conductivity. With equations 1.19, 1.18, and 1.12, one can find a direct relation between κ and C_v :

$$\kappa = \frac{1}{3} \rho C_v v_s \Lambda \quad (1.20)$$

where $\Lambda = v_s \tau$ is the mean free path, v_s is the speed of sound, and τ is the collision rate.

This kinetic relation is valid at low temperature, when collision processes conserve total phonon momentum.

Thermal conductance (K) and thermal conductivity (κ) are related via the following equation :

$$\kappa = K \frac{L}{S} \quad (1.21)$$

where L is the length of the sample and S the section.

As it has been said, thermal conductivity is an intensive property and conductance an extensive one. In the equation 1.20, one can notice the dependence with the mean free path of the conductivity.

At low temperature, in a nanowire for instance, the mean free path depends on the geometry of the system studied. Therefore thermal conductivity also depends on the system studied. It is then more appropriate to describe heat transport at the nanoscale with thermal conductance. Thus when two samples do not have the same size, a consistent normalization is needed. This normalization must take into account the size difference, which includes the mean free path. A model made by Casimir [4] will help us to fulfill this condition.

1.4.3 The Casimir model

In a previous section, the mean free path (MFP) has been defined as the distance between two inelastic collisions. The probability of a collision decreases with respect to the temperature. Therefore the mean free path increases. When it becomes larger than the dimensions of the system, the most probable collision will be with the surface. No other collision processes can happen in a single crystal nanowire at low temperature. Casimir, in 1938, postulates that a surface is diffusive [4]. In diffusive surfaces, incident phonons are systematically absorbed and

re-emitted following Planck's law. This corresponds to an infinitely rough surface (the surface is rough at all length scales). The surfaces of the nanowires act as black bodies for phonons. In a nanowire, the MFP is then limited by the cross section. With the kinetic equation (equation 1.20) Berman *et al.* demonstrate that it leads for the thermal conductance [5]:

$$K_{Cas} = 3.2 \times 10^3 \left(\frac{2\pi^2 k_B^4}{5\hbar^3 v_s^3} \right)^{(2/3)} \frac{e \times w \Lambda_{Cas}}{L} T^3 \quad (1.22)$$

where $\Lambda_{Cas} = 1.12\sqrt{e \times w}$ is the phonon Casimir mean free path for a rectangular shape phonon conductor, e refers to the thickness and w to the width of the nanowire, L being its length and v_s the sound velocity. In this model it is assumed that the mean free path does not depend on temperature.

In this quite simple model, the thermal conductance presents a cubic dependence with temperature. This dependence is in good agreement with experiments [7, 8, 9]. The limit for this model happens when the surface cannot be considered as diffusive. In other words, some phonons are specularly reflected on the surface due to their large wavelength.

1.4.4 The Ziman model

As shown in the previous section, the limit of the Casimir model occurs when one cannot consider the surface as diffusive for every phonon wavelength. This limit will be determined by the object which is reflected by the surface, the phonon in our case.

To illustrate this process, an analogy with a ball bouncing to a wall can be made. If the roughness of the wall is large compared to the diameter of the ball, the outbound may go in every possible direction. On the other hand if the diameter is larger than the roughness, then the ball will bounce according to Snell's law. It is a specular reflection. For the phonons, the diameter of the ball will be its wavelength. If the wavelength is small compared to the mean value of the roughness, then the surface will be diffusive. On the other hand, if the wavelength is larger than the mean value of the roughness, then a specular reflection happens for the phonon. This will contribute to increase the phonon MFP.

To describe this effect, Ziman and coworkers [5, 3] consider a phonon coming normally to the surface. This phonon has a probability p to have a specular reflection. p will depend on both the roughness of the surface and on the wavelength of the phonon. Thus, one may write $p(\lambda, \eta)$; η being the root mean square of deviation of the height of the surface. One may call η the asperity parameter, qualifying the roughness.

The calculation of $p(\lambda, \eta)$ can be done using rather simple arguments. It is the same as a wave reflecting on an irregular surface. A reflected wave (whose wavelength is λ) will have a phase shift ϕ by amounts depending on the height $y(x)$ of the surface at the position x , measured

1.4. Phonon transport at low dimensions and low temperatures

above or below some reference level parallel to the surface. ϕ is given by :

$$\phi = 4\pi y(x) / \lambda \quad (1.23)$$

The statistic of this phase shift, especially its variance, is what is interesting. The variance is defined by :

$$\overline{\phi^2} = \frac{16\pi^2}{\lambda^2} \eta^2 \quad (1.24)$$

The exact solution of the reflected wave is not interesting in our case. The only waves we are interested in are those running back along the path of the incident one. The probability of having such reflected waves gives the probability of having a specular reflection :

$$p(\lambda, \eta) = \exp(-\pi \overline{\phi^2}) = \exp\left(-\frac{16\pi^3 \eta^2}{\lambda^2}\right) \quad (1.25)$$

However the description of a single parameter η is too restrictive to apply to real surfaces. A more realistic way is to take into account a distribution probability $P(\eta)$ for η itself. It is now possible to define an average value of $p(\lambda)$:

$$\overline{p(\lambda)} = \int_0^\infty P(\eta) \exp\left(-\frac{16\pi^3 \eta^2}{\lambda^2}\right) d\eta \sim \int_0^{\lambda/4\pi} P(\eta) d\eta \quad (1.26)$$

This means that one of the priorities will be to determine the distribution of asperities in our sample. It has already been done in our group [10]. I will show the result in the chapter 2.

In the rest of the thesis I will only speak about $\overline{p(\lambda)}$, even when it will be written $p(\lambda)$ or p .

1.4.5 The universal quantum of thermal conductance

In 1988, two groups independently demonstrated the quantization of electron transport through a single ballistic channel [11, 12]. A ballistic channel is when electron's movement is impeded only negligibly by scattering. The conductance (G) changes in quantized steps of $g_0 = e^2/h$ when channels are open, through a gate voltage (see figure 1.7). To achieve that, one can be in the adequate conditions defined by the sample. It was a real technological challenge, and was made possible by using both cryogenics and microelectronic techniques.

One-dimensional phonon transport should also be quantized, as shown in 1983 by Pendry and coworkers [13]. It has then be formally demonstrated by Rego and Kirczenow in 1998 when the heat carrier are confined within dimensions that are small compared to their characteristic

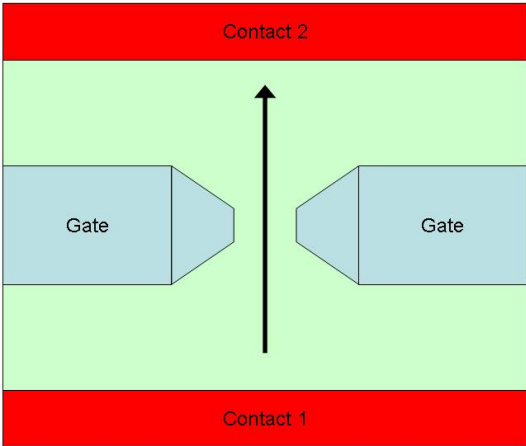


Figure 1.7: Schematic representation of a quantum point contact. When a voltage is applied to the gate, one can control the conductance from contact 1 to contact 2. In appropriate conditions, defined by the sample, the electrical conductance is found to vary in discrete steps of $g_0 = e^2/h$ with respect to the applied gate voltage.

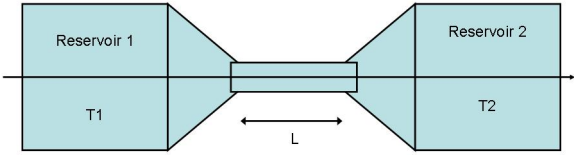


Figure 1.8: Schematic representation of a nanowire connected to two thermal reservoirs. If $T_1 > T_2$, then heat will flow along the x axis from reservoir 1 to 2.

1.4. Phonon transport at low dimensions and low temperatures

wavelengths [14]. They started with the Landauer energy flux for a nanowire connected to a hot and a cold reservoir (see figure 1.8) :

$$\dot{Q} = \sum_{\alpha} \int_0^{\infty} \frac{dk}{2\pi} \hbar \omega_{\alpha}(k) v_{\alpha}(k) [f_{hot} - f_{cold}] \xi_{\alpha}(k) \quad (1.27)$$

where α is the mode index, $\omega_{\alpha}(k)$ is the dispersion relation for the phonon with wave vector k , $v_{\alpha}(k)$ is the group velocity, $f_i(\omega) = 1/(e^{\hbar\omega/k_B T_i} - 1)$ represents the thermal distribution of phonons in the reservoirs, and $\xi_{\alpha}(k)$ is the transmission probability through the wire.

Two assumptions can be made. The cross sectional area of the wire is small enough (hundreds of nm²) to produce finite gaps in the dispersion relation; And the contact between the thermal reservoirs and the ballistic quantum wire is perfectly adiabatic ($\xi_{\alpha}(k) = 1$). The thermal conductance K is defined by $K = \dot{Q}/\Delta T$, where $\Delta T = T_{hot} - T_{cold}$ is the temperature gradient between the two reservoirs. One can then introduce K in equation 1.4.5 and solve it. For the massless mode (the one which $\omega(k=0) = 0$, i.e. the acoustic branches), it gives the remarkable result :

$$K = \frac{k_B^2 \pi^2}{3h} \left(\frac{T_R + T_L}{2} \right) N_{\alpha} \quad (1.28)$$

Where N_{α} is the number of massless modes. As it has been seen, 4 acoustic branches exist in a nanowire. In the limit $\Delta T \rightarrow 0$ this result leads to :

$$K_Q = \frac{k_B^2 \pi^2}{3h} 4T \quad (1.29)$$

This conductance is quantized for each mode. Furthermore, in this formula, no condition on the material, nor on the sample, nor on the heat carriers, is required. This means that this formula is also valid for the electrons (it can be found with the Wiedemann-Franz law, see section 1.6, and has been measured by Chiatti *et al.* [15]) and photons (it has been formally measured by Meschke, Guichard and Pekola [16]). The universal quantum conductance by the phonons has been measured in only one experiment by Schwab *et al.* [17, 18]. Unfortunately this measurement has never been reproduced. A more precise description of this experiment will be presented on section 2.2.4.

To conclude, a universal quantum of thermal conductance has been shown theoretically [13, 14] and measured [15, 16, 18]. The conditions required to have this conductance are : ballistic heat carrier in a one dimensional wire and a transmission coefficient between the wire and the reservoirs close to one. As the dominant phonon wavelength is inversely proportional to the temperature, in a nanowire, one may see the transition when the transport can be considered as one dimensional (K_Q) or three dimensional (K_{cas}). This has been plotted in figure 1.9. The transmission coefficient will be discussed in the next section.

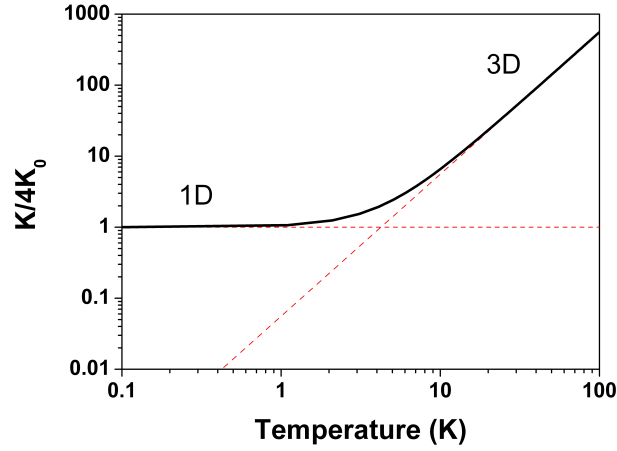


Figure 1.9: Theoretical thermal conductance normalized by four times the quantum of thermal conductance with respect to the temperature. One can see the transition between a one-dimensional behavior at low temperature and a three-dimensional behavior at high temperature.

1.4.6 The junction with the thermal bath

The difference in the density of states between a one-dimensional and a three-dimensional medium leads to boundary reflection of propagative waves. A nanowire is connected to two thermal reservoirs. A thermal resistance (or thermal conductance) appears at the interface. If this conductance has the same order of magnitude or lower than the conductance of the wire then it must be taken into account in our measurements. Therefore one must know the value of the contact conductance because it may impact the measurements presented in this thesis.

One of the first and complete theoretical works has been made by Cross and Lifschitz [19]. Their starting point is the Landauer energy flux equation. They are studying it in the approximation that the temperature gradient created is small compared to the temperature of the sample. This leads, as in the previous section, to a conductance determined by the transmission coefficient. To calculate the transmission coefficient, they use two models. The first one gives the transmission for all modes and all wave vector. It uses a scalar approach. A scalar field, the displacement for instance, is calculated with a basic wave equation ($\partial^2 \phi / \partial t^2 = v^2 \nabla^2 \phi$). The problem lies in the system chosen for the study and especially the surface of this system. Cross and Lifschitz use the geometry shown in figure 1.10. On the edges, they used a stress free condition. Then, they solve for each mode the propagative wave both inside the nanowire and the reservoir. To calculate the total transmission coefficient, one must integrate over all the modes. Their work is based on previous results by Angelscu *et al.* [20].

So Cross and Lifschitz have performed a full calculation of the transmission coefficient for the scalar case. Then they present another calculation, where the dispersion relation and the

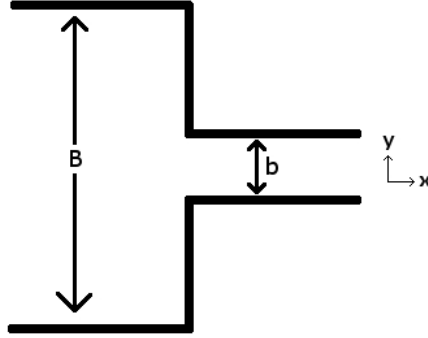


Figure 1.10: Geometry for the calculation of the transmission coefficient. Stress-free boundary conditions are assumed on the edges.

displacement are given by the relation between stress and strain tensors. The full development can be found in any standard text on elasticity, for example Landau and Lifshitz [21]. The dispersion relation can be calculated numerically. To have an analytical result, one must use a Taylor expansion. Then when the wave vector k is small in comparison with the inverse of the width of the nanowire ($bk, Bk \ll 1$; b and B are the dimensions shown in figure 1.10, k is the wave vector), one can find analytical results for both dispersion relation and transmission coefficient. Both models give in this approximation the same results. This leads to a transmission coefficient :

- $T(k \rightarrow 0) = 4bk$ for the longitudinal mode;
- $T(k \rightarrow 0) = 0.6bk$ for the torsional mode;
- $T(k \rightarrow 0) = 2.3bk$ for the flex bend mode;
- And $T(k \rightarrow 0) = (bk)^3/3$ for the in-plane bend mode.

This work was performed for a rectangular nanowire connected to a two dimensional thin plate.

The same work has been made by Chang and Geller [22] in the case of a cylindrical nanowire connected to a semi infinite three dimensional solid. The new relations to calculate the transmission coefficient in this case are :

- $T(k) = 1.91(bk)^2$ for the longitudinal mode;
- $T(k) = 1/6 * (bk)^4$ for the torsional mode;
- And $T(k) = 0.268(bk)^5$ for the two flexural modes.

Then the transport will be dominated by longitudinal phonons at low temperature (i.e. low energy phonons). Prasher and Majumdar have calculated the thermal conductance with the transmission for the longitudinal case [23] :

$$K_c = \frac{2\pi^3}{15} \frac{k_B^4}{\hbar^3} \frac{0.923 b^2}{v_s^2} T^3 \quad (1.30)$$

where b is the radius of the nanowire.

This result will be of importance as it gives a numerical value for the contact conductance. It may be compared to our experimental results. The wire conductance and the contact conductance are in series. If the theoretical value of the contact conductance is higher than our measured conductance, it will be a sign that the contact conductance plays no role in our measurements. This will be further explained in detail in chapter 3.

Another interesting study was made by Chalopin *et al.* [24]. The nanowires studied have square edges from 1 nm to 10 nm, and the temperature ranges from 1 K to 100 K. They use the diffusive limit approximation : $t_{wire \rightarrow bath} = C_{bath}v_{bath}/(C_{bath}v_{bath} + C_{wire}v_{wire})$; C_{bath}, C_{wire} are the heat capacity of the bath and the wire respectively, v the group velocities. The product $C.v$ is calculated from the temperature derivatives of the heat fluxes. To do so, one needs to know the total dispersion relation in both the nanowire and the thermal bath, and then determines the group velocities and the eigenfrequencies. The contact conductance is then $K_C = t_{wire}C_{wire}v_{wire}$. They compare this conductance to the intrinsic conductance of the nanowires, which is estimated to be four times the universal quantum of thermal conductance. They found the thermal contact conductance to be smaller than the intrinsic conductance of the nanowire. This means that contact conductance dominates the heat exchange in the case of these nanowires. This work however considers the wire as a perfect one-dimensional structure. It should not be the case in our works, since the section of our nanowires are bigger than the dominant wavelength.

Other interesting works were made with other methods. For instance, W.-X Li, T. Liu, and C. Liu [25] used a scattering matrix method to calculate transmission coefficient through an abrupt junction. This work was made from wires of dimension 15×15 nm, 18×18 nm and 20×20 nm. They are joined to a cavity of dimension 20×20 nm. This is quite different than the junction between a nanowire and bulk material. Also, these authors made their study for temperature between 0.1 K and 1 K. They found that the transmission coefficient is strongly impacted by the junction. The thermal conductance does not follow the same behavior for the smaller wire. Green function was also used in a work of J. Li *et al.* [25]. However they investigate an atomic wire, which is very different than our samples.

Nevertheless all these works shows that transmission coefficient can be affected by an abrupt junction between the nanowire and the thermal bath.

To decrease the influence of the contact, one can adapt the shape of the interface. Rego and Kirczenow [14] demonstrated that a nanowire, having a catenoidal contact with the reservoir, should have a transmission coefficient close to one within a certain range of temperature. Their model is only valid for longitudinal plane waves. They calculated the equation of motion for a wire which cross section varies as a \cosh^2 . Tanaka *et al.* implemented this work including all the acoustic branches and the two lowest optical modes [26]. They found similar results as Rego's group. The transmission coefficient should be close to one, leading to a plateau at four times the universal quantum of thermal conductance. This is quite exciting because

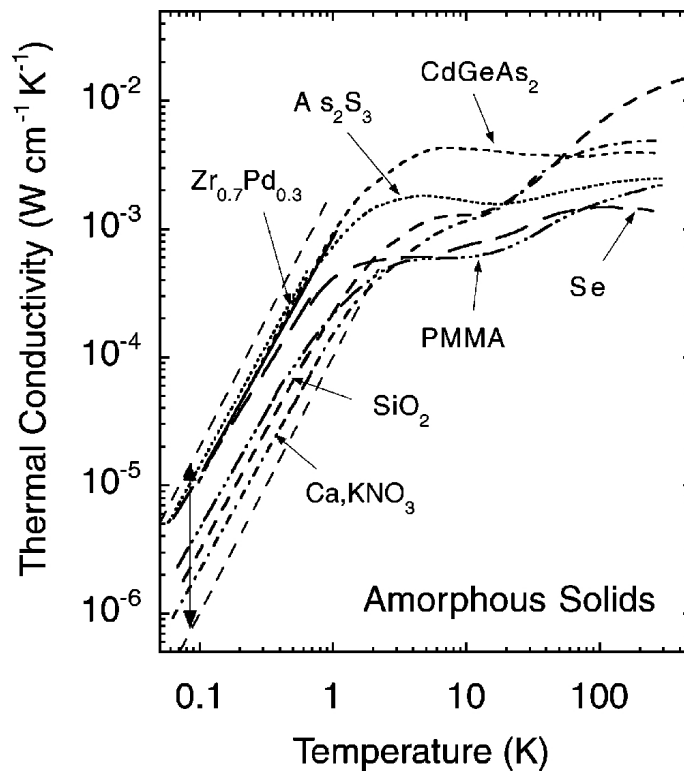


Figure 1.11: Thermal conductivity of several amorphous solids. This figure is taken from the review by Pohl *et al.* [27]. The conductivities of all glasses measured to date below 1 K lie in the range spanned by the two dashed straight lines shown here, separated by the double arrow.

such a nanowire is realizable with our fabrication process. However the temperature range of the plateau should be between 10 mK and 100 mK, just under the minimum temperature available with our refrigerator. In chapter 3 measurements made on this kind of sample will be presented.

1.5 Phonon inside amorphous materials

Until now, phonons have been described in the case of crystalline materials. In such materials, it is quite relevant to describe the atoms as masses linked by strings. However in amorphous materials this description is not appropriate. Furthermore, in these materials, the chemical composition and the physical structure at the microscopic level could hardly be more diverse. And yet, at temperatures below 1 K, the behavior of almost all amorphous materials is qualitatively similar [27]. These common features include a nearly linear specific heat and a thermal conductivity roughly proportional to T^2 (see fig. 1.11). As thermal conductivity is concerned, not only is this universality qualitative but also quantitative. In one order of magnitude, nearly all measured thermal conductivities can be found. Moreover, around 1-10

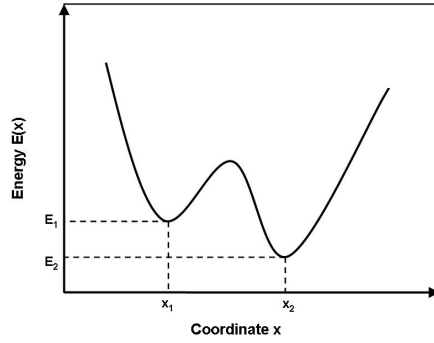


Figure 1.12: Energy E of the system as a function of a generalized coordinate x , measuring position along a line connecting two nearby local minima of E .

K, there is always a plateau, the thermal conductivity being approximately constant over about a decade in temperature. At higher temperatures, the thermal conductivity becomes roughly proportional to the temperature. In spite of much theoretical effort, this universality remains poorly understood.

The predominant explanation up to date to understand the physic of amorphous materials at low temperature was made almost simultaneously by Phillips [28] and Anderson, Halperin and Varma [29, 30]. The main hypothesis of this model is as follow : in any glass system there should be a certain number of atoms (or group of atoms) which can sit more or less equally in two equilibrium positions (see figure 1.12). Then, these authors investigate the case in which only tunneling allows transitions between the two states. In this case, these authors found that the specific heat is given by :

$$C = \frac{\pi^2}{6} k_B^2 T n(0) \quad (1.31)$$

where $n(0)$ is the density of tunneling states (number of tunneling states per unit volume) for the energy barrier close to zero. Determining the exact value of $n(0)$ is not possible. However one can find it by a fit of experimental data, and see if it is consistent with available information. For instance, Anderson *et al.* [29] found for fused silica : $n(0) = 0.04$ states per eV, per SiO_2 group. The total number of group of atoms with energy barrier close to zero is then estimated as $1/250$ of the total number of SiO_2 group. They claim that it seems to be a reasonable number.

The thermal conductivity can also be calculated through the kinetic relation with heat capacity (equation 1.20). The only problem is for defining the mean free path in this expression. As the mean free path is given by the collision rate, it will not be the same as in a crystalline material. Beside, the phonons which contribute to the thermal transport may not be the same that the

ones which contribute to the specific heat. The idea of Anderson *et al.* is to consider that the phonons which have a resonant tunneling through the two energy wells are involved in the thermal transport. Then the mean free path can be written as :

$$\Lambda = \frac{1}{\sigma \nu} \quad (1.32)$$

where σ is the scattering cross section and ν the number of resonant scatterers per unit volume.

Determining σ can be done using the relation $\sigma = 4\pi v_s^2 / \omega^2$ with the frequency ω coinciding with the splitting energy of the two level system. However the density of resonant scatterers is not easy. To estimate it, one must introduce unknown parameters describing the two level system. Anderson and coworkers finally found for the mean free path :

$$\Lambda = \frac{1}{\pi^2 v_s^2} \frac{\omega_0^3}{n(0) D} \omega^{-1} \quad (1.33)$$

where $\hbar\omega_0$ is an energy of the same order of magnitude as the zero-point energy and D is a parameter depending on the material.

The fact that the mean free path is inversely proportional to the frequency fully agrees with experimental studies [31]. This is quite intuitive. In other words, the phonons which contribute the most to the heat transport are the phonons with the highest wavelength ($\omega = \nu/\lambda$). However, one can argue that the heat capacity was previously demonstrated to be linear with the temperature. With the kinetic relation (equ. 1.20), this would mean a proportionality between the MFP and the frequency. This is not true, because at temperatures around 1 K and higher, for most of the amorphous materials, the heat capacity is cubic dependent to the temperature. The heat capacity dependence with respect to the temperature is thus : $C = A.T + B.T^3$, where A and B are parameters, which depend of the materials studied [31, 32].

This model does not take into account the anomalous amorphous materials (the ones which do not exhibit the universality behavior). If the model were complete, one should have an explanation for these exceptions. The model could be adapted with the fact that the energy barrier is too high to have any tunneling state, for instance. This should come from the fact that the lattice is overconstrained. However it is not the case for the anomalous materials detected [27].

Leggett was also critical towards this model [33]. In their formulas, Anderson *et al.* use many assumptions concerning the two level system. But these assumptions are sometimes made rather to fit the experimental data, than with a proper physical argument. Leggett takes the example of the ultrasound velocity shift. The ultrasonic attenuation per unit wavelength can be expressed considering very general assumptions by a Kramer-Kronig relation to the

coefficient α of $\ln T$ in the ultrasound velocity shift $\Delta c/c$. In the two level system model, α is given by :

$$\alpha = \frac{\gamma_t^2 (dn/d\epsilon)}{\rho v_t^2} \quad (1.34)$$

where ρ is the mass density, v_t the speed of transverse sound, $dn/d\epsilon$ the density of states of the two level system per unit energy, and γ_t the two level system transverse phonon coupling constant.

These four parameters are completely independent inputs. However, all the four parameters fluctuate by less than a factor of ten in a significant number of materials, and the maximum fluctuation of α is a factor 1.8. Such a random coincidence make one feel that something is missing in the model. Leggett also developed a model using an analogy with the Ising model for a spin glass. However, this model does not give the proper order of magnitude for the thermal (and acoustic) properties.

To conclude, the physics of heat transport in amorphous materials is still far from being fully understood. The mean free path of the phonons is still a characteristic length which can give a useful piece of information on the underlying physics. Therefore, further studies of the mean free path may help to get a better understanding of the thermal properties of amorphous materials, especially at low temperature.

1.6 Thermal transport by electrons

Similar to the calculation of the phononic heat capacity, the electronic heat capacity can be calculated by $C_{e^-} = \partial U / \partial T$ [1]. The mainly used approximations are a free electron gas, with a Fermi level large compared to the electrons thermal energy. These approximations give the result that the specific heat of electrons is linearly dependent on the temperature :

$$C_{e^-} = \frac{\pi^2}{3} D(E_F) k_B^2 T \quad (1.35)$$

where $D(E_F)$ is the electrons density of state at the Fermi level. This linear dependence implies that in metallic materials, at low temperature, the electronic heat capacity is higher than the phononic one (which is cubic with respect to the temperature, cf. equation 1.13).

The kinetic description used to determine the phonon thermal conductivity does not take into account the behavior of the statistics of the carrier. For electrons, one can make the same calculation as for the phonons. It leads to the following expression for the thermal conductivity of electrons :

$$\kappa_{e^-} = \frac{1}{3} \rho C_{e^-} v_f l_{e^-} \quad (1.36)$$

where ρ is the mass density, v_f is the Fermi speed and l_e is the electronic mean free path. As the Fermi velocity is three orders of magnitude higher than the speed of sound, in metals the thermal transport will be dominated by the electrons. In semiconductor materials, and at low temperature, the electrons cannot move (the thermal energy is not high enough for electrons to cross the semiconductor gap). Therefore, the thermal transport will come from the phonons.

A final note can be made on the Wiedmann-Franz law, a relation linking the thermal (K) and electronic (G) conductance in metals :

$$\frac{G}{K} = \frac{\pi^2 k_B^2}{3e^2} T = L_0 T \quad (1.37)$$

where L_0 is the Lorentz number equal to $2.45 \cdot 10^{-8} \text{ W}\Omega\text{K}^{-2}$, and e is the elementary electronic charge equal to $1.602 \cdot 10^{-19} \text{ C}$.

This law has been experimentally verified [1]. It is understandable as electrons transport both heat and electricity. Moreover it is interesting to notice that by replacing the electronic conductance by the quantum of conductance $G_0 = 2e^2/h$ then the thermal conductance equals the quantum of thermal conductance, as defined in section 1.4.5.

1.7 Nanophononics

Electronics has enabled technological developments that have transformed many aspects of our lives. Phononics, however still need to be further developed. This can be explained by multiple reasons. Phonons are massless and chargeless, which make them difficult to control. Furthermore, no good heat conductor material, neither good heat insulator material are available. As heat flows in all materials, heat is difficult to control. Another reason which makes the development of phononics difficult is when two bodies are in contact. In this case a thermal resistance will appear. And typically this resistance is on the same order of magnitude than the intrinsic material thermal resistance.

In everyday life, however, signals encoded by heat prevail over those encoded by electricity. Manipulate and control temperature should result in energy savings improvements, and also more accurate electronic devices. Thermoelectricity, for instance, allows the direct conversion of temperature differences to electric voltage and vice-versa. Up to date, however no efficient devices can be used on a power plant scale. To improve the thermoelectric effect, one needs a material with a high electrical conductivity and a low thermal conductivity. So if one manages to block phonons in a sample, this will pave the way to exciting technological developments.

In the phononic field some experiments have already been made[34]. A thermal diode, in which the heat flux in one direction is lower than in the opposite direction, has already been made by Chang and coworkers in 2006 [35]. They saw a conductance up to 7% greater in one

direction than in the other. A proposed version of a thermal transistor has been made by Baowen Li and coworkers [36]. Just as the case of an electronic-transistor, it can either act as thermal switch, or as a modulator that adjusts the heat current continuously across a wide range. The realization of such a device may open a door to build phononic logic gates.

In our group, in 2010, a serpentine was introduced in a nanowire [37]. The comparison between such a nanowire and a straight one shows that phonon transport is affected. With this purely geometrical effect a reduction in the thermal conductance ranging between 20% and 40% has been measured. This kind of phonon blocking system could be used to thermally insulate suspended devices, such as nanoelectromechanical systems.

Another way to develop phononics comes through what has been done in photonics. The photonics field is also in development nowadays. More results than in phononics have already been achieved. The main reason is that in the photonics field a monochromatic laser is used, whereas in phononics, heat generates a broad distribution of phonons. For instance, photonic crystals, among those the dielectric (or Bragg) mirror is the most famous, are highly developed. The principle is that a periodic structure affects photon transport. The periodic structure can be the repetition of thin layers of dielectric, or inclusions or holes in a matrix,... Phononic crystals have been theoretically proposed with periodic structure. In 2001, Cleland and coworkers investigated the case of a suspended nanowire with a periodically patterned cross section [38]. At low temperature, when the wire can be considered as one dimensional and the transport ballistic, this geometry opens a gap in the dispersion relation. For a temperature range defined by the period of the variation, the phonon distribution passes through the gap frequency. Thus the thermal conductance should be reduced according to the amplitude variation. The same calculation can be done for holes in a membrane [39, 40, 41, 42].

All these systems are quite exciting, as they can control phonon flow, and are feasible with regular nanofabrication. The measurement of these systems however is quite challenging, as it means measuring conductances smaller than one picoWatt per Kelvin, the amount of heat will then be on the order of femtoJoules.

1.8 Conclusion

Theoretical tools to understand thermal transport in nanowire at low temperature have been presented. The heat carriers, known as phonons, have two characteristic lengths. When these lengths are around the same order of magnitude as the sample size, both classical and quantum effects are expected (reduction of the mean free path and quantization for instance). Finally, to measure the intrinsic thermal conductance of a wire, a transmission coefficient close to unity from the wire to the thermal bath is needed.

2 Experimental techniques for thermal transport in small systems and at low temperatures

2.1 Introduction

Measuring thermal conductance of nanosize objects at low temperature is quite challenging. Nowadays, measurements at low temperatures and thermal conductance measurements are well known. Nanotechnology has also been well developed today. Combining all these techniques introduces difficulties. For instance, the value of the quantum of thermal conductance is around 10^{-13} W/K. To measure it, as $K = P/\Delta T$, one needs a temperature gradient around 10 mK, which leads to a dissipated power P of 10^{-15} W. These small energies imply the use of a low noise electronic setup. These measurements must also be performed at sub-kelvin temperature on nanosize samples. Very few techniques allow to perform it, which explains the lack of extended thermal measurements on low dimensional systems at low temperature.

In this work, the 3ω method has been used. This method is adapted to low temperatures and nanowires measurements. The advantage of this technique is its relatively easy implementation (both heater and thermometer are realized by the same object which is called a transducer). This method also permits measurements of both thermal conductance and heat capacity. Its main disadvantage is that the transducer introduces parasitic thermal paths to the phonon transport. Also, for the 3ω method to be properly implemented, a local temperature must be defined along the wire. However, when phonons are ballistic, they do not thermalize the wire. Thus this method is not trustworthy at very low temperature (more details on this effect can be found in chapter 3).

In this chapter, after a presentation of the 3ω method applied to nanowires, adjustments to fit to membranes will be presented. Then the sample fabrication process will be shown. The final section presents previous measurements made in the group. These measurements are important to validate a normalization process. Nanowires of different sizes will be compared. This work was important to be able to perform further normalization. The last part of this chapter shows that other parasitic thermal paths do not affect our measurements.

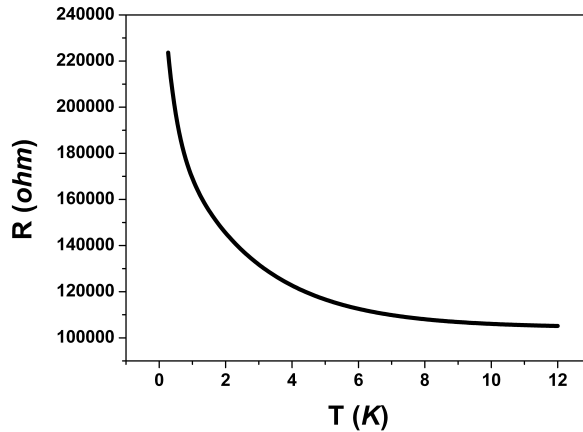


Figure 2.1: The resistance of a typical sample used in our measurements. Resistance varies significantly between 300 mK and 5 K, and remains above 100 k Ω below 10 K.

2.2 Measurement of thermal conductance

2.2.1 The 3ω method for nanowires

General principle

A measurement of thermal conductance is based on creating a temperature gradient (ΔT) after applying a heating power (P). Then, measuring the temperature gradient allows to know the thermal conductance as : $K = P/\Delta T$. In the case of the 3ω method, the power is created through a AC current in a transducer [43, 8, 44]. This transducer is used as a heater and a thermometer concomitantly. A resistive thermometric materials is used for such transduction. Niobium nitride - a metal undergoing a metal to insulator transition as the temperature is lowered - will be used for the thermometric transduction.

Niobium is a superconductor at low temperature. By doping it with nitrogen, one is able to transform it into an insulator at low temperature [45]. This happens because nitrogen creates a variation of the potential energy. Two phenomena are then in competition concerning electron transport : the electronic kinetic energy tends to delocalize the electrons; and on the contrary the disorder (introduced by the nitrogen) tends to localize them. At room temperature, the kinetic energy dominates, so NbN remains a conductor. At low temperature, the disorder introduced by the nitrogen dominates, inducing NbN to act as an insulator at $T=0$ K. This kind of materials are known as Mott-Anderson insulators [46, 47]. The resistance of the thin film continuously increases as the temperature decreases, making NbN a very good thermometer (see figure 2.1). One should be aware that the amount of nitrogen and the method used for deposition are critical elements for the disorder. Thus it will influence the metal to insulator transition, which is described by the slope of the resistance with respect to the temperature.

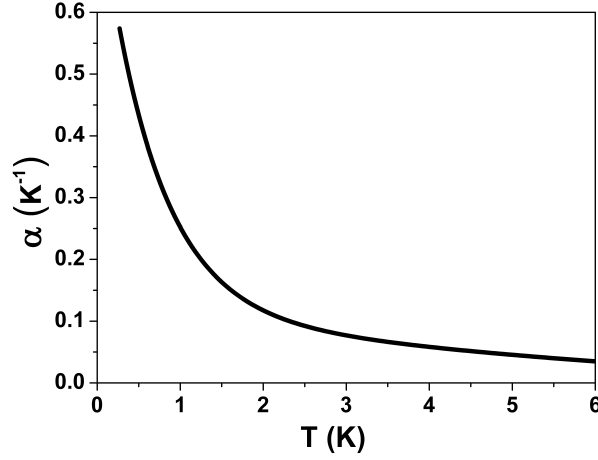


Figure 2.2: The temperature coefficient of a resistance measured on a typical nanowire. α is higher than 0.5 K^{-1} until 5K. Typical platinum thermometers have $\alpha_{Pt} = 4.10^{-3} \text{ K}^{-1}$ at room temperature. It illustrates that this NbN transducer is a very good thermometer.

The exact stoichiometry of the niobium nitride was measured by Rutherford backscattering spectrometry on thin films. But instead of writing the correct expression $\text{Nb}_1\text{N}_{1.6}$, the simplest notation NbN will be used [48].

The slope of the resistance will give the sensitivity of the thermometer. The best way to characterize this sensitivity is to calculate what is called the temperature coefficient α . For a material, at a temperature T_0 , α is given by (see figure 2.2 for a typical α of our samples) :

$$\alpha = - \left. \frac{1}{R(T_0)} \frac{\partial R}{\partial T} \right|_{T_0} \quad (2.1)$$

The 3 ω model

By depositing a thin layer of NbN on top of a suspended wire, it is possible to heat it with an AC current (see figure 2.3; $I_{ac} = I_0 \sin(\omega t)$), which induces a dissipated power $P = RI_{ac}^2$. Then, one can write and solve the equation of heat transfer :

$$\rho C_p \frac{\delta}{\delta t} T(x, t) - \kappa \frac{\delta^2}{\delta x^2} T(x, t) = \frac{I_0^2 \sin^2 \omega t}{LS} R(T(x, t)) \quad (2.2)$$

with the boundary conditions $T(0, t) = T_0$, $T(L, t) = T_0$, and $T(x, -\infty) = T_0$; where C_p , κ , R , and ρ are the volumetric specific heat, thermal conductivity, electric resistance and mass

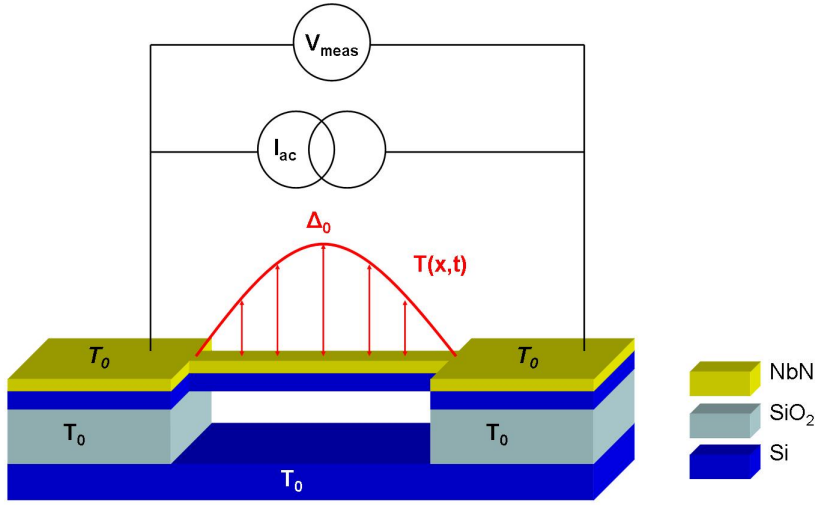


Figure 2.3: Schematic principle of the 3ω method. In black, the electronic circuit; in red, the temperature profile.

density of the sample at the substrate temperature T_0 , respectively; L is the length of the sample between voltage contacts, and S the cross section of the sample.

To solve this equation, one must know $R(T(x, t))$, which is tricky as it can be seen on the resistance profile shown in figure 2.1, with the temperature profile shown on figure 2.3. However, if the variation of temperature ($T(x, t) - T_0$) is small enough so that $R(T)$ can be considered linear, one can approximate the resistance by its two first terms of the Taylor series :

$$R(T(x, t)) = R(T_0) + R'(T_0) \cdot (T(x, t) - T_0) \quad (2.3)$$

Equation 2.2.1 can be solved by first using the impulse theorem. It leads to the result that ΔT can be represented as the integral of the responses of the sample to what can be called the instant force $b \sin^2(\omega t)$ at each time interval. Then an expansion in the Fourier series can be made, on the condition that the increase of temperature inside the wire is much lower than the temperature T_0 . It gives the temperature profile in the wire :

$$T(x, t) - T_0 = \Delta_0 \sum_{n=1}^{\infty} \frac{[1 - (-1)^n]}{2n^3} \times \sin \frac{n\pi x}{L} \left[1 - \frac{\sin(2\omega t + \phi_n)}{\sqrt{1 + \cot^2 \phi_n}} \right] \quad (2.4)$$

where $\cot \phi_n = 2\omega L^2 \rho C_p / \pi^2 n^2 \kappa$; and $\Delta_0 = 2I_0^2 R / (\pi^3 \kappa S / L)$ is the maximum rise of the temperature in the center of the wire. A noticeable fact is that the temperature will go from T_0 to $T_0 + \Delta_0$ at the frequency 2ω .

2.2. Measurement of thermal conductance

The temperature gradient Δ_0 is of importance. On figure 2.3 the temperature profile is represented. The highest temperature is at the center of the wire. Thus the heat will flow from the center to the extremities of the nanowire. The wire can then be seen as two wires in parallel of half the total length of the wire. It is also important to notice that Δ_0 must be small enough, as it has been said, to be able to develop the resistance in Taylor series and the temperature profile in Fourier series. Also, the heating power inhomogeneity caused by resistance fluctuations along the sample should be much smaller than the total heat power. This is given by the relation :

$$\frac{I_0^2 R' L}{\pi^2 \kappa S} \ll 1 \Leftrightarrow \Delta_0 \alpha \ll 2/\pi \quad (2.5)$$

Typically, $\Delta_0 \approx 10$ mK and $\alpha \approx 0.5$ K⁻¹ so this condition is usually fulfilled.

A last point regarding Δ_0 is that the measured conductance is an average measurement of the thermal conductance over the range of temperature T_0 to $T_0 + \Delta_0$. Δ_0 being small compared to T_0 assures that the temperature of the nanowire can be estimated as T_0 .

The small variation of temperature induces a small variation of resistance. This variation can be written as :

$$\delta R = \frac{R'}{L} \int_0^L [T(x, t) - T_0] dx = R' \Delta_0 \sum_{n=1}^{\infty} \frac{[1 - (-1)^n]^2}{2\pi n^4} \left[1 - \frac{\sin(2\omega t + \phi_n)}{\sqrt{1 + \cot^2 \phi_n}} \right] \quad (2.6)$$

One can notice that this variation appears at the frequency 2ω . The total resistance of the NbN will be $R_{tot} = R + \delta R$. The voltage can then be written : $V = RI_{ac} + \delta RI_{ac} = V_{1\omega} + V_{3\omega}$. As δR is small compared to R , the inequation $V_{1\omega} \gg V_{3\omega}$ will be always fulfilled. In the $V_{1\omega}$ signal, the information on thermal properties is hidden by the ohmic part. The 3ω component however has only one term, which is related to thermal properties. $V_{3\omega}$ can be written as (using the root mean square notation) :

$$V_{3\omega} \approx \frac{4I^3 R^2 \alpha}{\pi^4 K \sqrt{1 + (2\omega\gamma)^2}} \quad (2.7)$$

where α is the temperature coefficient of the thermometer (see equation 2.1), I is the root mean square value of the current (all the values will now be the root mean square of the signal), K is the thermal conductance and $\gamma = (LS\rho C_p)/(\pi^2 K)$ is the thermal time constant of the nanowire. The last term is very important, because it will determine the high and low frequency limit.

When $\gamma\omega \rightarrow \infty$ equation 2.7 can be written as :

$$V_{3\omega} \rightarrow \frac{4I^3 R^2 \alpha}{\pi^4 K \omega \gamma} = \frac{I^3 R^2 \alpha}{4\omega \rho C_p L S} \quad (2.8)$$

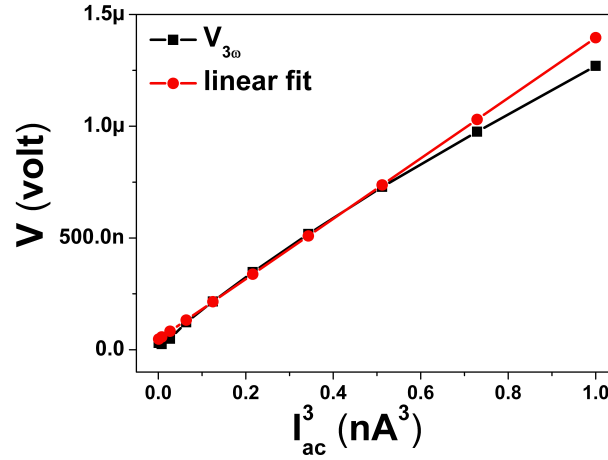


Figure 2.4: In black, $V_{3\omega}$ versus the current at the power three; in red, a linear fit of the lowest values of $V_{3\omega}$.

In this high frequency regime, the heat stored in the system does not have time to relax toward the heat bath. Hence the temperature will stay stable at Δ_0 . This explains the dependence of $V_{3\omega}$ to heat capacity only. However, as $V_{3\omega}$ is inversely proportional to the frequency, the signal will be very weak. This regime is called quasi-adiabatic.

On the other hand, the low frequency limit gives the thermal conductance. The low frequency regime occurs when $\gamma \rightarrow 0$. In other words, when the frequency is lower than the one corresponding to the relaxation time of the nanowire ($\tau = C/K$). In this quasi-static regime, equation 2.7 becomes :

$$V_{3\omega} \rightarrow \frac{4I^3 R^2 \alpha}{\pi^4 K} = \frac{IR' \Delta_0}{\pi^3} \quad (2.9)$$

The temperature will vary slowly enough from T_0 to its maximum value $T_0 + \Delta_0$ (see figure 2.3). The system will be sensitive to the propagation of the heat, i.e. the thermal conductance.

Preliminary measurements

Before analyzing the data, one must be convinced that this method is adequate. Thus preliminary measurements need to be performed.

As it has been said in the first part, the thermometer needs to be calibrated before any measurement, by measuring its resistance versus the temperature. This will allow the calculation of the temperature coefficient α (see equation 2.1).

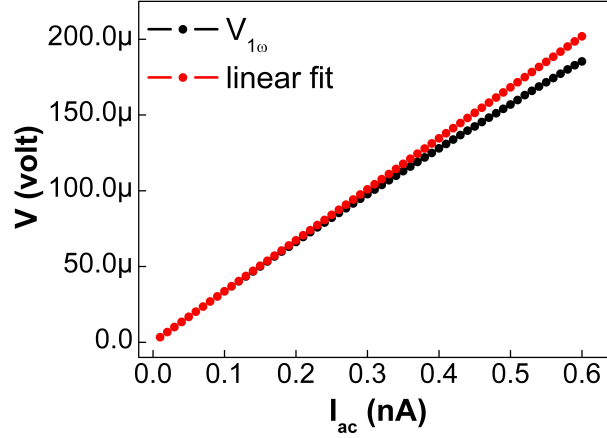


Figure 2.5: In black, $V_{1\omega}$ versus the current; in red, a linear fit of the lowest value of $V_{1\omega}$.

As one can see in equation 2.7, $V_{3\omega} \propto I^3$. This proportionality needs to be verified, to be sure that the measured $V_{3\omega}$ is coherent with the theoretical value. In the figure 2.4, one can see $V_{3\omega} \propto I^3$ at low current. When the current increases, the temperature inside the nanowire increases too. As it has been said, Δ_0 must be low enough for the 3ω method to be performed. Especially, one needs to be sure that $R(T)$ can be considered as linear for the range of temperature Δ_0 . At high current this will not be the case. This effect is also seen at the fundamental frequency of the signal, see fig 2.5.

Measuring the thermal time constant (γ) is very important to know in which regime the measurements will be done (low or high frequency). A simple way to measure it, is to fit $V_{3\omega}$ with respect to the frequency by $A/\sqrt{1+(B\omega)^2}$; where $B = 2\gamma$ (cf equation 2.7). This has been done in the figure 2.6. The measurement leads to $\gamma \approx 200\mu s$. This sample has a length of $5\mu m$ and a section of $200nm \times 100nm$. This value for γ does not fit the expected volumetric specific heat which is two orders of magnitude lower than the measured value [1, 49]. This is probably because other cutoff frequencies play a role. We do not know yet where do these cutoffs come from. However the presence of the plateau at low frequency implies that below 10Hz, the regime is in a proper quasistatic regime.

In figure 2.7, the electronic setup used in our experiments is represented. The current is generated by an ultra low distortion function generator (DS 360, by Stanford Research System, less than 0.001% total harmonic distortion), and a voltage-current converter (LC01, developed at the Institut Néel) that permits to deliver a very low current (to below 1 nA). The voltage is measured with a lock-in amplifier (SR830, by Stanford Research System, the input impedance is 10 M Ω) after being amplified by a low noise preamplifier (EPC1, developed by the Institut Néel, and sold by Celians; the noise is less than $2nV/\sqrt{Hz}$ at 1 Hz). The low noise electronic allows a highly sensitive measurement of the third harmonic of the signal, which is typically

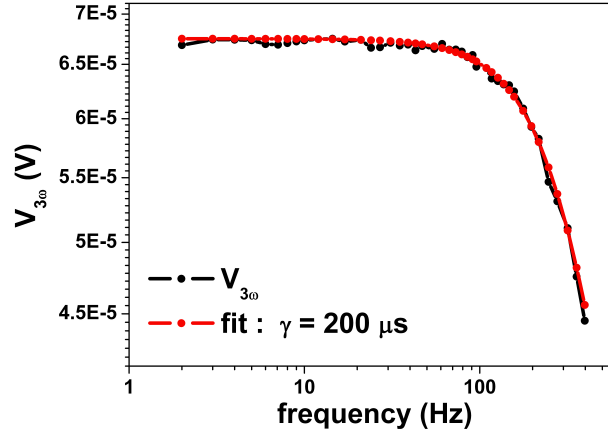


Figure 2.6: In black, $V_{3\omega}$ versus the frequency; in red, the fit of $V_{3\omega}$ explained in the text. This measurement was performed at 1.7K.

200 times lower than the first harmonic ($V_{1\omega}/V_{3\omega} = 200$).

The value of this ratio is actually quite low, and implies that $V_{3\omega}$ can be directly measured. In most common 3ω method, the temperature coefficient α is smaller 10^{-3} K^{-1} . This leads to a ratio $V_{1\omega}/V_{3\omega}$ to be around 10^5 . In that case, a Wheatstone bridge must be used to get rid of some part of the first harmonic of the signal. As it has been said, this is not the case for our measurements on nanowires.

2.2.2 The 3ω method for membranes

In this work, some 3ω measurements have also been made on SiN thin membranes elaborated by Hossein Ftouni. In the case of such membranes, the basis of the 3ω method are the same. An extensive description will then not be given [50, 51].

By coupling the 3ω method to Völklein geometry [52], one can make measurement of the in-plane thermal conductivity of a membrane [50] (figure 2.8). Typical dimensions of these membranes are 1 mm long, $150 \mu\text{m}$ wide, and 100 nm thick. A transducer centered on the membrane is used to both create an oscillation of the heat flux and to measure the temperature oscillation at the third harmonic using in that case a Wheatstone bridge set-up (figure 2.9).

The main difference with the 3ω method for nanowires is this Völklein geometry. In this geometry, the transducer is put on the center of the membrane. The thermal conductance studied is not along the transducer (as it is the case for the nanowire measurements) but between the transducer and the thermal bath (fig 2.8). The temperature is given by the 1 D

2.2. Measurement of thermal conductance

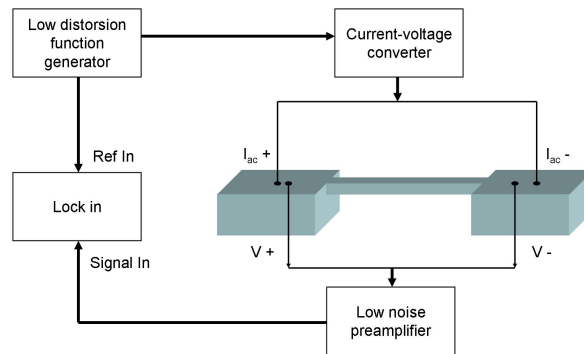


Figure 2.7: Schematic figure of the electronic setup. Some HF filters can be added to reduce the noise.

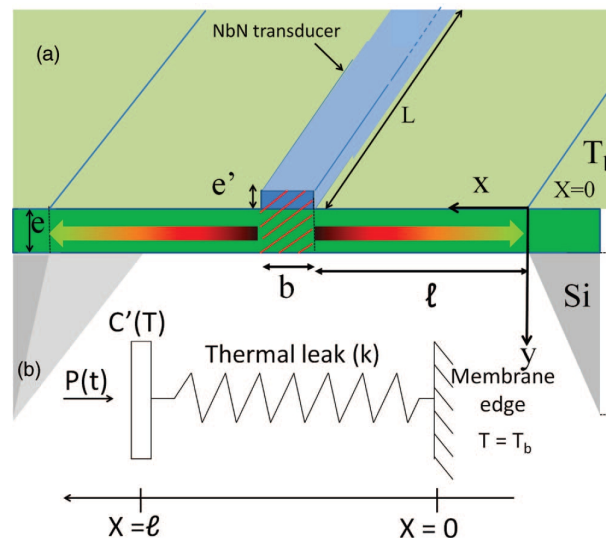


Figure 2.8: (a) Schematic of the membrane on which the NbN transducer has been deposited. e is the thickness of the membrane and e' the thickness of the NbN transducer. C' is the specific heat of the hatched area in red. The arrows represent the heat propagation. The hot point corresponds to the transducer (the red part of the arrows), whereas the cold point is at the edge of the membrane (the yellow part). (b) Schematic of the thermal system [50].

Chapter 2. Experimental techniques for thermal transport in small systems and at low temperatures

heat diffusion equation :

$$\frac{\partial^2 T(x, t)}{\partial x^2} = \frac{1}{D} \frac{\partial T(x, t)}{\partial t} \quad (2.10)$$

where D is the diffusivity of the membrane. Calculations using a 2D model give approximately the same results. The initial and boundary conditions are : $T(x, 0) = T_b$ and $T(0, t) = T_b$; where T_b is the bath temperature. Solving equation 2.10 gives the expression of the absolute value of the temperature $T_m(l)$:

$$T_m(l) = \frac{P_0}{K_p [1 + \omega^2 (4\tau^2 + \frac{2l^4}{3D^2} + \frac{4\tau l^2}{3D})]^{1/2}} \quad (2.11)$$

where $P_0 = RI_0^2/4$ is the dissipated power, K_p the thermal conductance, $\tau = C'/K_p$ is a thermal time constant of the system (C' is the heat capacity of the hatched area in figure 2.8).

Another difference with the nanowire, is the presence of the Wheatstone bridge. In the case of these membranes, putting the same transducer on top of the bulk sample is possible. Therefore two almost identical resistances are deposited on the sample, one on the suspended membrane, and one on the bulk part. A Wheatstone bridge can be made using these two resistances (see fig 2.9). This will decrease the 1ω component of the signal to have a better signal to noise ratio for the 3ω . However, with a Wheatstone bridge, the dissipated power can only be made through an AC voltage (on the contrary to nanowire, where an AC current can be used). This will give a different value of the 3ω component compared to the previous calculation. Using the temperature profile obtained in equation 2.11, $V_{3\omega}$ is given by (using the RMS notation) :

$$|V_{3\omega}| = \frac{\alpha V_{ac}^3 (R_1 + R_v) R_e^2}{2K_p (R_1 + R_e)^3 (R_1 + R_{ref} + R_v) [1 + \omega^2 (4\tau^2 + \frac{2l^4}{3D^2} + \frac{4\tau l^2}{3D})]^{1/2}} \quad (2.12)$$

where α is the thermometer temperature coefficient (equ. 2.1); R_1 , R_v , R_e , and R_{ref} are the resistances as defined in figure 2.9.

Like in the nanowire study, we are interested in thermal transport. We thus try to work in the quasi-static regime. Equation 2.12 can then be simplified for the low frequency limit. When ω is low enough to neglect the last term of the denominator in equation 2.12, $V_{3\omega}$ can be written in a simpler form :

$$|V_{3\omega}| = \frac{\alpha V_{ac}^3 (R_1 + R_v) R_e^2}{2K_p (R_1 + R_e)^3 (R_1 + R_{ref} + R_v)} \quad (2.13)$$

One may notice that in this case the proportionality $V_{3\omega} \propto V_{ac}^3$ is still valid. It is presented in figure 2.10. $V_{3\omega}$ with respect to the frequency has also been characterize to ensure that the

2.2. Measurement of thermal conductance

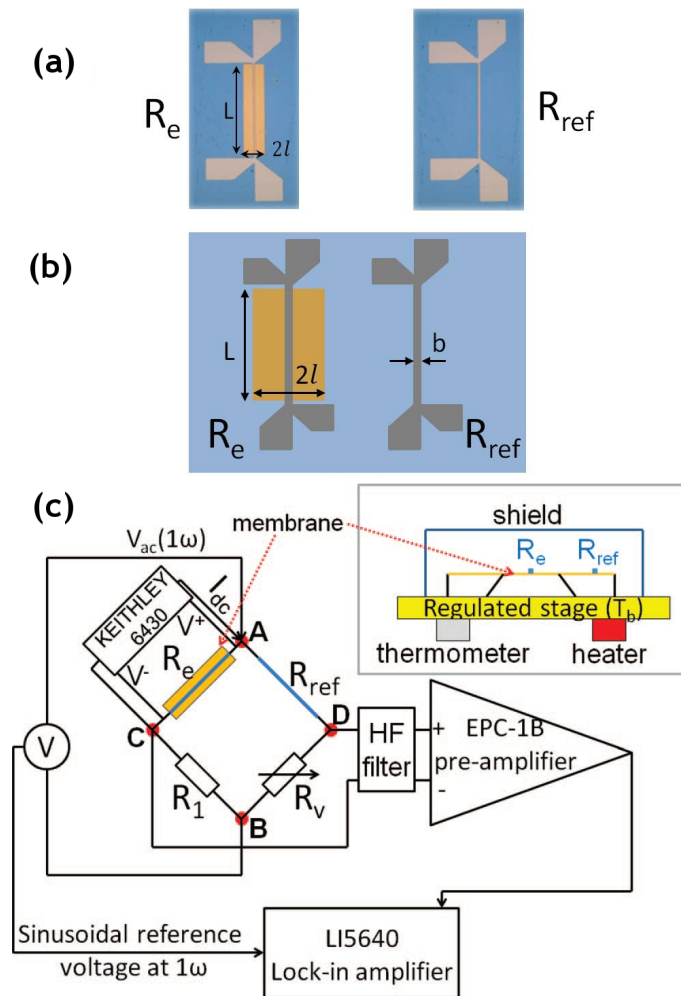


Figure 2.9: (a) and (b) : Photograph of the two NbN thermometers deposited on the membrane and on the bulk region. (c) Schematic of the electrical measurement system including HF filter, preamplifier, and lock-in amplifier. A, B, C, and D represent the nodes of the Wheatstone bridge. The $V_{3\omega}$ is measured between C and D. The transducer is referred to as R_e and the reference resistance as R_{ref} . The insert presents a schematic of the membrane fixed on the temperature regulated stage covered by a thermal copper shield [50].

Chapter 2. Experimental techniques for thermal transport in small systems and at low temperatures

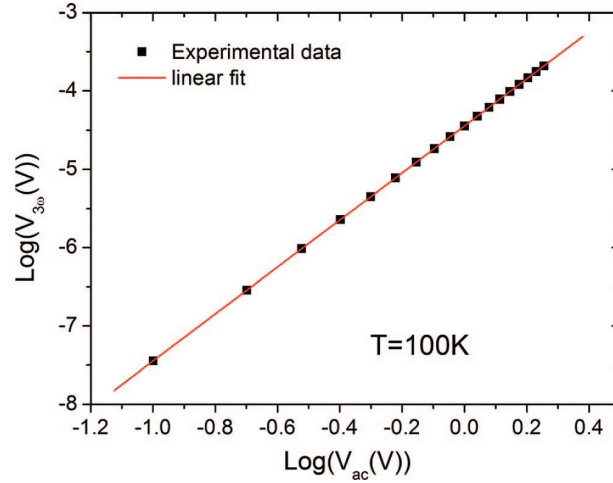


Figure 2.10: [50] $V_{3\omega}$ signal as a function of the voltage applied across the Wheatstone bridge (V_{ac}) in logarithmic scales. The linear fit is in a very good agreement with experimental data.

measurements will be performed in the quasistatic regime. As one can see in figure 2.11, that for frequencies below 10 Hz, the regime is quasistatic.

The 3ω method has been successfully adapted to measure the in-plane thermal conductance of thin suspended membranes. The main difference with the 3ω method for the nanowires, is that for the membranes, the heat propagates perpendicularly to the NbN transducer, i.e. along the membrane width (for the nanowires heat propagates along the transducer, thus along the length of the wire). I will present measurements on silicon nitride membrane in chapter 5. These measurements have been made with Hossein Ftouni.

2.2.3 The Helium 3 fridge

All the measurements performed during my PhD were done on the same Helium 3 fridge. The principle of such a fridge is to pump a liquid He^3 bath to cool it down. The minimum temperature this fridge can reach is 270 mK. The cooling system consists in two circuits. One Helium 4 circuit, which serves as a primary stage to reach 1 K; the other with Helium 3 cools the system down to 270 mK. Schematic representation of a He^3 refrigerator has been drawn on figure 2.12.

The sample is installed on a sample holder and glued with a PMMA resist. The sample holder is made in copper, and has gold strips which allows the connection of the samples by micro-bonding, a heating resistance (50 Ohms) and a commercial Ge thermometer resistance. It is placed in a calorimeter under cryogenic vacuum, to isolate the sample from gas exchange. The Helium 3 circuit and the 1K chamber are also in this vacuum chamber. The calorimeter is put on a liquid Helium 4 cryostat (see fig 2.12).

2.2. Measurement of thermal conductance

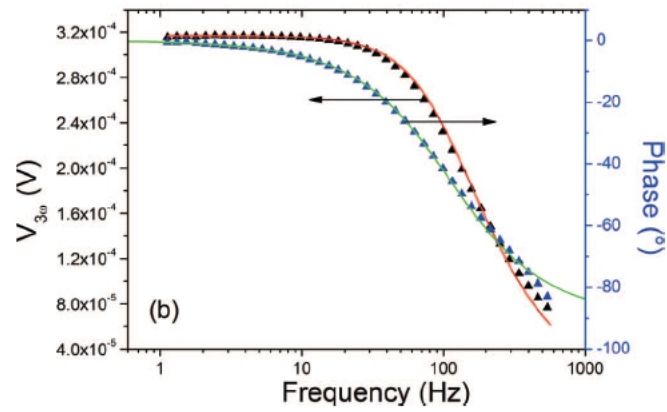


Figure 2.11: [50] $V_{3\omega}$ absolute value and phase signal as a function of the frequency and their respective fits (solid lines). The presence of the plateau below 10 Hz ensures the quasistatic regime.

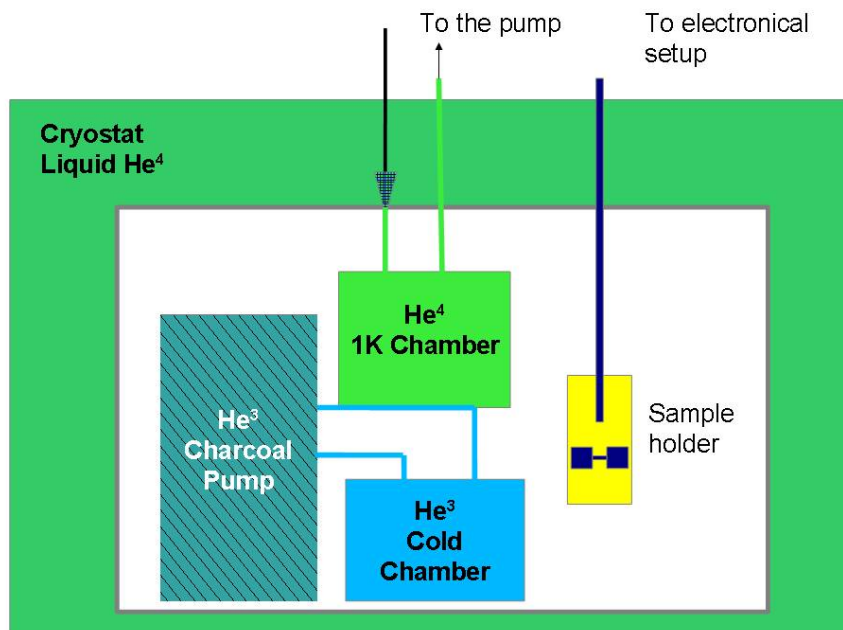


Figure 2.12: Schematic representation of the Helium 3 fridge used for the measurements. The vacuum chamber is in white. One can notice the closed circuit for helium 3.

Chapter 2. Experimental techniques for thermal transport in small systems and at low temperatures

The He^3 circuit consists in a charcoal pump and a cold He^3 chamber. This circuit is totally closed to avoid He^3 losses. The Helium 3 will become liquid in a capillary, thermally linked to the 1K chamber. The He^3 liquid is stored in the cold chamber. This chamber is also linked to the charcoal pump. This pump consists in a large amounts of porous charcoal. By heating it, it is possible to totally outgas the trapped He^3 . Then it will slowly absorb Helium 3 from the cold chamber. When the pumping speed and the pressure are stabilized, it is possible to reach temperatures as low as 270 mK. However, once the charcoal is saturated with He^3 , it will no longer be able to pump it. Another heating cycle is needed to reach again 270 mK. Typically, it is possible to keep the temperature below 300 mK for 6 hours.

2.2.4 Other method of measurement

Performing thermal measurement of nanowires at low temperature is so challenging that, not many experimental studies have been performed. As it has been said, the problem lies in the small energy exchange which takes place in this kind of systems. Creating and detecting a signal under the femtojoule at low temperature is quite difficult. As thermal conductance is concerned, the general principle is rather simple : one needs to create a temperature gradient through a power dissipation, and then measure this gradient.

In the late nineties, T. S. Tighe, J. M. Worlock, and M. L. Roukes developed a experimental device which allows thermal conductance measurements of nanowires [53]. In their experiments, they had a $3 \mu\text{m}^2$ suspended membrane, connected by four $5 \mu\text{m}$ long bridges (whose cross section is around $200 \text{ nm} \times 300 \text{ nm}$) to a thermal reservoir (see fig. 2.13). All this is made in *i*-GaAs. Then they connect two meandering $n+$ GaAs conductor on the membrane through the bridges. This pair of meanders will act as a transducer : the source will heat and the other unbiased will act as a thermometer. The phonon thermal conductance is obtained by heating the source transducer with a small DC current while monitoring the electron temperature of the unbiased sensor. Their results are in good agreement with the Casimir-Ziman model. This method, however has two drawbacks. Firstly, it requires many steps of lithography; Secondly the bridges had $n+$ GaAs conductor on top of them. A parasitic thermal path is then created and falsified some of their measurements. Especially for temperatures below 2.5 K this path becomes increasingly important.

K. Schwab, J.L. Arlett, J.M. Worlock, M.L. Roukes improved this device (see fig 2.14) [17, 18]. First they replaced the $n+$ GaAs by niobium in the bridges. On the membrane, instead of the pair of meandering, they put two Cr/Au resistors. The detection was performed by utilizing DC SQUID-based noise thermometry. In this technique, the temperature of a resistor is measured by placing it within a superconducting circuit that tightly couples it to a SQUID which amplifies the Nyquist current noise generated by the resistor. All their samples are made out of silicon nitride, because this material is easier to manipulate. They claim that even in such an amorphous material, ballistic transport is achieved for temperatures below 1 K. Finally they made their bridge with a width varying as a catenoid (\cosh^2). This could increase

2.2. Measurement of thermal conductance

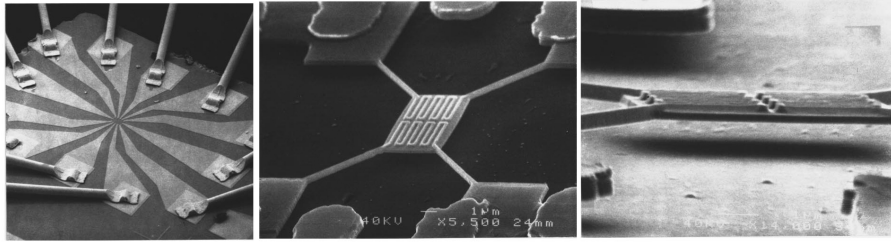


Figure 2.13: SEM picture of the device used by Tighe *et al.* [53]. On the left an overall view of a device. In the center : enlarged view of the membrane and the four bridges. One can see the pair of meandering on top of the membrane. On the right : an side view of the device.

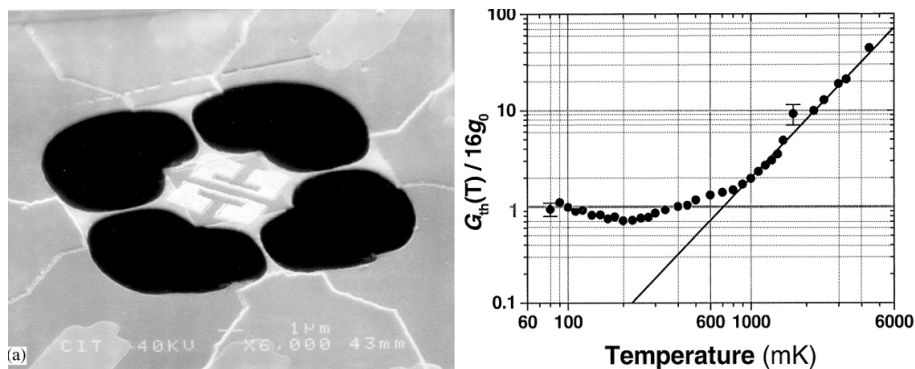


Figure 2.14: On the left : SEM picture of the device used by Schwab *et al.* [17, 18]. One can see the catenoidal shape of the wires. On the right, the thermal conductance normalized by 4×4 times the quantum of conductance in a log-log scale. The conductance seems to follow the three-dimensional behavior for temperature above 1 K, and approach sixteen times the quantum of conductance for temperature below 200 mK.

the transmission coefficient between the wire and the thermal reservoirs. They found that the thermal conductance approaches a plateau which value corresponds to the universal value of thermal conductance (see fig 2.14). Since 2000, no further measurement has been made with the same device, or independently reproduced.

In the group of Majumdar, a device to make thermal conductance measurements has been developed in 2003 [54, 55]. This device consists in two membranes of SiN_x connected to a thermal reservoir by five SiN_x beams (see fig 2.15). On each membrane a platinum electrode has been patterned and connected to the electronic setup through Pt on the beams. Each electrodes can act as both a heater and a thermometer for each membrane. An individual Si nanowire is deposited between the two membranes, and will then thermally connect them. This device allows measurements in a temperature range between 20 K and 320 K. They found a quite good agreement with the Debye model for the nanowire with a diameter larger than 50 nm, and a significant variation for the ones with a smaller diameter. They say that this

Chapter 2. Experimental techniques for thermal transport in small systems and at low temperatures

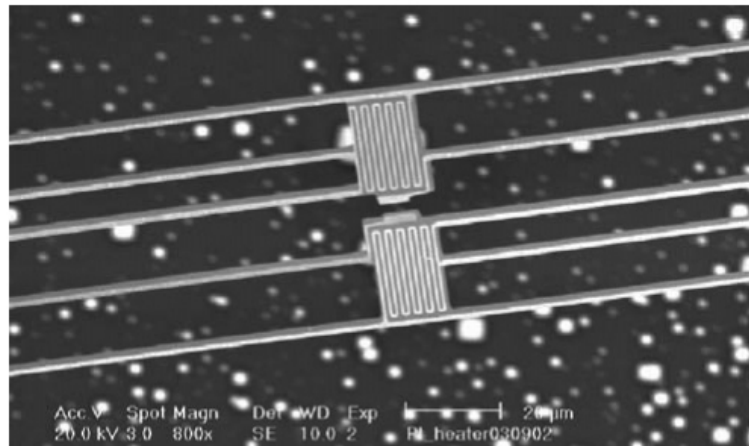


Figure 2.15: SEM picture of the suspended device used in the group of Majumdar [55]. One can see the two membranes with their platinum electrodes. In this device, some electrodes are available to measure the thermoelectric power of the nanowire which connect the two membranes. One can hardly distinguish the carbon nanotube between these two membranes.

variation may come from a variation in the dispersion relation. As it has been said in chapter 1.3.1 due to the smaller radius of the nanowire, a folding of the dispersion relation may happen.

In their experiments, nanowires are self grown and then deposited on the sensitive part of the sensor. If this allows a more accurate control of the geometry of the nanowire, it also introduces a higher thermal contact resistance. But this useful device still allows them to measure the thermal conductance of carbon nanotube [55], of controllably roughened Si nanowires [56], and others samples. If one is able to connect the membranes through a single nanowire with the same material (not by deposition, but by a lithography process), then it is possible to get rid of the thermal contact. It should be possible to make measurements at temperature below 100 mK, without any parasitic electronic thermal conductance. Such a device is currently being developed in our group.

Other methods exists for measuring thermal properties. For instance, pump-probe techniques allow measurements of phonons which are excited and measured by a laser beam [57, 58]. In this case, the physical properties used for thermometry is the variation of the reflectance with temperature. The problem with this technique is that a laser beam has a size of few micrometers. It is rather difficult to have a resolution below this spot size, thus to measure nanoscale structures.

Finally a way to make phonons measurements has been developed at Cornell university by the group of Robinson [59]. They adapt previous work made in the seventies with experimental millimeter-sized devices to micrometer-size [60]. These works use the fact that in a Josephson junction, phonons can be emitted. A Josephson junction is a superconductor-insulator-superconductor junction. By applying a DC bias voltage (which energy is eV), one can shift

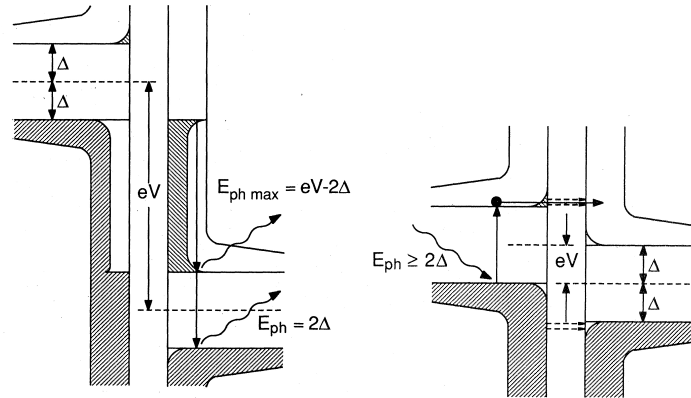


Figure 2.16: [61] Left : Josephson junction generation by quasiparticle relaxation ($E_{ph} \leq eV - 2\Delta$) and recombination ($E_{ph} \approx 2\Delta$). eV is the bias voltage and must be higher than the gap 2Δ . Right : Josephson junction detection of phonons which energy is higher than the gap. Here the bias voltage must be smaller than the gap.

the two Fermi levels. We will say that the left superconductor will have the higher Fermi level. Then an electron pair in the left superconductor may tunnel through the insulator to the right superconductor. If the bias energy eV is larger than the superconducting gap 2Δ , this electron pair will then transfer its excess energy to phonons through two mechanisms : relaxation and recombination (see fig 2.16). Relaxation induced phonons have energy around (but not longer than) $eV - 2\Delta$. Recombination induced phonons have energy around (but no less than) 2Δ . Thus this technique creates almost monochromatic phonons at these two energies. One can notice that the relaxation induced phonons constitute the part of emitted phonon spectrum whose energy may be controlled. The main drawback of this generation is that the emitted phonons are mainly along one direction. If the Josephson junction is put on the surface of a Si substrate, the phonons will mostly be emitted perpendicularly to the surface.

The detection of the phonon takes place in another Josephson junction. In this junction, the bias energy is smaller than the superconducting gap. A phonon with energy at least as large as 2Δ can transfer its energy to a Cooper pair. This pair then contributes to the tunneling current across the junction (see fig 2.16).

In the device made by Robinson *et al.*, generation and detection are both made by SQUIDS (two Josephson junctions in parallel). This was made because in a single Josephson junction, a current appears. This current avoids the phonon creation (and detection) process. In a SQUID, by applying a magnetic field, one can get rid of this current. The phonon signal to noise ratio is therefore enhanced. Furthermore, because of the direction of the emitted phonons, they made their SQUID on both sidewalls of what they called a mesa (see figure 2.17).

The aim of their first measurements was to prove that their device was properly functioning. To do so, they used different generator-detector pairs of SQUIDS, as shown in figure 2.17.

Chapter 2. Experimental techniques for thermal transport in small systems and at low temperatures

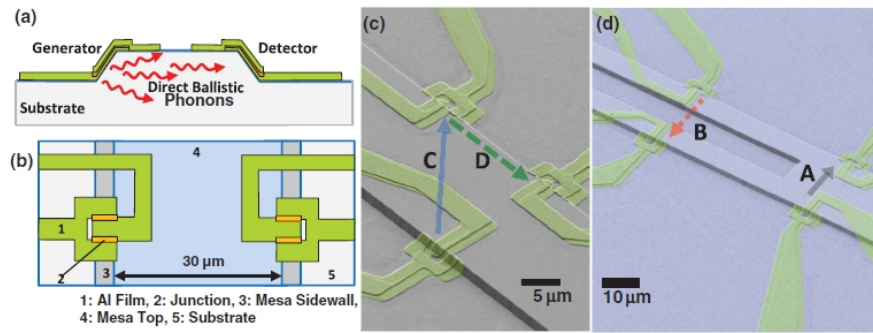


Figure 2.17: [59] (a) and (b) are a cross view and top view of the schematic diagram of phonon generator and detector. (c) and (d) are SEM picture of their device. Each phonon generator-detector pair is indicated by an arrow pointing from the generator to the detector. The detector in pair **C** is also used as the generator in pair **D**. Pair **B** is identical to **A** except that the ballistic path in **B** is interrupted by a trench etched into the mesa. The measurements confirm that phonons travel in line-of-sight from generator to detector.

During each set of measurements, they applied to the phonon generator a fixed AC current modulation $\delta I_{gen} = 15$ to 36 nA, with a stepped DC current $I_{gen} = -1.5$ to 1.5 μ A (with the RMS notation). With a lock-in amplifier, they measured the variation of current inside the detector δI_{det} . The ratio $\delta I_{det} / \delta I_{gen}$ is linked to phonon transport properties. It is not straightforward to directly get information on the phonon transport with this ratio. However, by comparing this ratio for different pairs, one can get several pieces of information. For instance the ratio in the pair **A**, which is facing on each side of the mesa, is significantly higher than the one in the pair **B**, which is separated by a trench. The pair **C**, which is facing on each side of the mesa with an angle around 45° , has almost the same ratio as the pair **A**. Finally the pair **D**, which lacks a line-of-sight between generator and detector, has almost the same ratio as pair **B**.

Their results show that phonons are truly emitted along a direction. However, the fact that the $\delta I_{det} / \delta I_{gen}$ ratio is not null for pair **B** and **D**, suggests that indirect transmission occurs by a scattering process within the silicon. These measurements are of great importance to validate their device. Further measurements are expected to provide a better understanding of this ratio. Also, instead of a trench, they can place some nanowires inside the mesa, to evaluate the impact on the phonon transmission. It is very interesting, as they do not look for thermal phonons. Their phonons are almost monochromatic, and they can control the phonon wavelength. Thus it should be possible to investigate more in detail monochromatic phonon transport in different geometries.

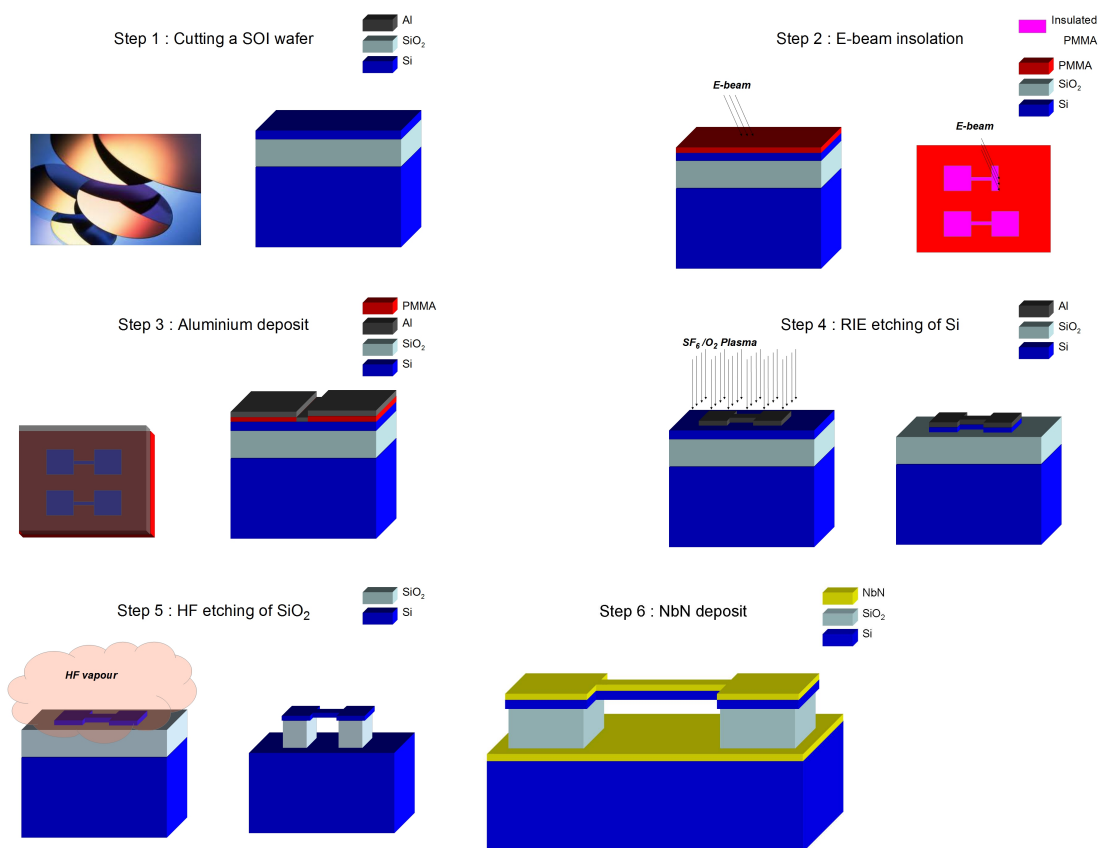


Figure 2.18: Schematic representation of the different steps of the lithographic process.

2.3 Fabrication

2.3.1 Silicon nanowires

The fabrication of single crystal silicon nanowires has been realized with the regular method of e-beam lithography. Wafers of 200 mm of silicon on insulator (SOI) provided by SOITEC have been used. These wafers are made of a thin layer of 350 nm of silicon on top; a layer of 1 μm of silicon oxide (SiO₂); and 500 μm of bulk silicon. The aim of this lithography is to design a nanowire (having dimensions of about 10 μm \times 100 nm) that is doubly clamped at two pads (having dimensions of about 100 μm \times 100 μm). By an etching process, it is possible to suspend the wire while the pads are still attached to the bulk substrate. In figure 2.18 the different steps are shown.

E-beam lithography

First, the Si layer on top of the wafer is thinned by thermal oxidation followed by a liquid hydrofluoric acid (HF) desoxidation, in order to have a 100 nm (or 200 nm) thin silicon layer. Then the wafer is separated into 1 cm² squares. Approximately 50 nanowires can be made

Chapter 2. Experimental techniques for thermal transport in small systems and at low temperatures

on each square. A thin layer of a polymer resist (PMMA, diluted at 4%) is spun on top of the sample. Then the sample is introduced in a SEM (scanning electron microscope). It is possible to control the beam of the SEM, through a machine made by the RAITH company. The minimal area size of the beam is 4 nm. A roughness under 10 nm is then expected. This allows us to create any wanted shape of nanowire. The beam of electrons will break the bounds of the polymer. An MIBK/IPA solution will dissolve the resist which has been insulated.

Then an aluminum thin layer (30 nm) is evaporated on all the sample. It will fill the holes or be on top of the resist. This Al layer will act as a mask for the following etching process. A NMP bath at 70°C will then remove the resist, and the Al on top of it. On the sample, aluminum with the wanted shape will stay on top of the sample.

The sample is then put on a reactive ion etching (RIE) chamber. A SF_6/O_2 plasma will etch the silicon isotropically, whereas the aluminum will not be affected. In one minute and thirty second, 100 nm of Si will be etched. A basic solution (MF319) will remove the aluminum of the sample. The sample will then consist in pads and nanowires of silicon on top of oxide silicon.

Vapor HF etching

The aim is then to suspend the nanowires without affecting the pads. Hydrofluoric acid (HF) etches oxide silicon but is inert to silicon. It means that in a HF bath, the SiO_2 will be removed, but both nanowires and pads will not be affected. For a short time, just a small amount of SiO_2 will be etched. In order to avoid sticking processes (drop of liquid which breaks the sample), HF vapor will be used instead of liquid HF. The sample is stuck to a Teflon lid regulated at 45 °C. The lid is put right over a HF solution. Vapor HF will then etch the SiO_2 anisotropically. Typically, in half an hour, 2 μm is etched. As the wire is 100 nm width, and the pads are $100 \times 100 \mu\text{m}^2$ large, twenty minutes are enough to ensure that the wire is suspended whereas the pads will still be attached to the bulk substrate. On the samples, one can find 50 suspended nanowires doubly clamped to two pads linked to the substrate.

Deposition of the NbN transducer

As it has been said in section 2.2.1, a transducer is needed for using the 3ω method. In our study, the transducer is made of NbN. The resistance of this material is highly sensitive to the deposition conditions and can be tuned. Thus a calibration of the deposition is needed, in order to have a good sensitivity at the temperature range of the study. The sensitivity of a thermometer is given by its temperature coefficient $\alpha = (1/R)(dR/dT)$ (see section 2.2.1).

A way to have an estimate of the temperature coefficient is to measure the resistance at room temperature and the resistance at 70K (the liquid nitrogen temperature). The ratio between these two resistances is called the resistive ratio, RR. The He^3 fridge provides a temperature range between 0.3K and 10K, $RR \approx 3$ leads to a temperature coefficient around one in this range of temperature.

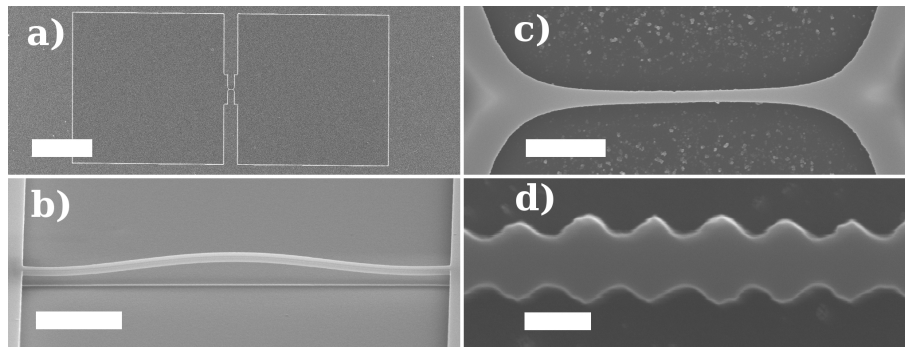


Figure 2.19: Some nanowires realized during this work. The scale bar for a) is $100\ \mu\text{m}$, for b) is $2\ \mu\text{m}$, for c) is $2\ \mu\text{m}$, and for d) is $200\ \text{nm}$.

The NbN deposition is made in a RF sputtering setup. Argon and nitrogen gases are first introduced in the deposition chamber. A RF voltage will produce a plasma. This plasma etches atoms of a niobium target. Within the Ar/N plasma, Nb atoms will also be present. The deposition can then begin. First we will deposit the NbN on sapphire samples. After the deposition, the RR is measured on the sapphire. By adjusting some deposition parameters (concentration and pressure of the gases, time of deposition, distance to the Nb target,...) it is possible to change the RR. For instance, raising the frequency of the pulse RF voltage reduces the RR. Once the RR is close to the value needed on the sapphire samples, the Si sample is introduced in the machine to make the deposition.

The final step is an annealing. Cycling the NbN at 150°C for 6 hours ensures that the resistance of NbN will not change over thermal cycling.

Once the NbN is deposited the sample is ready to be measured. All that needs to be done is to micro-bound the sample to the sample holder. In our case aluminium wires are used. In figure 2.19 several nanowires made during my PhD are shown.

2.3.2 Fabrication of Si_3N_4 nanowires and slabs

During my thesis, I also worked on silicon nitride samples. Measurements on these samples will be presented in the chapter 5. As the impact of reduced dimension on thermal transport of amorphous materials is interesting, different kinds of sample will be made. Here the fabrication of Si_3N_4 nanowires and Si_3N_4 slabs will be presented.

The SiN nanowires

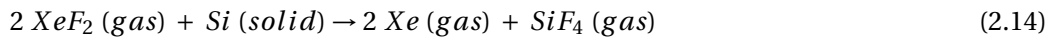
The fabrication of Si_3N_4 nanowires is basically the same as for Si nanowires. The wafers consist in a thin layer of $100\ \text{nm}$ (or $50\ \text{nm}$) of silicon nitride (Si_3N_4 , which will be called SiN from now), and bulk undoped silicon. The SiN layer was made with an internal stress of $0.85\ \text{GPa}$.

Chapter 2. Experimental techniques for thermal transport in small systems and at low temperatures

The steps of lithography are the same as the ones for the Si nanowire fabrication until the suspension process. As silicon, SiN is also etched by a SF₆/O₂ plasma. However HF does not etch the silicon. An anisotropic etching process, selective to silicon without etching silicon nitride, is required.

The XeF₂ etching process

The xenon difluoride gas does not etch any SiN, SiO₂, aluminum, nor PMMA but selectively etches Si. This is very convenient as it allows to perform the suspension of the SiN nanowire in a final step. Only the NbN needs to be protected from the XeF₂. To do so, a PMMA resist is good enough, which is convenient as PMMA is easily placed and removed. The chemical reaction is the following :



As the resulting gases prevent the continuation of the process, one needs to evacuate them. The process consists in cycles of less than a minute to permit the evacuation. The cycle time and the number of cycles will have a great influence on the etching speed and on the anisotropy of the etching. Environmental parameters such as temperature and XeF₂ pressure will have an effect too. With the table top etcher used in my PhD (Xetch e1 made by Xactix company), all these parameters except the temperature can be monitored.

Calibration of the etching process has been done. 10 cycles of 30 seconds with a pressure of 1.5 torr of XeF₂ allows to etch 2 μm of silicon. This is enough to suspend the SiN nanowires while the pads are still attached to the Si bulk.

The SiN slabs

In this work, the slabs are beams which lengths are between 10 μm and 20 μm, and width between 1 μm and 2 μm. As the size of the slabs is much bigger than the nanowires, a regular photolithography can be used to make them. This process is well known, so it will not be described in this manuscript. These slabs were made by Dr. Kunal Lulla.

2.3.3 Fabrication of the SiN membranes

The fabrication of the membranes has been made by Hossein Ftouni. The different steps of lithography are shown on figure 2.20. The membranes have a typical length of 1.5 mm and a typical width of 150 μm. These sizes are very large compared to the slabs and the nanowires. The membrane is released by etching the rear face of the wafer.

The membrane needs the NbN transducer to be precisely centered (see section 2.2.2), contrary to nanowires (and slabs), where the NbN is deposited uniformly over the whole sample. This

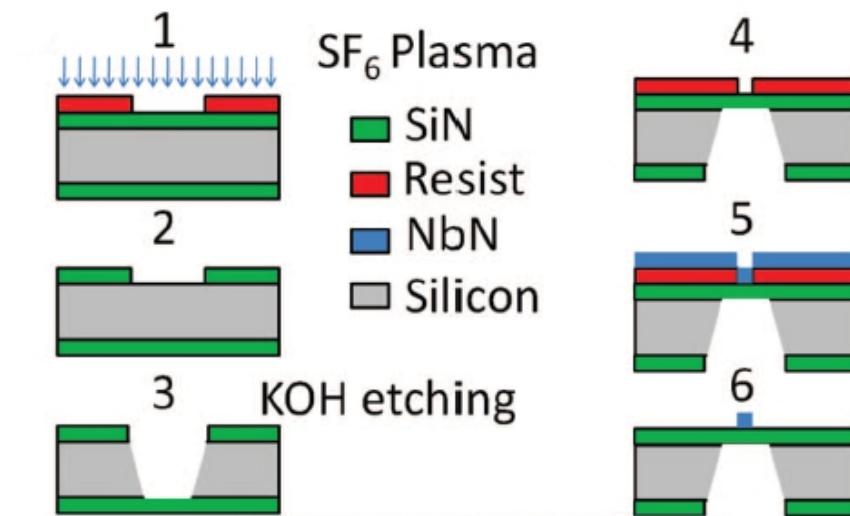


Figure 2.20: (1) The patterns of the membranes are created by photolithography. (2) The unprotected SiN is removed by SF_6 RIE. (3) The silicon is anisotropically etched in a KOH solution. (4) The thermometers are obtained by a lift-off process; the area is patterned by photolithography. (5) NbN is deposited by reactive sputtering. (6) The resist and NbN layer are removed using a wet procedure.

will be done by a photolithographic process (figure 2.20).

2.4 Previous measurements of silicon nanowires

2.4.1 Introduction

Straight silicon nanowires have already been investigated in the group [8, 10, 37]. The measurements will be presented by comparing the conductance measured with the Casimir model and then by combining it with the Ziman model. The conductance will then be compared to the contact conductance calculated by Chang and Geller [22, 62]. The influence of both length and width will also be studied. In a final part the parasitic thermal paths inside the NbN and at the NbN-Si interface, which may perturb the measurements will be evaluated and discussed.

2.4.2 Comparison with the Casimir-Ziman model

These models have been described in the part 1.4. As a reminder, the Casimir model is based on the fact that the phonon mean free path (MFP) is limited by the cross section of the system

Chapter 2. Experimental techniques for thermal transport in small systems and at low temperatures

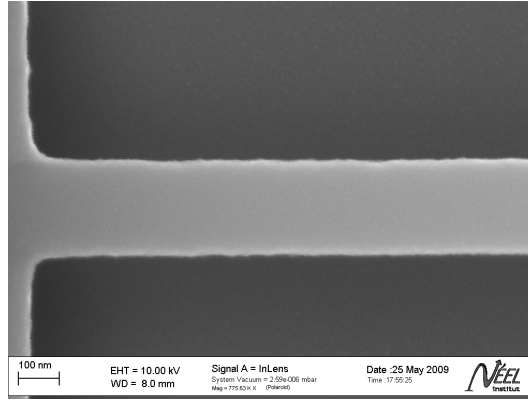


Figure 2.21: SEM picture of a nanowire which width is 200 nm. One can see that the mean value of the roughness is under 5% of the width.

[4]. For the thermal conductance, it leads to [5] :

$$K_{Cas} = 3.2 \times 10^3 \left(\frac{2\pi^2 k_B^4}{5\hbar^3 v_s^3} \right)^{(2/3)} \frac{e \times w \Lambda_{Cas}}{L} T^3 = \beta_{Cas} T^3 \quad (2.15)$$

Where $\Lambda_{Cas} = 1.12\sqrt{e \times w}$ is the Casimir MFP for a rectangular shape phonon conductor, e refers to the thickness and w to the width of the nanowire, L being its length; v_s is the speed of sound, which was set to 6500 m/s, the mean value of the speed of sound of the transverse (5840 m/s) and longitudinal (8400 m/s) acoustic phonons. β_{Cas} is the proportionality factor between the conductance and the cubic temperature. It is then defined as the Casimir conductance at 1 K.

The mean free path may be modified, as it has been explained in section 1.4.4, by the model of Ziman. In this case, the mean free path becomes [3] :

$$\Lambda_{Ziman} = \frac{1+p}{1-p} \Lambda_{Cas} \quad (2.16)$$

Where p is the probability for a phonon to have a specular reflection at the surface of the nanowire. p depends on the probability distribution $P(\eta)$ for the mean value of the roughness η : $p = \int_0^{\lambda/4\pi} P(\eta) d\eta$; where λ is the dominant wavelength of the phonons. One needs to determine this distribution. A distribution given by $P(\eta) = \exp(-\eta/\eta_0)/\eta_0$ is in good agreement with the SEM picture shown in fig. 2.21. As defined in section 1.4.3, η_0 is the mean value of the roughness. The probability p of having a specular reflection at the surface is then expressed by :

$$p = \int_0^{\lambda/4\pi} P(\eta) d\eta = 1 - \exp\left(-\frac{\lambda_{Dom}}{4\pi\eta_0}\right) \quad (2.17)$$

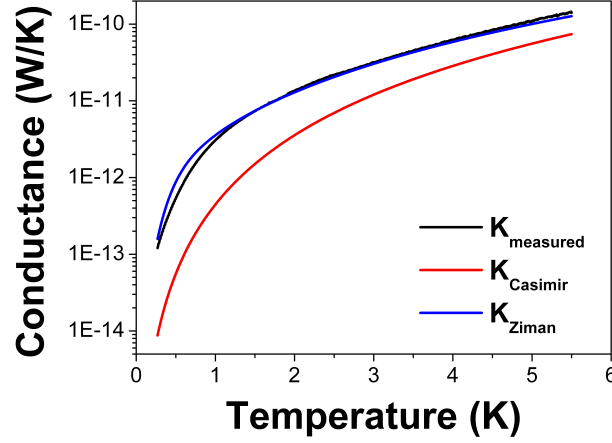


Figure 2.22: In black : thermal conductance of a Si nanowire of dimension $10\mu\text{m} \times 150\text{nm} \times 100\text{nm}$; In red : the conductance obtained with the formula by Casimir (equ. 1.22); In blue : the conductance obtained with the effective mean free path (equ. 2.18).

η_0 is not exactly known, and is specific to the studied nanowire. However with the usual e-beam lithography, one can expect a mean value of roughness around 5 nm. In figure 2.21 a close-up picture of a nanowire is presented. One can see that the surface is quite smooth, with a mean value of the roughness around 5 nm.

The mean free path, as modified by Ziman, diverges when the temperature approaches zero. This is not physically correct. At the boundary between the nanowire and the thermal reservoirs (what has been called the pads in section 2.3) the phonons are scattered because of a difference in the density of states. One can use Matthiessen's rule for the collision rate : $\tau^{-1} = \tau_{surface}^{-1} + \tau_{boundary}^{-1}$. The mean free path is the product of the collision rate and the speed of sound. As the speed of sound is the same along the nanowire, one can write :

$$\Lambda_{eff}^{-1} = \Lambda_{Ziman}^{-1} + L^{-1} \quad (2.18)$$

where L is the length of the nanowire.

In figure 2.22 the conductance measured in a $5\mu\text{m} \times 150\text{nm} \times 100\text{nm}$ Si nanowire is shown. The conductance obtained with equation 2.15 and the conductance obtained by replacing the Casimir mean free path by the effective mean free path (equation 2.18) have also been plotted.

All these conductances behave similarly. $K_{Casimir}$ is an order of magnitude below the measured conductance. For K_{Ziman} , the mean value of roughness η_0 has been set to 4 nm. The mean free path varies between 2 μm and 200 nm, which is in a very good agreement with the nanowire size. This validates the Casimir-Ziman model. It means that in such a nanowire,

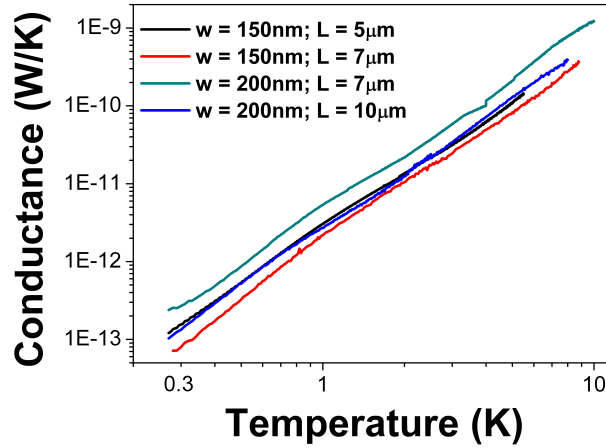


Figure 2.23: Thermal conductance of four nanowires in a log-log scale. w is the width and L is the total length of the nanowire. All the wires have the same 100 nm thickness.

phonons act as in a three dimensional sample. The scattering at the surface is a mix between specular and diffusive reflection. Normalization within the framework of the Casimir-Ziman model is therefore very consistent.

2.4.3 Influence of the dimensions

As the wires size measured during my PhD are not strictly the same, it is important to have a proper normalization. In the previous section, it has been shown that the Casimir-Ziman model can be used. In this section, nanowires with different sizes will be presented. The conductance of four nanowires are shown in figures 2.23 and 2.24. They have the same thickness, 100 nm. Their widths are 150 nm and 200 nm. Their total lengths are 5 μm , 7 μm and 10 μm . As a reminder, the 3ω method heats the wire in the center, so that a single wire acts like two wires, of half the length, in parallel.

In figure 2.23, the conductances without any normalization are presented. All these conductances have the same behavior. One can notice that for nanowires with the same width, the larger the length, the lower its conductance. It is the contrary for two wires with the same length : the larger the width, the higher its conductance. This is consistent with what is expected.

In figure 2.24, conductances have all been normalized by dividing them by the Casimir-Ziman conductance at 1 K, β_{Cas} (cf equation 2.15). The mean free path is modified by the Ziman model. All the conductances become very close to each other. This means that the normalization is consistent. In chapters 3 and 4, this normalization will be used.

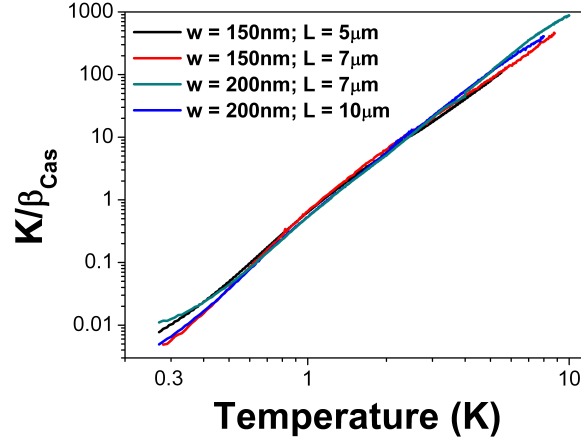


Figure 2.24: Thermal conductance of four nanowires divided by β_{Cas} in a log-log scale. For all the range of temperature, the samples keep almost the same effective conductance.

2.4.4 Influence of the contact

As it has been shown in section 1.4.6, a contact resistance may appear at the junction between the nanowire and the pads (i.e. : the thermal reservoirs). This contact conductance has been calculated (see section 1.4.6) [22, 23] :

$$K_c = \frac{2\pi^3}{15} \frac{k_B^4}{\hbar^3} \frac{0.923 b^2}{v_s} T^3 \quad (2.19)$$

where b is the radius of the nanowire, in our case it will be half the width of the nanowire. This conductance has been plotted with the measured conductance of a $10\mu\text{m} \times 150\text{nm} \times 100\text{nm}$ nanowire (figure 2.25). In this figure four times the universal quantum of thermal conductance is also represented (see section 1.4.5) :

$$K_0 = \frac{\pi^2 k_B^2 T}{3h} \quad (2.20)$$

This conductance should be the conductance of a one-dimensional wire with no contact resistance to the thermal reservoir.

One can see in the figure 2.25 that the contact conductance is one order of magnitude higher than the measured conductance. This means that the contact conductance should not affect our measurements, as this conductance is in series with the wire conductance. The transmission from the wire to the thermal reservoir should not be a limiting factor in our experiments. However the geometry used in the theoretical work consists in a cylindrical nanowire connected to a three-dimensional reservoir. In our case, it is a rectangular nanowire

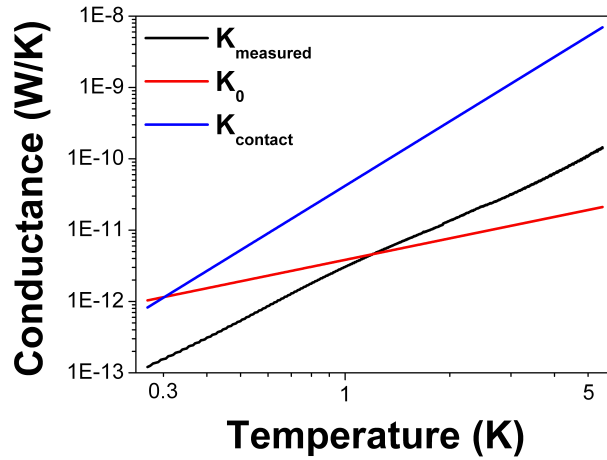


Figure 2.25: In black : Thermal conductance of a Si nanowire of dimension $10\mu\text{m} \times 150\text{nm} \times 100\text{nm}$; In red : four times the universal quantum of thermal conductance; In blue : the contact conductance obtained with formula 2.20.

and the reservoir is a three-dimensional silicon oxide. This can introduce deviations from the theory. Further investigations on the contact have been made and will be presented in chapter 3.

If the universal quantum of thermal conductance is on the same order of magnitude than the measured conductance, it does not behave the same. It is not surprising, because even in the ideal case (perfect transmission), the conductance should be quantized below 300 mK [14, 26]. This is because the phonon dominant wavelength is on the same order of magnitude as the cross section of our nanowire ($\lambda_{Dom} = 200\text{ nm}$ at 0.5 K). Thus the wire cannot be considered as one dimensional concerning phonon transport.

However, one can notice that at 300 mK, the contact conductance is on the same order as the quantum of thermal conductance. It means that thermal contact resistance should have an effect on the conductance when the temperature is below 300 mK for a one-dimensional wire.

2.4.5 The other parasitic thermal paths

A NbN transducer has been deposited on top of the wire. This transducer introduces several parasitic thermal conductances which may disrupt the phonon thermal conductance in silicon (see fig 2.26). One needs to ensure that the thermal properties are actually coming from the phonons inside the silicon. Several theoretical works allow to calculate the different values of these parasitic thermal paths.

The signal is carried through electrons for both heating process and temperature measurement.

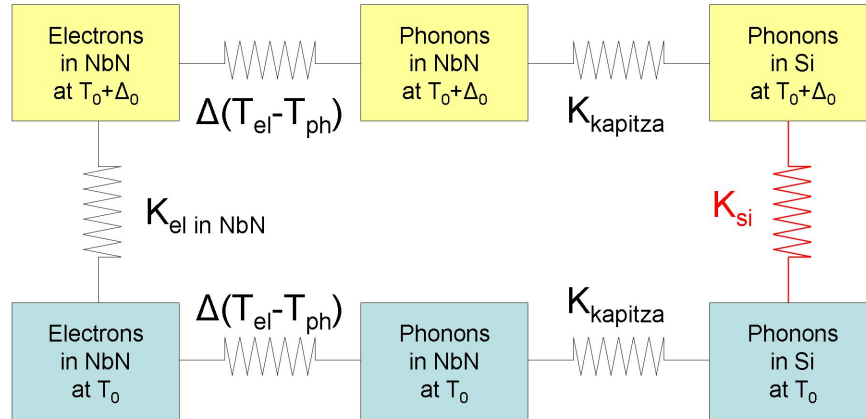


Figure 2.26: Schematic representation of the heat transfer in this system. One want to have the thermal conductance measured equal to the thermal conductance of phonons inside the Si (in red).

However we are interested in the heat carried by phonons. One needs to be sure that the two baths (electrons and phonons) are thermalized. This can be checked using the formula by Wellstood *et al.* [63]. This formula allows determining the difference in temperature between the electro bath and the phonon bath in the NbN: $T_{e^-}^5 - T_{ph}^5 = P / (Vol \cdot g_{e-ph})$; T_{e^-} and T_{ph} are the temperature of electrons and phonons bath respectively; P is the electronic power; Vol is the volume of the metal; and g_{e-ph} is a electron-phonon coupling constant depending on the material. A numerical application gives at 1K, a difference of temperature for electron and phonon baths under 1 mK (For a typical measurement : $P = 2.10^{-13} W$; $Vol = 7.10^{-14} cm^3$; $g_{e-ph} = 1000 W/K^5/cm^3$). This difference is negligible as the increase of the temperature inside our sample is around 10 mK.

Concerning the thermal conductance, two parasitic thermal paths may change the measured conductance. The first one is in parallel with the phonon conductance. It is the thermal conductance of electrons inside the NbN (called K_{e^-}). The other one, which is in series, is the thermal conductance at the interface between the NbN and the Si (known as the Kapitza conductance $K_{Kapitza}$). In order to be sure that the conductance measured ($K_{measured}$) is the conductance of phonons inside the Si, the condition $K_{e^-} \ll K_{measured} \ll K_{Kapitza}$ must be fulfilled. The thermal conductance of electrons inside the NbN can be known by the Wiedmann-Franz law : $K_{e^-} R = L_0 T = 2.44 \cdot 10^{-8} T$. This has been plotted in figure 2.27.

The Kapitza conductance comes from a lattice mismatch between NbN and Si [61]. Two main models can be used to determine such a mismatch : The acoustic mismatch model (AMM) and the diffuse mismatch model (DMM). In the AMM, phonons are governed by continuum acoustics and the interface is treated as a plane. Thus, no scattering events happen. Phonons

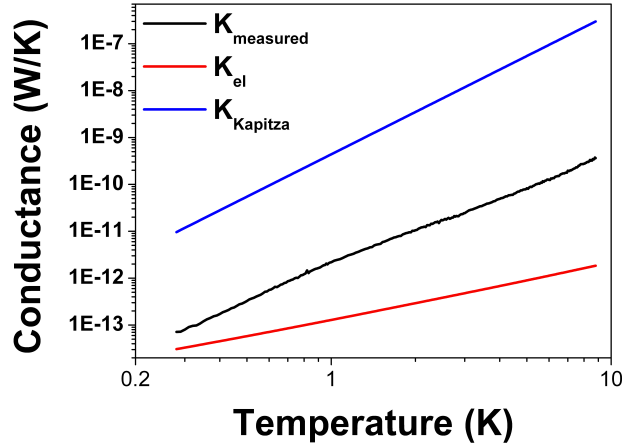


Figure 2.27: In black the thermal conductance measured with the 3ω method; In red the electronic conductance; and in blue, the Kapitza conductance. For details, see the text.

may be reflected, may change their direction but without any energy loss. In the DMM the extreme opposite is used : all the phonons are diffusely scattered at the interface. At low temperature (below 60 K), both model give the same formula : $K_{\text{Kapitza}} = T^3 \cdot S_{\text{exch}} / r$; where S_{exch} is the exchange surface in cm^2 and r a number depending on the materials in contact. This formula is valid for both gas-solid and solid-solid contacts. For solid-solid contact the r number is almost the same for AMM and DMM. For our NbN-Si contact, r has been set to twelve [61].

This Kapitza conductance has also been plotted in the figure 2.27; one can see that $K_e \ll K_{\text{measured}} \ll K_{\text{Kapitza}}$. Therefore, the measured conductance is the expected conductance of phonons inside the silicon.

2.5 Conclusion

All the tools needed to perform measurements at low temperature on silicon wires have been presented in this section, from the fabrication, to the measurements. Measurements on straight nanowires have allowed to ensure a normalization within the framework of the Casimir-Ziman model. In this model, the mean free path, which is related to the size of the wire, has a significant effect on the conductance. It will then be possible to modify the conductance by adjusting the nanowire shape.

As it has been shown, parasitic thermal paths do not affect our measurements. The influence of thermal contact conductance has been quickly investigated. Further investigation is needed, and will be presented in the next chapter.

3 Investigation of the thermal transport at the junction between a nanowire and a thermal bath

3.1 Introduction

The study of the thermal transport at the junction between a nanowire and the thermal reservoir is of great importance. As we want to investigate the thermal conductance of a nanowire, we need to be sure that the contact has no effect on the measured conductance. In this chapter, the conductance of nanowires with different shapes of contact will be presented. The design of the contact was made to look like a catenoid (see figure 3.1). This shape should normally have the larger reduction of the contact resistance (i.e. a transmission coefficient close to 1)[14].

3.2 Theoretical works

The most adapted model for thermal contact resistance seems to be the one developed by Chang and Geller [22], because no approximation on the size of the nanowire has been made. Also, in this model, they investigate the transmission coefficient of a cylindrical nanowire to a three-dimensional thermal bath, which is quite similar to our samples.

In this case, shown in figure 3.2, one can write the energy flux as :

$$H^+ = \frac{1}{2\pi} \sum_m \int_0^\infty dk v(k) \hbar \omega_m(k) n(\omega_m(k)) \quad (3.1)$$

where m denotes the modes, k is the wave vector of the phonon, ω_m is the frequency of the m mode, $v(k) = d\omega_m(k)/dk$ is the group velocity, and $n(\omega_m(k))$ is the phonon distribution function, Bose-Einstein distribution in our case.

With the group velocity, it is possible to transform the integral to an integral over frequencies :

$$H^+ = \frac{1}{2\pi} \sum_m \int_{\omega_m}^\infty d\omega \hbar \omega_m(k) \frac{1}{\exp\left(\frac{\hbar\omega}{k_B T}\right) - 1} \quad (3.2)$$

Chapter 3. Investigation of the thermal transport at the junction between a nanowire and a thermal bath

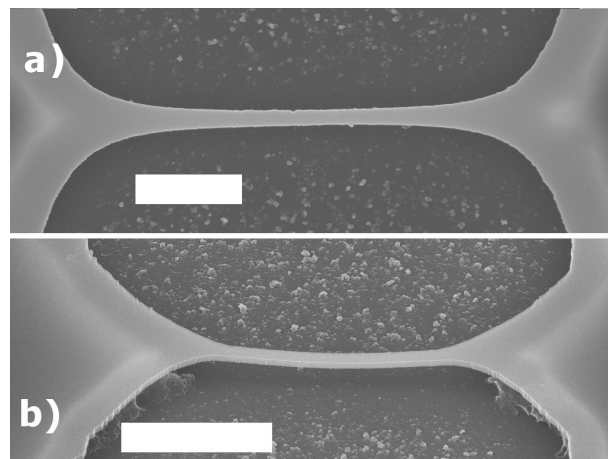


Figure 3.1: SEM picture of two nanowires with a catenoidal-like shaped interface. The scale bars for a) and b) is $2 \mu\text{m}$.

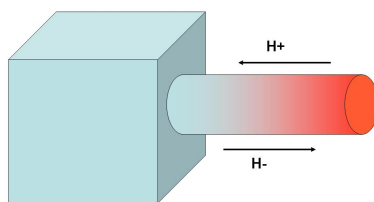


Figure 3.2: Schematic description of the energy flux in a nanowire to a three-dimensional thermal bath.

where ω_m is the cutoff frequency of the m th mode.

The thermal conductance is given by subtracting the analogous expression H^- for the left-moving phonons (in fig. 3.2) given by eq. 3.2. The temperature for the left-moving phonons is the reservoir temperature T , whereas it is the temperature $T + \delta T$ for the right-moving phonons. The thermal conductance is then given by :

$$K(T) = \lim_{\delta T \rightarrow 0} \frac{H^+(T + \delta T) - H^-(T)}{\delta T} \quad (3.3)$$

Assuming that the transmission between the nanowire and the thermal reservoir is not perfect, one can write :

$$K(T) = \frac{d}{dT} \left(\frac{1}{2\pi} \sum_m \int_{\omega_m}^{\infty} d\omega \hbar \omega_m(k) \frac{1}{\exp\left(\frac{\hbar\omega}{k_B T}\right) - 1} t(\omega) \right) \quad (3.4)$$

where $t(\omega)$ is the transmission coefficient. In this work it is assumed that this coefficient is the same for transmission from the nanowire to the thermal reservoir than from the thermal reservoir to the nanowire.

After calculating the derivative, one find the general expression :

$$K(T) = \frac{\hbar^2}{k_B T} \sum_m \frac{1}{2\pi} \int_{\omega_m}^{\infty} d\omega \frac{t(\omega) \omega^2 \exp\left(\frac{\hbar\omega}{k_B T}\right)}{\left(\exp\left(\frac{\hbar\omega}{k_B T}\right) - 1\right)^2} \quad (3.5)$$

Determining the transmission coefficient is therefore essential to know the thermal conductance. Chang and Geller find the transmission coefficient for each mode (for silicon nanowire) :

$t(\omega) = 1.91(b\omega/v_l)^2$ for the longitudinal mode;

$t(\omega) = 1/6 * (b\omega/v_{tor})^4$ for the torsional mode;

And $T(\omega) = 0.268(b\omega/v_{flex})^5$ for the two flexural modes.

At low frequency (which means at low temperature, as we are looking for thermal phonons) only the longitudinal mode contributes. Then Prasher, Tong and Majumdar give an analytical form for the thermal conductance [23] :

$$K_c = \frac{2\pi^3}{15} \frac{k_B^4}{\hbar^3} \frac{0.923}{v_s^2} \frac{b^2}{v_s^2} T^3 \quad (3.6)$$

where $b = \sqrt{section}$ is the radius of the nanowire, v_s is the group sound velocity for the longitudinal mode.

Chapter 3. Investigation of the thermal transport at the junction between a nanowire and a thermal bath

As mention earlier, to compare nanowires with different sizes, the framework of the Casimir model will be used. The conductance will be divided by β_{Cas} . Therefore the normalized theoretical contact conductance can be written as :

$$K_c/\beta_{Cas} = 4.7 \times 10^{-4} \frac{k_B^{4/3} L}{\hbar \Lambda} T^3 \quad (3.7)$$

In the case where the transmission coefficient is close to one and when the nanowire acts like a one dimension channel, the conductance becomes quantized. By replacing $t(\omega)$ by one, equation 3.5 gives for each mode (the four acoustic modes) :

$$K_Q = \frac{k_B^2 \pi^2}{3h} T \quad (3.8)$$

where h is the Planck constant.

Tanaka, Yoshida and Tamura [26] demonstrate that a plateau corresponding to four times the quantum of thermal conductance should appear for a temperature value of $T_b = 2\pi\hbar v_s/k_B\vartheta$. ϑ is a characteristic length. It is defined as, if w is the width which varies along the x axis : $w(x) = e \cosh^2(x/\vartheta)$. It can be seen as the length of the wire over which the cross-sectional area can be regarded as uniform. For our samples, the temperature T_b is around 100 mK. This is a temperature lower than our range of study. No quantization effects will be expected, even if the transmission coefficient is close to one.

3.3 Measurements and normalization

In figure 3.3 thermal conductances for three nanowires with a catenoidal shape interface are represented. Their geometrical parameters are presented in the table 3.1. Thermal conductance for a straight nanowire, the contact conductance of equation 3.2, and four times the quantum of thermal conductance are also shown. In inset the conductances normalized to four times the quantum of conductance are represented. As expected from previous measurements, no plateau can be seen.

For all the samples, the contact conductance is almost one order of magnitude higher than the measured conductances for temperatures above 0.5 K. Below 500 mK, one sample shows a significant increase of its thermal conductance. It becomes quite close to the contact conductances. The other samples present an opposite effect. Their conductance tends to drop, even below the conductance of the straight sample.

Even if all measured conductances do not have the same value, their behavior seems quite similar. In order to compare them, the normalization with β_{Cas} has been done. For the contact conductance and the quantum conductance, the size used for normalization will be the same as that of the straight nanowire.

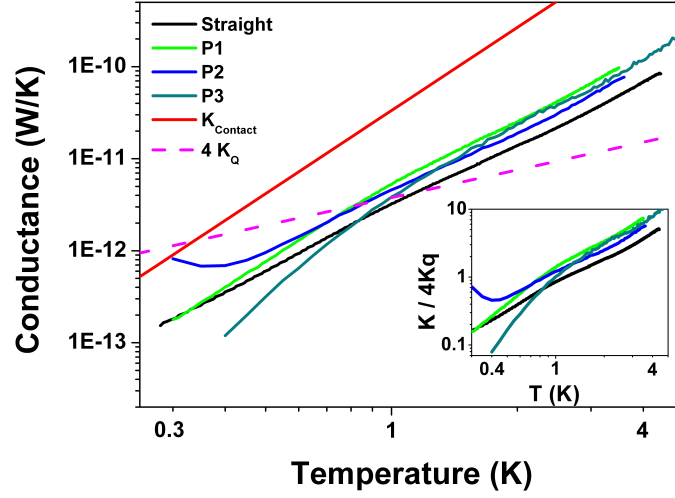


Figure 3.3: Measured thermal conductance of a straight nanowire (size : $10 \mu\text{m} \times 200 \text{ nm} \times 100 \text{ nm}$) and three nanowires with a profiled shape interface with the thermal bath (see figure 3.1). In red the contact conductance (cf equation 3.2) is represented and in dashed line, four times the universal quantum of thermal conductance (K_Q). The inset shows the measured conductances normalized by four times K_Q .

Sample	Effective length (μm)	width (nm)	thickness (nm)	MFP at 1 K (nm)
straight	5	200	200	860
P1	2.9	200	200	830
P2	3.5	200	200	800
P3	2.8	200	200	760

Table 3.1: Geometrical parameters of the nanowires presented in this chapter. The effective length is the length corresponding to the straight cross section of the nanowire. The effective MFP at 1 K is also represented.

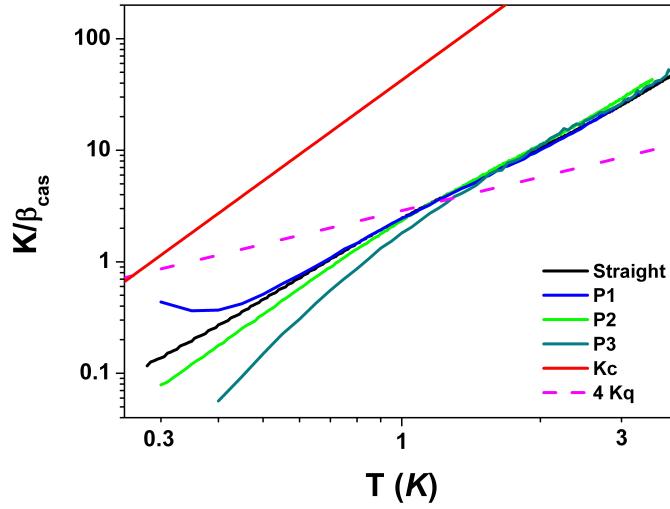


Figure 3.4: The conductances of the same sample as in figure 3.3 normalized by β_{Cas} (see equation 2.15). For the contact conductance (K_C) and the quantum conductance ($4K_q$), the size used for the normalisation is the same as for the straight nanowire. All samples have the same conductance for temperatures above 1.5 K.

To do this normalization one needs to know the length of the wire. However, with a shape such as figure 3.1, it is quite hard to define the length. With SEM picture of the sample (fig 3.1), one can estimate the length of the straight part of the nanowire (see table 3.1). As one can see in figure 3.4, these values for the length give a K/β_{Cas} identical for all the samples for temperature above 1.5 K. These values of lengths are therefore accurate.

In figure 3.4 the conductances normalized by β_{Cas} have been plotted. One can see that above 1.5 K, all the conductances are very close to each other; and the contact conductance calculated by Prasher *et al.* [23] is more than one order of magnitude higher than these measured conductances. These results clearly indicate that the measured conductances are the intrinsic conductance of the wires; meaning the transmission coefficient between the nanowire and the thermal bath is close to one above 1 K.

Below 1 K, the conductances have a very different behavior. This could originate in the measurement method itself. The maximum rise of temperature Δ_0 must be much lower than the temperature of study. If this is not fulfilled, then the temperature in the nanowire cannot be considered as the same than in the thermal bath [44]. In our measurements, at 300 mK, Δ_0 is 10 mK in the straight wire, 25 mK in P1, 3 mK in P2, and 30 mK in P3. As the difference is less than 10 %, it should not influence our measurements. So experimental problem linked to the temperature amplitude oscillation in the 3ω method can be discarded.

The reason for such a large dispersion may come from the mean free path. For the 3ω method

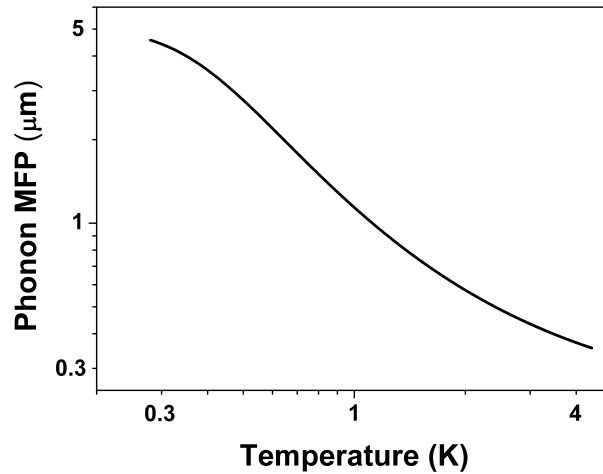


Figure 3.5: Phonon MFP for the straight nanowire. For temperature below 1 K, the MFP becomes larger than the $1 \mu\text{m}$.

to be implemented, one needs to write and solve locally the equation of heat transfer. To do that, it is essential to define a local temperature inside the nanowire. Following studies made by Hartmann and coworkers [64, 65, 66] local temperature is only expected to exist in systems with effective interactions, meaning with energy exchange. When a specular reflection happens at the surface however, no energy is exchanged. Thus there is no physical meaning of speaking about temperature in a volume smaller than $vol_{min} = \Lambda_{phonon}^3$. This is not physically obvious, as it means that the temperature, which is an intensive property, becomes dependent on the MFP, i.e. on the sample studied.

Below 1 K, the phonon MFP becomes larger than $1 \mu\text{m}$ (see fig 3.5). The volume of the nanowire is $5 \mu\text{m} \times 0.2 \mu\text{m} \times 0.2 \mu\text{m}$. Thus the limit of the local temperature notion is reached. The 3ω method becomes not relevant for sub-Kelvin temperature and should be replaced by a more appropriate method.

3.4 Conclusion

In this chapter, it has been demonstrated that heat flows well from the wire to the thermal bath for temperature above 1 K. The measured conductances correspond indeed to the intrinsic thermal conductance of the nanowire. For temperature below 1 K, some dispersion on the measured conductances implies that the 3ω method may have reached its limit. This comes from the fact that as the temperature decreases the phonon mean free path increases. Thus the local temperature, necessary to solve the heat transfer equation and then apply the 3ω method, cannot be defined inside the wire. A new method is needed to perform measurements below 1 K.

4 Modification of phonon transport in corrugated nanowires

4.1 Introduction

Up to now, the phonon-boundary scattering has been treated as a combination of diffusive and specular reflection in the Casimir-Ziman model. It has been shown that this treatment is in a very good agreement with the experimental data in straight nanowires. When Ziman and coworkers calculated the mean free path (MFP), they considered a phonon coming normally to the surface. They did not take into account the direction of the reflected phonon. If backscattering processes occur, then the reflected phonon flows in the direction opposite to the heat flux. Thus it may decrease the MFP. In a straight nanowire, no backscattering can happen. However in a sawtooth nanowire, as described by Arden L. Moore and coworkers [67], backscattering occurs. In their paper, these authors show that a sawtooth shape of the surface affects the MFP, and therefore the thermal conductance. The sawtooth wire is represented on figure 4.1. The arrows represent phonons specularly reflected at the surface. This may be a new exciting way to manipulate heat flux at the nanoscale.

The same idea was used by Rajbapour and coworkers [68]. In this study, the transmission between two materials was investigated with an interface boundary designed with sawtooth shape (see figure 4.1).

In this chapter, the thermal conductance of corrugated nanowires is investigated. In these nanowires the surface has been periodically patterned (see figure 4.2). This design should increase considerably the probability of phonon-boundary scattering. In table 4.1, the characteristics of each nanowire are shown. Four corrugated nanowires will be compared to a straight nanowire.

4.2 Measurements

In figure 4.3, the measured conductances are presented. One can notice that the samples have almost the same conductance, both in order of magnitude and behavior. This analysis

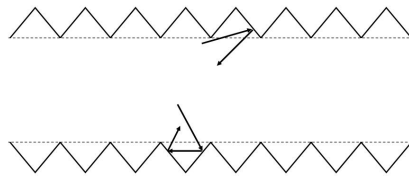


Figure 4.1: Schematic diagram of the sawtooth nanowire [67]. The arrows represent phonons which are specularly reflected at the surface. The same geometry was made in the study by Rajbapour *et al.*, but instead of investigating the reflection at the interface between a Si nanowire and the vacuum, these authors are looking for the transmission across a sawtooth interface between two materials.

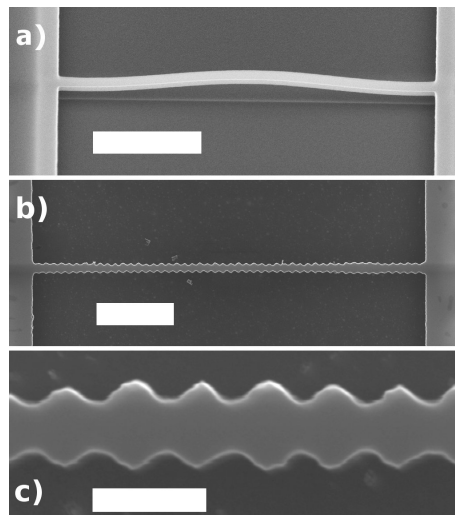


Figure 4.2: SEM images of the straight (a) and the corrugated (b) nanowires; (c) corresponds to the top view of the corrugated nanowire. The scale bars correspond to (a) $2\ \mu\text{m}$, (b) $2\ \mu\text{m}$, and (c) $300\ \text{nm}$.

4.2. Measurements

Sample	L (μm)	w_{min} (nm)	w_{max} (nm)	period (nm)	MFP (nm)	MFP_N	b	p
straight	5	200	200	0	909	1	2.27	0.60
C1	4.4	130	250	200	114	0.13	2.52	-0.32
C2	5	140	245	200	181	0.2	2.74	-0.10
C3	5	160	260	200	356	0.39	2.54	0.22
C4	4.4	230	250	200	140	0.15	2.6	-0.27

Table 4.1: Geometrical parameters and physical data extracted from the thermal conductance measurements of the straight and corrugated nanowires (C_i). w_{min} and w_{max} designate the minimum and maximum width of the corrugated nanowires and L their length. The thickness of the silicon wires is equal to 200 nm. MFP_N is the MFP of the wire divided by the MFP of the straight nanowire.

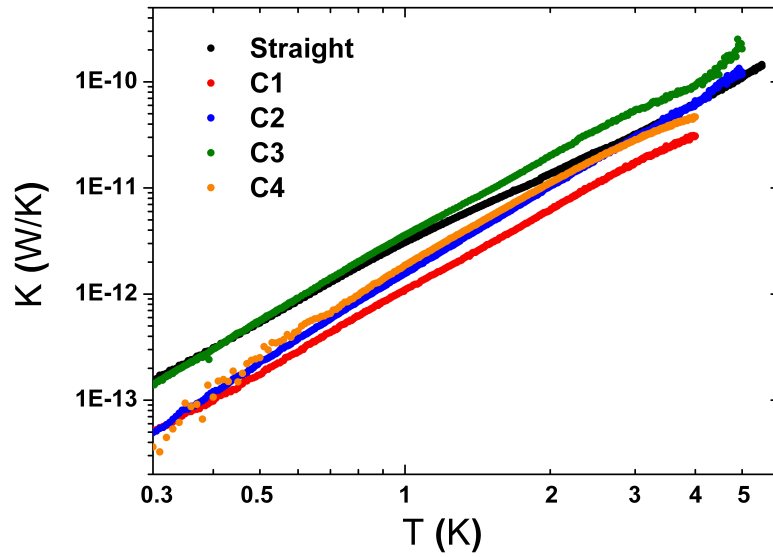


Figure 4.3: Thermal conductance versus temperature for a straight nanowire and four corrugated nanowires in the log-log scale. The slopes of the conductance of all these samples are quite similar.

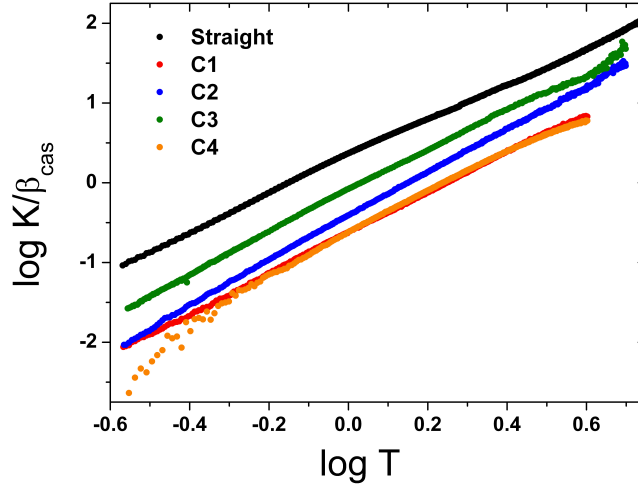


Figure 4.4: Log-log plot of the normalized thermal conductance of the straight and four corrugated nanowires versus the temperature. As expected the straight wire has a higher conductance than the corrugated ones. the difference in the corrugated should be linked with the difference in their MFP. One can see the linear relation between the logarithm of the normalized conductances with respect to the logarithm of temperature.

of the data must be carefully done. As one can see in table 4.1 the lengths and cross section are not the same for all these wires. The normalization within the framework of the Casimir-Ziman model must be done. The scientific objective of these experiments is to measure the influence of the corrugation on the MFP of the phonons. With the Casimir-Ziman model, MFP depends on both temperature and the sample cross section. MFP is thus hard to calculate in the presence of a corrugated surface. As thermal conductances are linear in a log-log scale, it means that $K \propto T^b$; b is the exponent of the temperature power law, which should be close to 3 for three dimensional samples (see equation 1.22). Thus, the effective MFP should be proportional to the temperature. Writing this mathematically gives : $\Lambda_{eff} = c.T^\delta$; where c and δ are unknown factors. As δ is quite hard to extract from measurements, we will consider the MFP to be temperature independent. This can be done because the Casimir conductance has almost the same behavior as the measured conductance (as it was seen on section 2.4).

For the normalization, the Casimir MFP will be used : $\Lambda_{Cas} = 1.12\sqrt{e.w}$; where e is the thickness of the nanowire and w its width. It leads to :

$$K/K_{Cas} = \Lambda_{eff}/\Lambda_{Cas} \tag{4.1}$$

Then $\log(K/\beta_{Cas})$ will be plotted. As it is proportional to the logarithm of the temperature,

one can write :

$$\log(K/\beta_{Cas}) = a + b.\log(T) = 10^a.T^b \quad (4.2)$$

and find graphically the factors a and b . Here, 10^a can be considered as the product between the effective MFP and the Casimir MFP (see equation 4.1). In the Casimir model b is equal to three. The difference between b and 3 is linked to what has been previously called δ (which is the temperature power law of the effective MFP). However, we have no proof that δ is exactly the difference between b and 3. This is the reason why we decide to neglect the temperature dependence of the MFP.

On figure 4.4, the conductances normalised by β_{Cas} are presented. The width used in the Casimir formula (β_{Cas}) is an average value of the corrugated width. The effective MFP and the b factor can be found on the table 4.1. Moreover, from the effective MFP, the p factor of the Ziman model can be deduced ($\Lambda_{eff} = (1 + p)/(1 - p)\Lambda_{Cas}$).

4.3 Impact on the mean free path

As one can see in table 4.1, the MFP in the corrugated sample is almost an order of magnitude smaller than in the straight nanowire. This effect can only be attributed to the corrugation. Moreover, for samples C1, C2, and C4, the effective MFP is patently smaller than the smallest section of the nanowires, demonstrating a phonon flux weaker than the one expected in the Casimir limit. For the straight sample, the phonon MFP is two times higher than the nanowire width. It is a signature of ballistic phonons. As the factor p is equal to 0.6 for the straight wire, we found negative values for C1, C2 and C4. A negative value is not physically sound, as it is a probability of having a specular reflection. As proposed by Moore *et al.*, this reduction of p , down to negative values, is a signature of the presence of strong phonon trapping in the wire due to multiple phonon scattering or even backscattering.

For the nanowire C3, the MFP is not as reduced as in the others nanowires. However, there is still a reduction of a factor 4 compared to the straight nanowire. The difference in value with the other nanowires may come from a difference of the roughness in the nanowire C3. If C3 has a smoother surface than the others nanowires, it may explain this difference. This will be discussed with a Monte Carlo simulation.

To illustrate the difference in the MFP, in figure 4.5 the effective MFP of the nanowire C1 has been plotted together with the MFP in the straight nanowire and the Casimir MFP. The fact that the MFP of the corrugated is on the order of the corrugation illustrates the phonon trapping inside what one can call the cavity of the surface. Moreover, it is clear that the MFP in the corrugated nanowire is much smaller than the Casimir limit. It means that a corrugated surface has the same effect as introducing internal scattering in a nanowire.

A way to ensure that the reduction in MFP is really due to multiple scattering is to make a

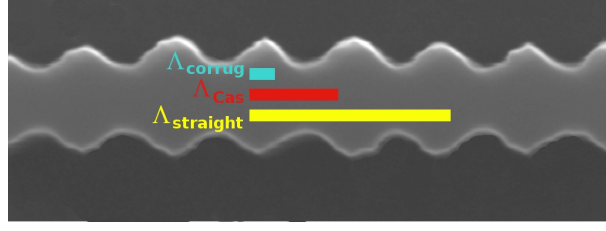


Figure 4.5: The Casimir MFP ($\Lambda_{Cas} = 220 \text{ nm}$), the effective MFP in the straight nanowire ($\Lambda_{straight} = 454 \text{ nm}$), and the corrugated nanowire C1 ($\Lambda_{corrug} = 57 \text{ nm}$) are compared to the actual geometry of the corrugated nanowire. One can see that the MFP of the corrugated wire is much smaller than the width, whereas the MFP of the straight wire is much higher.

Monte-Carlo simulation (MC). As multiple scattering effects involve a corpuscular behavior for the phonons, it is particularly well handled by a Monte Carlo analysis. Ali Rajabpour of the Imam Khomeini International University and Sebastian Volz of the Laboratoire d'Energétique Moléculaire et Macroscopique made a simulation using the ray tracing principle [68]. The principle is that phonons are emitted from one side of the wire with a random initial direction and a random initial position. The frequency dependence is discarded. The phonons are then tracked until leaving the wire through one of its sides. The ratio between the number of phonons reaching the other side $N_{through}$ to the initial number of phonons N defines the transmission $T = N_{through}/N$. The only scattering mechanism is generated by the surfaces and was modeled by different specularities parameters ranging from $p = 0$ to $p = 1$ as reported in figure 4.6; the value of the parameter p derived from the thermal measurement of the straight nanowire is $p = 0.6$. The transmission coefficients can then be related to the MFP through the relation :

$$T = \frac{1}{1 + \frac{3}{4} \frac{L}{\Lambda}}. \quad (4.3)$$

In this equation, Λ stands for any MFP and L is the length of the wire.

In figure 4.6, the results of the simulation are compared to the experimental MFP. One can see that the trend of the simulation is in good agreement with experiment, especially for samples C1, C2 and C3. Those samples may have different local roughness, hence different values for the parameter p . Here the parameter p represent the local probability of a specular reflection, whereas in table 4.1 p represented the global probability of a specular reflection.

One can find a MFP value significantly close between MC simulation and experiments, when p is adequately adjusted. One can say that MC simulations support the experimental fact that in the presence of corrugation, the MFP is strongly reduced. This reduction may be attributed to the occurrence of phonon multiple scattering, which is inherent to the ray tracing method.

The sample C4 shows a behavior which cannot be described by the simulations. However,

4.4. Impact of the corrugation on the dispersion relation

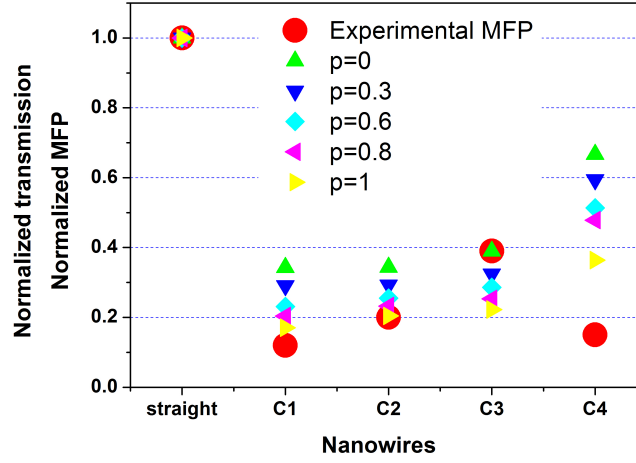


Figure 4.6: The red full circles are the experimental MFP normalized by the MFP in the straight nanowire. The Monte Carlo simulations have been performed with different parameters p (see the figure legend). The transmissions obtained by the MC simulations are normalized to the transmission in the straight wire.

other mechanisms may be responsible for such an MFP reduction. Two scenarios of phonon scattering have recently been proposed which could explain a thermal transport far below the Casimir limit: coherent effects, involving correlated multiple scatterings of phonons [69], or strong phonon scattering induced by highly perturbed surfaces (core defects and surface ripples) [70]; validating such scenarios would require further experimental and theoretical investigations.

4.4 Impact of the corrugation on the dispersion relation

Cleland and coworkers investigated the phonon propagation in a periodically modulated nanowire [38]. The nanowire has almost the same shape as our corrugated nanowires. However their study is made in the absence of scattering processes, i.e. for ballistic phonons in a one dimensional wire. This is not our case. It should happen at lower temperature. Nevertheless their results are quite interesting, as they investigate the effect of corrugation on the dispersion relation. In a so called phononic crystal, they found that a gap should open in the dispersion relation for the longitudinal mode (see figure 4.7). The frequency of the center of gap ω_0 is determined by the period of the modulation $2\pi/G$: $\omega_0 = c_l G/2$; c_l being the velocity of the longitudinal mode. The magnitude of the gap $\Delta\omega$ will be dependent of the amplitude of the corrugation ϵ : $\Delta\omega = \epsilon\omega_0$. This calculation has been made using the longitudinal displacement.

With this study [38] we can calculate the characteristic values of the gap for our nanowires. We find that the gap may open around 100 GHz, with a magnitude of 40 GHz. As the tem-

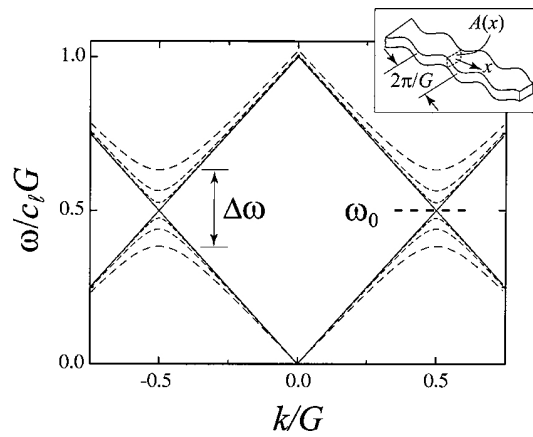


Figure 4.7: Calculated dispersion relation for a straight nanowire (full line) and for phononic crystals with different amplitudes of corrugation (dashed lines). The insert shows such a phononic crystal nanowire. The gap $\Delta\omega$ for a modulation ratio $\epsilon = 0.5$ is indicated, as is the band-gap center frequency $\omega_0 = c_l G/2$.

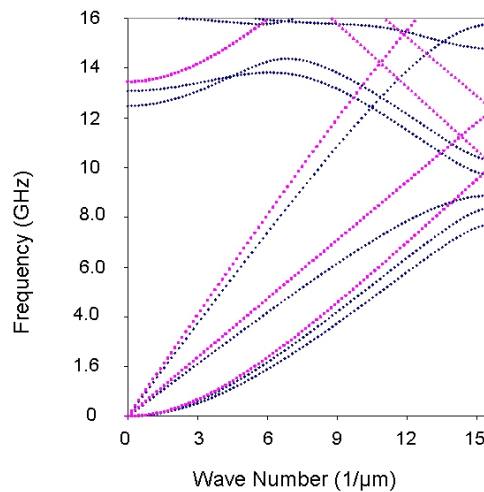


Figure 4.8: Dispersion relation of the sample C2 in dark blue, and the dispersion relation of the straight in magenta. One can see that a small gap opens at 9 GHz.

perature ranges from 300 mK to 5K, the phonon dominant frequency, which is given by $\omega_{Dom} = 4.25k_B T/h$, ranges in our measurements from 30 GHz to 400 GHz (ω at 1 K is around 100 GHz). This means that for ballistic phonon only, a reduction of 40 % may be expected at 1 K for the longitudinal mode due to the phononic crystal effect. As the phonons are mainly diffusive, this reduction is rather small and cannot be discriminated from the multiple scattering effect.

Anne-Christine Hladky and coworkers (from the Institut d'Electronique de Microélectronique et de Nanotechnologie) calculate the dispersion relation for the straight nanowire and the corrugated C2, for all modes. This is shown on figure 4.8. One can see that a gap opens at 9 GHz, which is much smaller than the expected value from the study of Cleland *et al.*. At higher frequency, the confinement introduced by the size of the nanowire folds the modes. This folding induces a broad dispersion on any frequencies. Hence no gap can be seen. A modification of the average sound velocity (which is defined for the i mode as $v_i = \partial\omega/\partial k$) may happen. However this cannot be easily calculated with this model for the dominant phonon frequency.

4.5 Conclusion

We have shown a significant reduction in the phonon MFP in monocrystalline silicon nanowires related to the presence of multiple reflections induced by corrugated surfaces. In the best case, the effective MFP has been reduced by more than a factor of nine compared to the one of the straight nanowire MFP. Consequently, heat transport has also strongly decreased below the Casimir limit. The hypothesis of multiple reflections for phonons is confirmed by the ray tracing analysis showing a strong diminution in the phonon transmission. The dispersion relation has been modified by the corrugation, but the effect happen for lower frequencies. To see the impact on the thermal conductance, one need to perform measurements at lower temperature. This work has been published in Applied Physics Letters [71].

5 Measurements on SiN structures

5.1 Introduction

In section 1.5, a model concerning thermal properties in amorphous materials has been presented. This model, using a two level system for the equilibrium position of an atom (or group of atoms), has some flaws. The origin of these two level systems is not well defined, the calculations for theoretical values of thermal properties requires parameters, and some anomalies with respect to this model cannot be explained. Therefore a phenomenological approach developed by Pohl and coworkers [27] will be used in this chapter.

Three kinds of samples were studied : nanowires, slabs and membranes. Actually, three nanowires two slabs and two membranes have been measured. As for samples of the same kind the measurements gave the same results, just one of each kind will be compared. Along with picture of the samples, a schematic representation with the dimensions of each samples is shown on figure 5.1. Also, the heat flux is represented. For both the nanowire and the slab, heat flows along the length, whereas for the membrane, heat is generated by the NbN transducer and flows to the edge.

5.2 The phenomenological approach

To analyze our results, we use the same approach as Pohl, Liu and Thompson [27]. In this review, the authors list thermal properties and internal friction of almost all the amorphous materials measured so far, on a total of over 60 different compositions. They are investigating bulk materials so thermal conductivity has been compared. Around 1 K, the thermal conductivity κ , is proportional to the square of the temperature. Combining this relation with the gas-kinetic picture (equ. 1.20 in section 1.4.2), one can write :

$$\kappa = \zeta_0 \cdot T^2 = \frac{1}{3} c_D v_s \Lambda \quad (5.1)$$

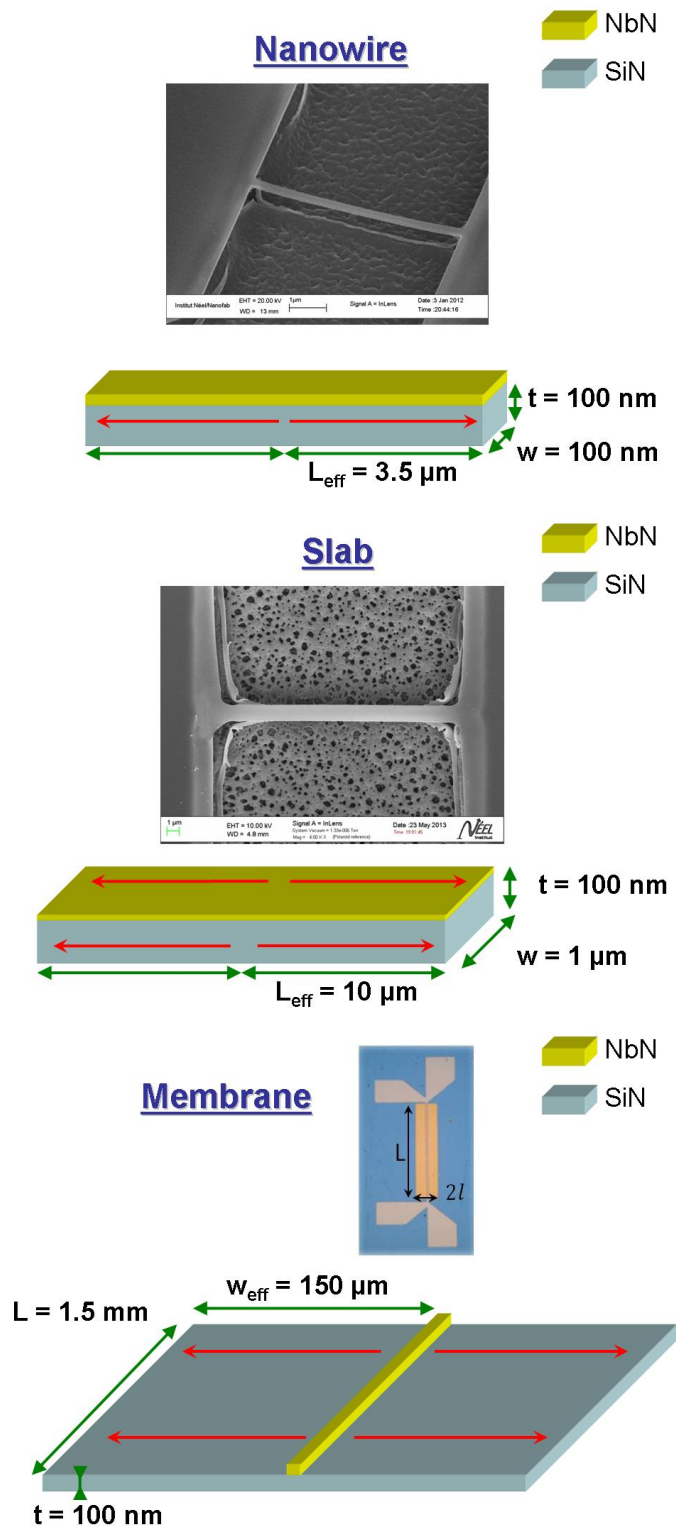


Figure 5.1: Pictures and schematic representation of the three SiN samples studied. The red arrows represent the heat flux. The green arrows the dimensions of these samples. The break at the right edge of the slab may impact the thermal transport. However, the verifications for the 3ω method ensure that the method is properly functioning.

5.2. The phenomenological approach

ζ_0 , is the proportionality factor, corresponding to the thermal conductivity at 1 K; c_D is the volumetric specific heat of the heat carrying phonons; v_s is the average speed of sound, which is 11000 m/s in the SiN of our study; and Λ is the phonon mean free path (MFP).

Pohl and coworkers used data on bulk or millimeter size films. In our case, the mean free path should strongly be affected by the small size of our samples. As the thermal conductivity, which is an intensive property, depends on the mean free path, it is not physically relevant to use κ in our case. However, there exists no proper model which describes accurately the physics of thermal transport inside amorphous materials. This phenomenological approach seems the best up to date. We will use this approach, but in order to not mix the thermal conductivity inside bulk SiN with the thermal conductivity inside our small samples, the notation $\kappa_{extensive}$ will be used to name the extensive concept of thermal conductivity.

Following this approach, one needs to know the specific heat. Inside amorphous materials, the Debye model is in a good agreement with the experiments for temperatures down to 1 K [31, 72]. In this model the specific heat is given by :

$$c_D = \frac{2}{5} \frac{k_B^4 \pi^2}{\hbar^3 v_s} T^3 \quad (5.2)$$

Combining equations 5.1 and 5.2 allow to write for the MFP :

$$\Lambda = \frac{15\hbar^3}{2\pi^2 k_B^4 \pi^2} \frac{\zeta_0 v_s^2}{T} \quad (5.3)$$

As it has been seen on Si nanowires, the MFP is of great importance for thermal transport. One can see that the MFP is inversely proportional to the temperature and depends on the speed of sound, and on the proportionality factor between the thermal conductivity and the square of the temperature (ζ_0).

To compare thermal measurements and acoustic attenuation measurements, Pohl *et al.* introduce what they call the relative inverse phonon mean free path. It is the ratio between the dominant phonon wavelength and the phonon MFP. With the dominant wavelength approximation ($\lambda_{dom} = h.v/4.25 k_B T$) this ratio is given by :

$$\frac{\lambda_{dom}}{\Lambda} = \frac{4\pi^3 k_B^3}{15\hbar^2 4.25} \frac{1}{\zeta_0 v_s} = 0.46 [J.K^{-3}.s^{-1}] \cdot \frac{1}{\zeta_0 v_s} \quad (5.4)$$

This relative inverse phonon mean free path depends on the investigated phonon modes (transverse or longitudinal). However, for both modes, its value is independent of the material (and its composition) and falls within a factor 20 for the materials reviewed by Pohl and coworkers. The order of magnitude of the relative inverse phonon mean free path is the same

for the transverse modes or the longitudinal. This is the reason why we will use an average value of both modes (so with an average value of the speed of sound).

The relative phonon mean free path is important for a theoretical reason. In the two level systems model, a parameter called the tunneling strength describes the coupling between the tunneling states and the lattice. The tunneling strength is given by [27]:

$$\xi_i = \frac{\bar{P}\gamma_i^2}{\rho v_i^2} \quad (5.5)$$

Where \bar{P} is the spectral density of the tunneling states, γ_i is the energy with which they are coupled to the plane-wave lattice vibrations, ρ is the mass density, and v_i is the speed of sound, with i indicating the phonon mode.

Pohl *et al.* demonstrate then the relation :

$$\frac{\lambda_{dom}}{\Lambda} \approx 12.5 \xi_t \quad (5.6)$$

As the relative inverse phonon mean free path, the tunneling strength is the same for almost all amorphous materials within a factor 20. It should be very interesting, if this model is relevant for our samples, to know if a size modification also modifies the tunneling strength.

The aim of our measurements will be to see if the universality behavior is still valid when the dimensions are reduced. If it is the case, then we will see how the mean free path is affected within the framework of this model. To do so, SiN nanowires, slabs, and membranes have been fabricated and measured.

5.3 Measurements on nanowires, membranes and slabs

The measurements have been performed on three kinds of samples shown on figure 5.1. The measurements on the nanowire and the slab have been realized with the same setup as described for the Si nanowires. For the membrane, the measurements have been realized with Hossein Ftouni, and the setup is the one with the Völklein geometry (see section 2.2.2).

In figure 5.2 the conductances of the nanowire, the slab and the membrane are shown in a log-log scale. The conductance of the nanowire looks like a square dependence for all the range of temperature (we found on the graph $K \propto T^{2.10}$). The conductance of the slab seems to show a slight deviation with the temperature squared for the lower temperatures (for $T > 0.5$ K we found $K \propto T^{1.87}$). For the membrane, the conductance is almost constant for temperatures between 0.3 K to 1 K. For temperatures above 1 K, the conductance increases also with a square dependence with respect to the temperature (in this case : $K \propto T^{2.47}$). Quantitatively, the conductance of the nanowire is almost 2 orders of magnitude below the conductance of the

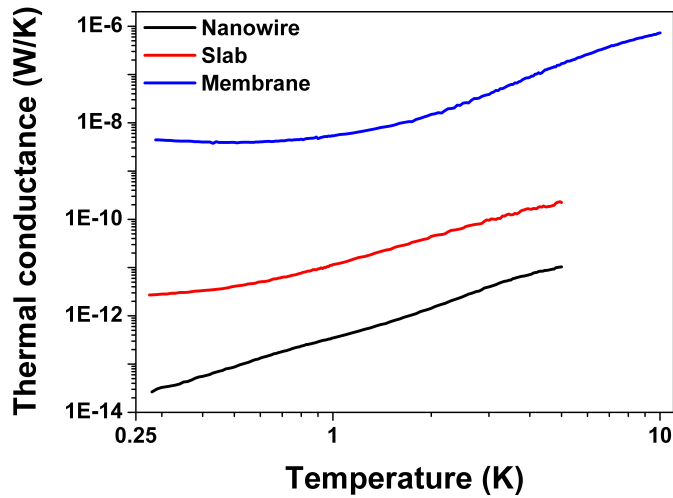


Figure 5.2: Thermal conductances of the nanowire (black), the slab (red), and the membrane (blue) in a log-log scale. The slope for the conductance of all these samples looks the same for temperatures above 2 K.

slab, and 6 orders of magnitude below the conductance of the membrane. This seems to agree with what one may expect (the smallest system has the smallest thermal conductance).

Following the phenomenological approach, the extensive thermal conductivities will be calculated. For the nanowire and the slab, the extensive thermal conductivity is given by : $\kappa_{extensive} = K.L_{eff}/w.t$; where K is the conductance shown on fig. 5.2, L_{eff} , w , and t , are the effective length, the width and the thickness respectively. These dimensions are indicated on figure 5.1. For the membrane, as the heat flows along the width, the extensive thermal conductivity is given by : $\kappa_{extensive} = K.w_{eff}/L.t$; where K is the conductance shown on fig. 5.2, w_{eff} , L , and t , are the effective width, the length and the thickness respectively.

It is important to remember that the extensive thermal conductivity is used to allow comparison and calculation of the mean free path. It is not the real thermal conductivity of the SiN.

In figure 5.3, the extensive conductivities of the samples are shown. Qualitatively, the extensive conductivities behave just as the thermal conductances. This is trivial, as just a normalization by the dimensions has been performed. Quantitatively, the difference between $\kappa_{extensive}$ decreases but is not zero. $\kappa_{extensive}$ for the slab is about twice $\kappa_{extensive}$ for the nanowire. And $\kappa_{extensive}$ for the membrane is three order of magnitude higher than for the nanowire. This difference must come from a difference in the phonon mean free path.

The dependency for the thermal conductivity with the square of the temperature is not obvious on figure 5.3. It is necessary to verify this dependence to apply the model made by Pohl *et al.*

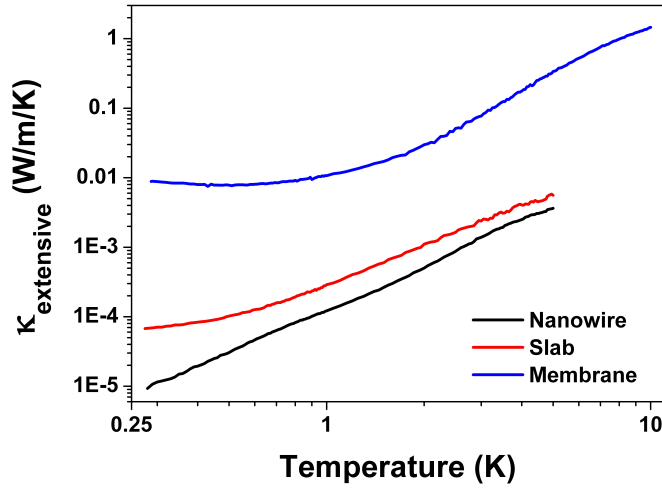


Figure 5.3: Extensive thermal conductivities of the nanowire (black), the slab (red), and the membrane (blue) in a log-log scale. Compared to the thermal conductances, the extensive thermal conductivities of the samples are closer to each others. The reason they do not have the same values (although all the samples are made out of the same material) is due to their small dimensions. In these different samples, the phonons do not have the same mean free path.

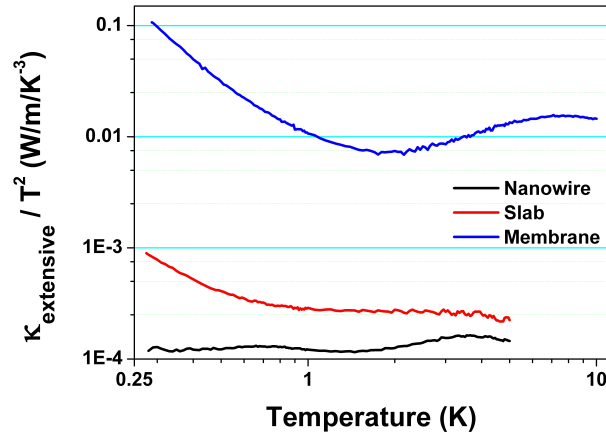


Figure 5.4: Thermal conductivity divided by the temperature squared of a nanowire (black), a slab (red), and a membrane (blue) in a log-log scale. $\kappa_{extensive}/T^2$ of the nanowire is quite constant for all the range of temperature. For the membrane and the slab, the variation of $\kappa_{extensive}/T^2$ is within a factor 2 for temperatures above 1 K.

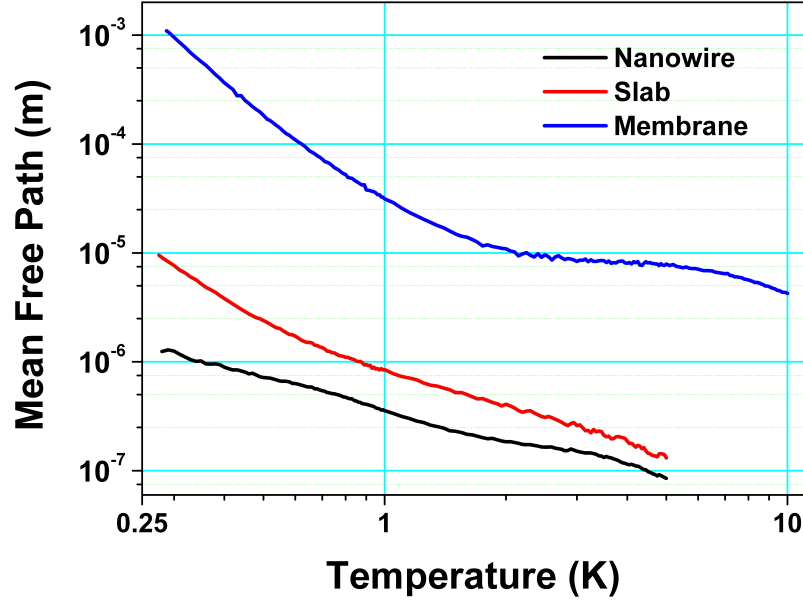


Figure 5.5: Mean free path of the nanowire (black), the slab (red), and the membrane (blue) in a log-log scale. As the mean free paths are very different in all these samples, an impact of the low dimensions of the samples is clearly evidenced by this figure.

To verify it, one can plot $\kappa_{extensive}/T^2$. This corresponds to what has been previously called ζ_0 . It has been done on figure 5.4. In this figure, one can see that $\zeta_0(T)$ for the nanowire is almost constant for all the range of temperature. Its value is $1.4 \times 10^{-4} \text{ W K}^{-3} \text{ m}^{-1}$. ζ_0 for the slab is around $2.5 \times 10^{-4} \text{ W K}^{-3} \text{ m}^{-1}$ for the temperatures above 1 K. And for the membrane $\zeta_0 \approx 1.5 \times 10^{-2} \text{ W K}^{-3} \text{ m}^{-1}$ above 5 K.

As for a quite large temperature range, ζ_0 is constant in all our samples, the model of Pohl and coworkers can be used. The mean free path can be then calculated, as it has been demonstrated with the equation 5.3. In this equation ζ_0 has been set independent of the temperature. In our case, we use the $\zeta_0(T) = \kappa_{extensive}/T^2$ shown in figure 5.4. The MFPs are represented on figure 5.5. For the nanowires, this value of MFP is quite consistent, as ζ_0 is almost constant for all measured temperatures. The MFP of the slab and the membranes for temperatures below 1 K must be taken with caution. For higher temperature, the model should be valid.

Quantitatively, the MFPs of both the nanowire and the slab seems quite consistent. At the lowest temperatures, the MFP approaches the value of the effective length. At the highest temperature, the MFP of the nanowire corresponds to the square root of the cross section ($100 \text{ nm} \times 100 \text{ nm}$). This is similar to the Casimir model. For the slab, at the higher temperatures the value of MFP is slightly above 100 nm. It has been shown, that in such a system, the lowest

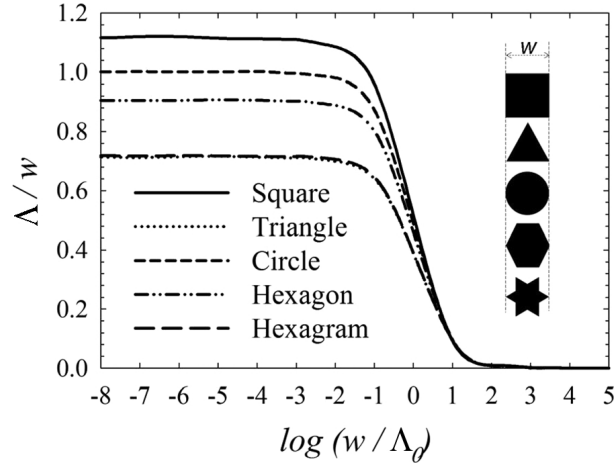


Figure 5.6: Figure taken from [74]. The ratio between the MFP (Λ) and the width (w) is plotted with respect to the log of the ratio between the width and the intrinsic MFP (Λ_0).

dimension (the thickness in our case) plays a key role in thermal transport [73].

In ref. [74] Wang and Mingo investigate the influence of this lowest dimension on the MFP. These authors calculate the MFP with respect to the ratio of the lowest dimension (w) by the intrinsic MFP due to bulk scattering process (Λ_0 , so the ratio is : w/Λ_0 , see figure 5.6). This calculation has been done for different shapes of wire and with different values of the width (the thickness remains the same). In the case of a rectangular section, when the ratio w/Λ_0 is smaller than 0.1, the MFP corresponds to 1.12 times the lowest dimension (i.e. the width). This is the case in the measured slab. And this calculation explains the fact that the MFP in the slab at the highest temperatures is close to 112 nm.

The case of the membrane is different. First of all, as it can be seen on figure 5.4, below 1 K the extensive conductivity does not depend to the power three with respect to the temperature. Therefore the values of MFP for temperatures below 1 K are not trustworthy. Then, in the nanowire and the slabs, the dimensions are on the same order of magnitude. For the membrane however, the cross section seen by the phonons is $100 \text{ nm} \times 1.5 \text{ mm}$. There is more than 4 orders of magnitude between the two dimensions. This huge aspect ratio induces an almost two-dimensional system. In their study, Wang and Mingo showed that in such a system, the MFP should be the same as in the bulk material. This is consistent with our measurements as the MFP in the membrane is almost constant around $10 \mu\text{m}$.

The last step of this approach is determining the relative inverse phonon mean free path (λ/Λ , equ. 5.4). This ratio is of importance for two reasons : firstly, because for almost all the amorphous materials the value is within a factor 20, whatever the method used to measure it. Secondly, in the two level systems model, this ratio is proportional to the tunneling strength. This tunneling strength is an adjustable parameter describing the coupling of the two tunneling states to the lattice (see equations 5.5 and 5.6), which should not change with

5.4. Comparison with the Casimir-Ziman model and the quantum of thermal conductance

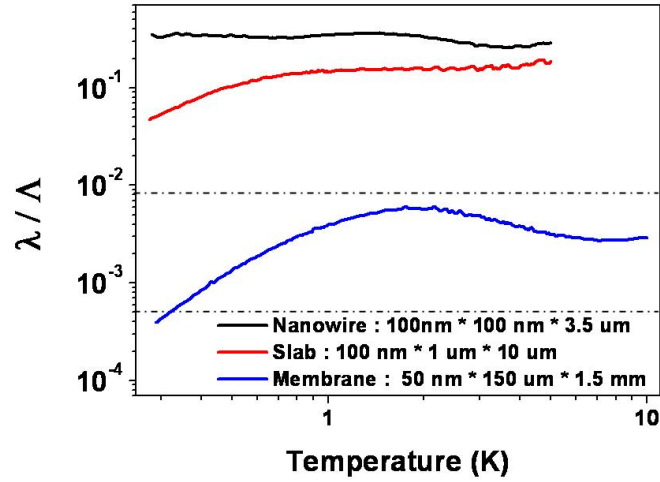


Figure 5.7: Relative inverse phonon mean free paths in the sample studied (same colors as the other figures) in a log-log scale. The values of this ratio for all the materials reviewed by Pohl *et al.* are between the two dashed lines. The membrane result in good agreement with these values, whereas the nanowire and the slab have much larger values.

the dimensions of the sample, at least between membranes and slabs.

The relative inverse phonon mean free paths have been represented for all the temperature range in figure 5.7. One can see that for the membrane, its value is within the range of the other materials reviewed by Pohl and coworkers. The nanowire and the slab have a much higher value of relative inverse phonon mean free path. In the framework of the tunneling state model, it can be interpreted as a more efficient coupling between the tunneling states and the lattice. This can come from the decreasing of the volume to surface ratio.

To conclude, this approach allows us to calculate the MFP in quite good agreement with theoretical works. The normalization with an extensive conductivity, although questionable on physical grounds, seems quite accurate with our measurements. The relative inverse phonon mean free path may give experimental values for further theoretical works. This is of great importance, because a theoretical model to explain the physics of phonon thermal transport inside amorphous materials is still lacking.

5.4 Comparison with the Casimir-Ziman model and the quantum of thermal conductance

In this section, we will briefly try to compare our measurements on the SiN nanowire to the Casimir-Ziman model and the quantum of thermal conductance.

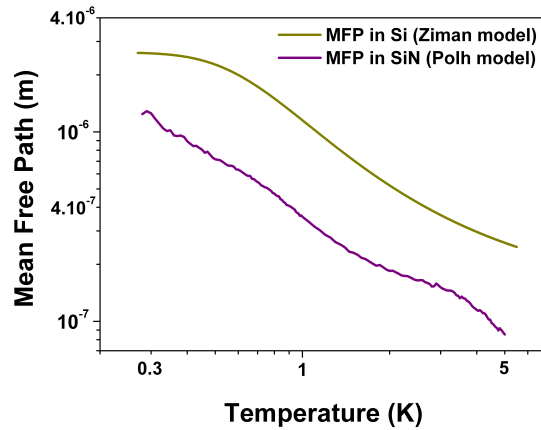


Figure 5.8: Mean free path in a Si nanowire (dark yellow) and in a SiN nanowire (purple). The nanowires have the same dimensions. One would expect to have the same MFP in both nanowires. However, even having the same order of magnitude is a proof of a certain consistency of the phenomenological model of Pohl and coworkers, even in the case of small size systems.

But firstly, it is of interest to compare the MFP in the SiN found with the model of Pohl *et al.* to the MFP of Si found with the Casimir-Ziman model. In figure 5.8 the MFP in the SiN nanowire, and in a Si nanowire of the same dimensions ($3.5 \mu\text{m} \times 100 \text{nm} \times 100 \text{nm}$) are plotted. The MFP of the Si nanowire has been plotted within the framework of the Casimir-Ziman model. These MFP have almost the same order of magnitude and behavior. This means that our interpretation within the framework developed by Pohl *et al.* is quite consistent. The difference in the values of these MFP may come either from a physical reason (the MFP in an amorphous material is smaller than in a crystalline material) or from a problem in the phenomenological model used for SiN.

Then, for the thermal conductance, the Casimir-Ziman model was used very successfully to interpret the data in the silicon nanowires. In the case of a SiN nanowire, one may want to use the same Casimir-Ziman model. The conductance in a SiN nanowire has a square dependence with respect to the temperature. The simple Casimir model cannot be used, as it predicts a cubic dependence with respect to the temperature for the conductance. This is evidenced by the figure 5.9. In this figure the thermal conductance of the nanowire used in the previous section (fig. 5.2) has been plotted, with the conductances obtained within the framework of the Casimir-Ziman model (cf. section 2.4) and K_0 (four times the universal quantum of thermal conductance; see section 1.4.5).

On this figure, one can see that even qualitatively, the conductance of the Casimir model does not correspond to the measured conductance. The conductance made with adjusting the MFP with specular reflection (K_{Zim}) may look like the measured conductance, but one order of

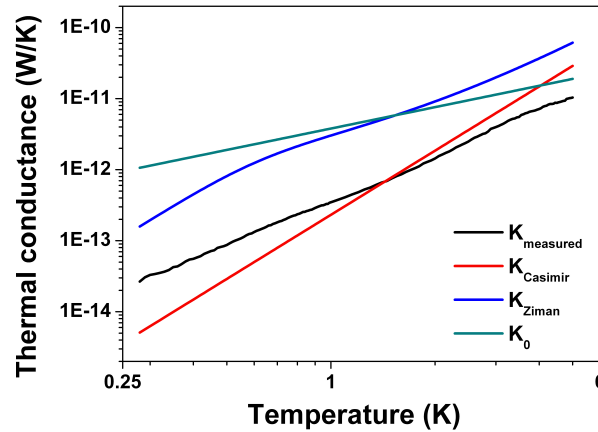


Figure 5.9: Thermal conductance of the SiN nanowire (in black), the conductance obtained by the Casimir formula (in red), the conductance with the effective mean free path obtained with the Ziman model (in blue), and four times the quantum of thermal conductance (K_0 , in dark cyan). On the contrary to Si nanowires, these conductances have not even the same behavior with respect to the temperature. The measured conductance is much smaller than the quantum of thermal conductance.

magnitude higher. Finally, the thermal conductance of the SiN nanowire is much smaller than the quantum of thermal conductance. The difference between these conductances increases when the temperature goes down. Quantum effects are therefore not expected, even for lower temperatures than those studied.

The conductance called K_{Zim} is the most comparable to the measured conductance. However the factor ten between these two conductances cannot be explained. To understand this difference, it requires the understanding of the physics inside amorphous materials. Indeed if the two level system is affected by the small size of our sample, this must change the thermal transport. This is not taken into account in the Casimir-Ziman, and should be investigated in order to have a good understanding of the physics inside nanowires in amorphous materials.

5.5 Conclusion

Measurements of thermal properties in SiN have been made on three kind of samples : a nanowire, a slab and a membrane. The behavior of the extensive thermal conductivity is qualitatively the same as other amorphous materials. The quantitative difference comes from the small size of the samples, which has been evidenced through the study of the mean free path. Theoretical works are still lacking to have a physical explanation of the transport inside bulk amorphous materials, and also in small systems. These measurements may help the understanding of the physics of phonons in amorphous materials.

Conclusion

During these three years, I have been able to develop successfully thermal transport measurements on low dimensional systems at low temperatures. This work contributes to the understanding various effects of nanoscale structuring on phonon transport.

Firstly, I have proved that the conductance measured is not limited by the contact conductance between the nanowire and the thermal bath. The heat can flow without major perturbations from the nanowire to a three dimensional thermal reservoir. This result was not obvious since several models predict an increasing contribution of the contacts to thermal transport as the temperature is lowered. This is not the case for our samples at the temperatures studied, where the transmission of heat is nearly perfect.

Then, measurements on corrugated nanowires show a surprising effect. The phonon mean free path is drastically reduced by multiple scattering and backscattering at the surface of the nanowire. This leads to a significant decrease of the thermal conductance. The Casimir limit, which is the lowest value for thermal conductance, has been exceeded in these corrugated nanowires. These experimental results are of great interest as it allows a new way to decrease the heat transport with potential application to new materials for thermoelectricity.

Measurements have also been performed in amorphous material samples with three different sizes (100 nm, 1 μm , 100 μm). By comparing with studies done on other amorphous materials, the mean free paths have been determined. The physics of phonons in amorphous materials is not completely understood. It has been shown that the phonon mean free path still plays a major role for the heat transport in these materials. These measurements may contribute to have a better understanding of the heat transport in amorphous materials.

In these works, measurements have been done down to 0.3 K. We are now convinced that the 3ω method cannot be used at lower temperature. Indeed, due to the increasing of specular reflection of phonons on the surface as the temperature is lowered, the phonons mean free path becomes too large compared to the actual length of the nanowire. In order to explore thermal transport at lower temperature, where ballistic transport plays a crucial role, the 3ω method needs to be dropped for a new experimental technique. A new generation of sensors are currently being developed in the group for that purpose. These sensors may pave the way to measurements in the quantum regime of thermal transport at very low temperatures.

Bibliography

- [1] G. Chen, *Nanoscale Energy Transport and Conversion*. Oxford University Press, 2005.
- [2] N. W. Ashcroft and N. D. Mermin, *Solid state physics*. 1976.
- [3] J. Ziman, *Electrons and Phonons*. Oxford University Press, 2001.
- [4] H. B. G. Casimir *Physica*, vol. 5, p. 595, Mar. 1939.
- [5] R. Berman, E. L. Foster, and J. M. Ziman, “Thermal conduction in artificial sapphire crystals at low temperatures,” *Proc. of the Royal Society*, vol. A231, pp. 130–144, Mar. 1955.
- [6] T. Klitsner and R. O. Pohl *PHYSICAL REVIEW B*, vol. 36, p. 6551, 1987.
- [7] W. Fon, K. C. Schwab, J. M. Worlock, and M. L. Roukes, “Phonon scattering mechanisms in suspended nanostructures from 4 to 40 k,” *Phys. Rev. B*, vol. 66, pp. 045302–, July 2002.
- [8] O. Bourgeois, T. Fournier, and J. Chaussy, “Measurement of the thermal conductance of silicon nanowires at low temperature,” *J. Appl. Phys.*, vol. 101, pp. 016104–3, Jan. 2007.
- [9] J. Cuffe, O. Ristow, E. Chavez, A. Shchepetov, P.-O. Chapuis, F. Alzina, M. Hettich, M. Prunnila, J. Ahopelto, T. Dekorsy, and C. M. S. Torres *PHYSICAL REVIEW LETTERS*, vol. 110, p. 095503, 2013.
- [10] J. S. Heron, T. Fournier, N. Mingo, and O. Bourgeois, “Mesoscopic size effects on the thermal conductance of silicon nanowire,” *Nano Letters*, vol. 9, no. 5, pp. 1861–1865, 2009.
- [11] B. J. van Wees, H. van Houten, C. W. J. Beenakker, J. G. Williamson, L. P. Kouwenhoven, D. van der Marel, and C. T. Foxon, “Quantized conductance of point contacts in a two-dimensional electron gas,” *Phys. Rev. Lett.*, vol. 60, pp. 848–850, Feb 1988.
- [12] e. a. Wharam, *D. A. J. Phys. C: Solid State Phys.*, vol. 21, p. L209, 1988.
- [13] J. B. Pendry *J. Phys. A: Math. Gen.*, vol. 16, p. 2161, Mar. 1983.
- [14] L. G. C. Rego and G. Kirczenow, “Quantized thermal conductance of dielectric quantum wires,” *Phys. Rev. Lett.*, vol. 81, pp. 232–, July 1998.

Bibliography

- [15] O. Chiatti, J. T. Nicholls, Y. Y. Proskuryakov, N. Lumpkin, I. Farrer, and D. A. Ritchie, “Quantum thermal conductance of electrons in a one-dimensional wire,” *Phys. Rev. Lett.*, vol. 97, p. 056601, Aug 2006.
- [16] W. P. J. P. Meschke, Matthias; Guichard, “Single-mode heat conduction by photons,” *Nature*, vol. 444, pp. 187–190, 2006.
- [17] K. Schwab, E. A. Henriksen, J. M. Worlock, and M. L. Roukes *Nature*, vol. 404, pp. 974–977, 2000.
- [18] K. Schwab, W. Fon, E. Henriksen, J. M. Worlock, and M. L. Roukes, “Quantized thermal conductance: measurements in nanostructures,” *Physica B: Condensed Matter*, vol. 280, pp. 458–459, May 2000.
- [19] M. C. Cross and R. Lifshitz, “Elastic wave transmission at an abrupt junction in a thin plate with application to heat transport and vibrations in mesoscopic systems,” *Phys. Rev. B*, vol. 64, pp. 085324–, Aug. 2001.
- [20] D. E. Angelescu, M. C. Cross, and M. L. Roukes *Superlattices and Microstructures*, vol. 23, p. 673, 1998.
- [21] L. Landau and E. Lifshitz, *Theory of Elasticity*. 1986.
- [22] C.-M. Chang and M. R. Geller, “Mesoscopic phonon transmission through a nanowire-bulk contact,” *Phys. Rev. B*, vol. 71, pp. 125304–8, Mar. 2005.
- [23] R. Prasher, T. Tong, and A. Majumdar, “An acoustic and dimensional mismatch model for thermal boundary conductance between a vertical mesoscopic nanowire/nanotube and a bulk substrate,” *J. Appl. Phys.*, vol. 102, pp. 104312–10, Nov. 2007.
- [24] Y. Chalopin, J.-N. Gillet, and S. Volz, “Predominance of thermal contact resistance in a silicon nanowire on a planar substrate,” *Phys. Rev. B*, vol. 77, pp. 233309–4, June 2008.
- [25] W.-X. Li, T. Liu, and C. Liu, “Phonon transport through a three-dimensional abrupt junction,” *Appl. Phys. Lett.*, vol. 89, pp. 163104–3, Oct. 2006.
- [26] Y. Tanaka, F. Yoshida, and S. Tamura, “Lattice thermal conductance in nanowires at low temperatures: Breakdown and recovery of quantization,” *Phys. Rev. B*, vol. 71, pp. 205308–12, May 2005.
- [27] R. O. Pohl, X. Liu, and E. Thompson, “Low-temperature thermal conductivity and acoustic attenuation in amorphous solids,” *Rev. Mod. Phys.*, vol. 74, pp. 991–1013, Oct 2002.
- [28] W. A. Phillips *Journal of Low Temperature Physics*, vol. 7, p. 351, 1972.
- [29] P. W. Anderson, B. I. Halperin, and C. M. Varma *The Philosophical magazine*, vol. 25, p. 1, 1972.

-
- [30] M. P. Zaitlin and A. C. Anderson, "Phonon thermal transport in noncrystalline materials," *Phys. Rev. B*, vol. 12, pp. 4475–4486, Nov 1975.
- [31] R. C. Zeller and R. O. Pohl, "Thermal conductivity and specific heat of noncrystalline solids," *Phys. Rev. B*, vol. 4, pp. 2029–2041, Sep 1971.
- [32] V. Narayanamurti and R. O. Pohl, "Tunneling states of defects in solids," *Rev. Mod. Phys.*, vol. 42, pp. 201–236, Apr 1970.
- [33] A. J. Leggett *Physica B*, vol. 169, pp. 322–327, 1991.
- [34] L. Wang and B. Li, "Phononics gets hot," *Physics World*, vol. 7, pp. 27–29, 2008.
- [35] C. W. Chang, a. A. M. D. Okawa, and A. Zettl, "Solid-state thermal rectifier," *Science*, vol. 314, p. 1121, 2006.
- [36] B. Li, L. Wang, and G. Casati, "Negative differential thermal resistance and thermal transistor," *Appl. Phys. Lett.*, vol. 88, p. 143501, 2006.
- [37] J.-S. Heron, C. Bera, T. Fournier, N. Mingo, and O. Bourgeois, "Blocking phonons via nanoscale geometrical design," *Phys. Rev. B*, vol. 82, p. 155458, Oct 2010.
- [38] A. N. Cleland, D. R. Schmidt, and C. S. Yung, "Thermal conductance of nanostructured phononic crystals," *Phys. Rev. B*, vol. 64, pp. 172301–, Oct. 2001.
- [39] J. O. Vasseur, P. A. Deymier, G. Frantziskonis, G. Hong, B. Djafari-Rouhani, and L. Dobrzynski *Journal of Physical and Condensed Matter*, vol. 10, p. 6051, 1998.
- [40] D. Vasseur, Djafari-Rouhani, Pennec, and Hladky-Hennion *Phys. Rev. B*, vol. 77, p. 085415, 2008.
- [41] A. Netsch, A. Fleischmann, and C. Enss *Journal of Physics: Conference Series*, vol. 92, p. 012130, 2007.
- [42] J. Tang, H.-T. Wang, D. H. Lee, M. Fardy, Z. Huo, T. P. Russell, and P. Yang., "Holey silicon as an efficient thermoelectric material," *Nano Lett.*, vol. 10, p. 4279, 2010.
- [43] D. G. Cahill, "Thermal conductivity measurement from 30 to 750 k: the 3 omega method," *Rev. Sci. Instrum.*, vol. 61, pp. 802–808, Feb. 1990.
- [44] L. Lu, W. Yi, and D. L. Zhang, "3 omega method for specific heat and thermal conductivity measurements," *Rev. Sci. Instrum.*, vol. 72, pp. 2996–3003, July 2001.
- [45] S. Marnieros, *Couches Minces d isolant d Anderson. Application a la bolometrie a tres basse temperature*. PhD thesis, Universite de Paris Sud (Paris XI), 1998.
- [46] P. W. Anderson, "Localized magnetic states in metals," *Phys. Rev.*, vol. 124, pp. 41–53, Oct 1961.

Bibliography

- [47] N. Mott *J. Non-Crystal. Solids*, vol. 1, p. 1, 1968.
- [48] O. Bourgeois, E. André, C. Macovei, and J. Chaussy *Rev. Sci. Instrum.*, vol. 77, p. 126108, 2007.
- [49] C. Buzzi, *Developpement de bolometre monolithiques silicium refroidies a 0.3 K pour le satellite FIRST*. PhD thesis, Universite Joseph Fourier, 1999.
- [50] A. Sikora, H. Ftouni, J. Richard, C. Hébert, D. Eon, F. Omnes, and O. Bourgeois, “Highly sensitive thermal conductivity measurements of suspended membranes (sin and diamond) using a 3w-volklein method,” *Rev. Sci. Instrum.*, vol. 83, p. 054902, 2012.
- [51] H. Ftouni, D. Tainoff, J. Richard, K. Lulla, J. Guidi, E. Collin, and O. Bourgeois, “Specific heat measurement of thin suspended sin membrane from 8 k to 300 k using the 3 omega-v[o-umlaut]lklein method,” *Review of Scientific Instruments*, vol. 84, no. 9, p. 094902, 2013.
- [52] F. Völklein *Thin Solid Films*, vol. 188, p. 27, 1990.
- [53] T. S. Tighe, J. M. Worlock, and M. L. Roukes, “Direct thermal conductance measurements on suspended monocrystalline nanostructures,” *Appl. Phys. Lett.*, vol. 70, pp. 2687–2689, May 1997.
- [54] D. Li, Y. Wu, P. Kim, L. Shi, P. Yang, and A. Majumdar, “Thermal conductivity of individual silicon nanowires,” *Appl. Phys. Lett.*, vol. 83, pp. 2934–2936, Oct. 2003.
- [55] C. Yu, L. Shi, Z. Yao, D. Li, and A. Majumdar, “Thermal conductance and thermopower of an individual single-wall carbon nanotube,” *Nano Letters*, vol. 5, no. 9, pp. 1842–1846, 2005.
- [56] J. Lim, K. Hippalgaonkar, S. C. Andrews, A. Majumdar, and P. Yang *Nano Lett.*, vol. 12, p. 2475, 2012.
- [57] C. Thomsen, H. T. Grahn, H. J. Maris, and J. Tauc, “Surface generation and detection of phonons by picosecond light pulses,” *Phys. Rev. B*, vol. 34, pp. 4129–4138, Sep 1986.
- [58] A. Huynh, N. D. Lanzillotti-Kimura, B. Jusserand, B. Perrin, A. Fainstein, M. F. Pascual Winter, E. Peronne, and A. Lemaitre, “Subterahertz phonon dynamics in acoustic nanocavities,” *Phys. Rev. Lett.*, vol. 97, p. 115502, Sep 2006.
- [59] J. B. Hertzberg, O. O. Otelaja, N. J. Yoshida, and R. D. Robinson, “Non-equilibrium phonon generation and detection in microstructure devices,” *Rev. Sci. Instrum.*, vol. 82, p. 104905, 2011.
- [60] H. Kinder, “Spectroscopy with phonons on $\text{Al}_2\text{O}_3: \text{V}^{3+}$ using the phonon bremsstrahlung of a superconducting tunnel junction,” *Phys. Rev. Lett.*, vol. 28, pp. 1564–1567, Jun 1972.

-
- [61] E. T. Swartz and R. O. Pohl, "Thermal boundary resistance," *Rev. Mod. Phys.*, vol. 61, p. 605, July 1989.
- [62] R. Prasher, T. Tong, and A. Majumdar, "Approximate analytical models for phonon specific heat and ballistic thermal conductance of nanowires," *Nano Lett.*, vol. 8, no. 1, pp. 99–103, 2008.
- [63] F. C. Wellstood, C. Urbina, and J. Clarke, "Hot-electron effects in metals," *Phys. Rev. B*, vol. 49, pp. 5942–5955, Mar 1994.
- [64] M. Hartmann, G. Mahler, and O. Hess, "Existence of temperature on the nanoscale," *Phys. Rev. Lett.*, vol. 93, p. 080402, Aug 2004.
- [65] M. Hartmann, G. Mahler, and O. Hess, "Local versus global thermal states: Correlations and the existence of local temperatures," *Phys. Rev. E*, vol. 70, p. 066148–, Dec. 2004.
- [66] M. Hartmann, "Minimal length scales for the existence of local temperature," *Contemporary Physics*, vol. 47, no. 2, pp. 89–102, 2006.
- [67] A. L. Moore, S. K. Saha, R. S. Prasher, and L. Shi, "Phonon backscattering and thermal conductivity suppression in sawtooth nanowire," *Appl. Phys. Lett.*, vol. 93, p. 083112, Mar. 2008.
- [68] A. Rajabpour, S. M. V. Allaei, Y. Chalopin, F. Kowsary, and S. Volz, "Tunable superlattice in-plane thermal conductivity based on asperity sharpness at interfaces: Beyond ziman's model of specularity," *Journal of Applied Physics*, vol. 110, no. 11, p. 113529, 2011.
- [69] J. Sadhu and S. Sinha *Phys. Rev. B*, vol. 84, p. 115450, 2011.
- [70] Y. P. He and G. Galli *Phys. Rev. Lett.*, vol. 108, p. 215901, 2012.
- [71] C. Blanc, A. Rajabpour, S. Volz, T. Fournier, and O. Bourgeois, "Phonon heat conduction in corrugated silicon nanowires below the casimir limit," *Applied Physics Letters*, vol. 103, no. 4, p. 043109, 2013.
- [72] P. D. Vu, J. R. Olson, and R. O. Pohl *J. Low Temp. Phys.*, vol. 113, p. 123, 1998.
- [73] D. G. Cahill, W. K. Ford, K. E. Goodson, G. D. Mahan, A. Majumdar, H. J. Maris, R. Merlin, and S. R. Phillpot, "Nanoscale thermal transport," *J. Appl. Phys.*, vol. 93, pp. 793–818, Jan. 2003.
- [74] Z. Wang and N. Mingo, "Absence of casimir regime in two-dimensional nanoribbon phonon conduction," *Applied Physics Letters*, vol. 99, no. 10, p. 101903, 2011.